

A STUDY OF THE TURN-ON

MECHANISMS IN THYRISTORS

Thesis presented for the Degree of

Doctor of Philosophy

of Brunel University

by

William Fong Yan

May 1975

## CONTENTS

Abstract

Acknowledgments

Chapter 1	Introduction	p.1
Chapter 2	Review of the $di/dt$ problem	p.6
2.1	General	
2.2	The diffusive model	
2.3	Lateral bias model	
2.4	Experimental work relating to the plasma spreading models	
Chapter 3	Experimental details	p.20
3.1	Specimen structure	
3.2	Measurement techniques	
Chapter 4	Results	p.34
4.1	Introduction	
4.2	Results of spreading velocity measurements	
4.3	Results of current gain measurements	
4.3.1	Results showing the positive feedback effect of the $V_{B0}$ junction capacitance	
4.3.2	Results on experimental rectangular devices	
Chapter 5	Discussions	p.38
5.1	Device designs affecting the spread. of plasma	
5.1.1	The values of current gains of the n-p-n and the p-n-p transistor sections	
5.1.2	Emitter shorts	

5.2 Discussion of results

Chapter 6 Theoretical developments p.43

6.1 Introduction

6.2 Assumptions made in evaluating  
the initial turned-on area

6.3 Evaluation of the initial turned-on  
area

6.4 Correlation of the diffusive model  
of plasma spread as proposed by  
Bergman and that by Longini and  
Melngailis

References

Tables

Figures

## ABSTRACT

Mechanisms of thyristor turn-on were studied.

An attempt was made to relate the 'on' plasma spreading velocity to the small signal current gain value of the n-p-n transistor section of the thyristor.

The extent to which the thyristor turns on initially largely affects the speed of turning-on the device. A model is proposed to calculate the initial turned-on area of thyristors.

## ACKNOWLEDGMENTS

I am deeply indebted to Professor C.A. Hogarth for his persistent encouragement and advice ever since I entered the field of semiconductors; in particular, during the course of writing up of this thesis.

I am also indebted to Dr. W Fulop for his supervision and many stimulating discussions during the progress of this work and Dr. R.J. Bassett for his valuable discussions and preparation of special devices used in this project.

I wish to express my thanks to the Library staff of Brunel University for their help in obtaining the necessary references, and to all colleagues and staff of the Physics Department for their guidance.

I am also indebted to Westinghouse Brake & Signal Co. Ltd. for providing me a studentship and necessary facilities to make the completion of this work possible. Also, the discussions with the members of staff of its Physical Research Laboratory, in particular, Mr.C.V. Miles and Mr.J.M. Garrett

were most valuable.

Thanks are also due to Mr.R.C. Irons for his useful discussions, reading the script and help in many ways.

Last but not the least, I have to thank my parents for their encouragement and guidance.

## CHAPTER 1

### INTRODUCTION

Silicon controlled rectifiers or thyristors are basically the semiconductor version of thyratrons. A detailed introduction to the historical background and basic principles of operation of the device has been given by Raderecht (1). Early publications on the device include those of Moll et al (2), Mackintosh (3,4), Jonscher (5,6), Misawa (7), Kuzmin (8,9), Somos (10,11), Muss and Goldberg (12), Gentry (13), Aldrich and Holonyak (14).

In brief, a thyristor is a four-layer p-n-p-n device, constructed as if a p-n-p transistor is connected to a n-p-n transistor as shown in figure 1. The device has two stable states in the forward direction, i.e. with the anode biased positively with respect to the cathode. In the 'off' state, the device blocks voltages, which could be as high as 6 kV, with only a minute leakage current of the order of milli-amperes, or less, passing through the device. In the 'on' state, the device may conduct a high forward current, e.g. 1000 A in large area devices, while the anode-to-cathode voltage is of the order of 1 to 2 volts. Switching of the device from the 'off' state to the 'on' state can be achieved by;

- a) Applying a high enough gate current to the p-base layer of the device, i.e. gate triggering.

- b) Applying a steep enough ramp voltage across the device, i.e.  $dv/dt$  triggering.
- c) Applying a forward voltage higher than the breakover voltage ( $V_{BO}$ ) of the device, i.e. voltage triggering.
- d) Shining light onto the p-base layer of the device, i.e. light triggering.

The most commonly used method for switching the device 'on' is gate triggering.

The requirement for switching thyristors to the 'on' state is that the sum of the small signal alpha values of the two transistor sections is equal to or greater than unity; i.e.

$$\alpha_{npn_0} + \alpha_{pnp_0} \geq 1$$

where  $\alpha_{npn_0}$  is the small signal low frequency a.c. common base current gain, alpha, of the n-p-n transistor section.

$\alpha_{pnp_0}$  is the small signal low frequency a.c. common base current gain, alpha, of the p-n-p transistor section.

When the device is switched 'on', it cannot be restored to the 'off' state by merely disconnecting the gate drive, because positive feedback of carriers inside the device keeps the sum of the alpha values of the two transistor sections in excess of unity. Switching the device 'off' requires the anode current to drop below the value of the holding current. This is normally achieved by disconnecting or reversing the voltage across

it. By doing so, the excess carriers inside the device, while it is in the 'on' state, are removed either by recombination or swept out of the device; the sum of the alpha values drops below unity and the device switches off.

Attempts have been made to produce devices that can be switched off by a negative gate signal, i.e. gate turn-off devices. However, this has always been more of a theoretical than a practical interest. Reversing the gate bias to extract excess carriers out of the device would create a high lateral current flowing in the gated base region. This would develop a high bias across the cathode p-n junction in the region furthest away from the gate contact. As a result, the cathode p-n junction in this region would breakdown and remain in the 'on' state, whereas the rest of the device would remain 'off'. All the load current would then be crowding in this 'on' region. The high current density thus created could destroy the device.

In the past decade, thyristors have mainly been used as high power or fast switching elements and development has been mainly directed towards problems relating to power dissipation, forward and reverse blocking capabilities (15), fast turn-on (16,17,18,19, 20,21), fast turn-off (11), and high  $di/dt$  (14,22,23, 24) or high  $dv/dt$  ratings (1,11,25).

Larger area devices are being used to accommodate the high currents that flow while the device is 'on'.

High resistivity, a wide n-base, and bevelling of the surface where the junctions emerge, have made higher blocking capabilities possible, while regenerative gates and gold doping are used to achieve fast switching. Shorted-emitters are employed to short out any displacement currents arising from suddenly-applied high bias voltages across the device, thus enabling better  $dv/dt$  ratings to be achieved.

$di/dt$  failure occurs when a fast-rise high forward current is allowed to flow through the device at the beginning of the 'on' state. As the 'on' region has not yet spread far enough to reduce the current density in that area, high power dissipation resulting in excessive thermal stress leading to mechanical stress can cause failure. This remains a continuing problem of high power, fast turn-on devices. Research was directed towards obtaining a larger initially turned-on area and faster spread of the plasma. Ring gate and regenerative gate devices were then developed to initiate such a larger area and a faster turn-on. Cordingly (26) developed an acoustic technique for investigating the  $di/dt$  capability of the device non-destructively. However, it is felt that if there is any method of estimating the spread of the initial turned-on plasma by using some simple measurements of basic parameters of the device, it would give some insight into the  $di/dt$  capability of the device.

As the width of the p-base layer in part determines the plasma spread (27) under specified conditions, such as a given 'on' current through the device, it was hoped to relate the n-p-n current gain value of the device to the spreading velocity of the plasma. The width of the p-base which determines both spreading velocity and current gain should thus establish a link between the n-p-n current gain values and the spreading velocity and the  $di/dt$  capability of the device. The n-p-n current gain values were measured using the three terminal method (28) proposed by Fulop and the spreading velocity was obtained by using the probing technique (29,30,39) described in Chapter 3.

## CHAPTER 2

### REVIEW OF THE $di/dt$ PROBLEM

#### 2.1. General

As outlined in Chapter 1, failure of thyristors will occur when a high current is allowed to flow through the device within a short time after the device has switched on. This is attributed to the high current density in the turned-on region which results in high power dissipation leading to thermal and mechanical stress in that area. A limit is thus imposed upon the rate of rise of the forward current that is to flow when the device is initially turned-on; this is normally referred to as the  $di/dt$  rating of the device.

The task of improving the  $di/dt$  capability of thyristors was tackled by previous workers in different ways. The general trend was either to increase the initial turned-on area, so as to give a lower initial 'on' current density (16,22,31), or to initiate a faster spreading mechanism by using auxiliary structures inside the device (18,19,21). Higher gate drives and longer gate-to-cathode perimeter lengths were employed to enlarge the initial turn-on area. However, as higher input gate power is required to switch the longer gate perimeter structure, these devices are less sensitive to trigger currents. Regenerative, inverse gate, and auxiliary gate devices were thus designed whereby the

'on' current flowing through the initial 'on' portion of the device is used as a secondary gate drive to turn on other parts of the device. Auxiliary gate devices also have a disadvantage, as these devices operate by first turning on the auxiliary or secondary thyristor, and then transferring the load current from the auxiliary thyristor to the main thyristor. The auxiliary device switches 'off' after the 'on' process is completed. This means that in the steady 'on' state, a certain area of the device, equal to the area of the auxiliary thyristor, is 'wasted' because it does not take part in carrying the 'on' current. Perhaps, the best type of device to use in achieving high  $di/dt$  ratings is the regenerative gate devices which have proved to have ratings of the order of  $600A/\mu\text{sec}$  at  $1kV$ <sup>as</sup> against the normal 30 to  $100A/\mu\text{sec}$  for large devices.

The study of the  $di/dt$  problem would not be complete without considering the velocity of spread of the 'on' plasma. Investigations into the mode of spreading was tackled both theoretically (32,33,34,35) and experimentally (20,36;37,38,39,40). Bergman (33), Longini and Melngailis (32) derived expressions for the plasma spreading velocity based on the pure diffusive flow of carriers. Deviations from the 'diffusive model' were observed (29,30) at high 'on' current levels. This was attributed to the fact that high lateral potential differences from the 'on' to the 'off' region exist which would influence the spread of the 'on' plasma (30). Ruhl (27), Somos (10),

Somos and Piccone (34) thus developed the 'lateral bias model' of the plasma spread which was based on the lateral field from the 'on' to the 'off' region of the device.

## 2.2 The diffusive model

Work on the diffusive model were first published by Longini and Melngailis (32) and Bergman (33). In this model, the diffusion of minority carriers from the 'on' to the 'off' region is considered to be the only mechanism responsible for the plasma spread. As the carrier densities in both base regions of the 'on' region, according to the current density, can be a few order of magnitudes higher than those appropriate to the 'off' region, carriers will diffuse down their concentration gradient from the 'on' to the 'off' region. This lateral diffusion of carriers is equivalent to the injection of gate current from the 'on' region to the 'off' region. The 'off' region next to the 'on' region will turn on when the sum of the p-n-p transistor section alpha values reaches unity. This newly turned-on region then contributes carriers to the neighbouring 'off' region. The process repeats itself and so the plasma spreads.

The velocity of propagation of the turned-on region was derived by Longini and Melngailis through the use of the continuity equation. The spreading velocity was assumed to be uniform throughout the

spreading process. Any electric field along the base regions that might influence the diffusion of carriers was considered to be negligible. Also, p-base and n-base layers were assumed to be of equal thicknesses. With these assumptions, Longini and Melngailis arrived at the following expression for the spreading velocity,

$$v_s = \frac{F}{N_0} - \frac{N_0}{F} \left( \frac{D}{\tau} + \frac{\pi^2 D^2}{a} \right) \text{----- (1)}$$

where  $\frac{2F}{\pi}$  is the flux of carriers that is fed to the 'off' region per unit base thickness per unit length of periphery of the 'on' region

$D$  is the diffusion constant of minority carriers

$\tau$  is the minority carrier lifetime

$a$  is the thickness of each base

$N_0$  is the maximum carrier density at the periphery of the 'on' region

From this, it can be seen that Longini and Melngailis have made two rather questionable assumptions. One is the uniform spreading velocity throughout the process and the other is the equality of the two base thicknesses. In fact, during spreading, carriers are diffusing out of the 'on' region so that the carrier concentration gradient from the 'on' to the 'off' region will drop as the spreading progresses, thereby reducing the speed of lateral flow of carriers. This will lead to a gradual decrease in the velocity of propagation of the 'on' region during the process unless the  $di/dt$  value of the forward

current is high enough to compensate<sup>for this</sup>. Also, in order to stand high voltages, the lower doped n-base is normally much thicker than the p-base. Longini and Melngailis however, have assumed the base thicknesses to be the same and thus their derivation has overlooked the variation of the spreading velocity and the differences in base widths.

Bergman, though using the same model, gave the spreading velocity of the 'on' region in terms of the rise-time of the 'on' load current pulse as follows,

$$v_s = 1.48 \sqrt{\frac{D}{t_r}} \text{ --- (2)}$$

where  $D$  is the ambipolar diffusion constant, taken as the mean of the electron and hole diffusion constants,

$t_r$  is the rise-time of the load current pulse and lies in the  $\mu\text{sec.}$  region. \* (see p.19)

Here, the rise-time is defined as the time taken for the load current to rise from 10% to 90% of its final value. This must not be confused with the rise-time defined by Misawa (6) which is the time taken for the load current to rise from 10% to 90% of the value at which the centre junction switches on. Even for non-inductive loads, the load current at which the centre junction of the device switches on might not be the true final value as the voltage across the device might not have dropped to a sufficiently low value. This is due to the high resistance of the <sup>switched on base</sup> ~~on~~ regions which <sup>have</sup> has not

yet been <sup>fully</sup> conductivity modulated. One could well say that the rise-time used by Bergman is the rise-time of the circuit load current.

As can be seen from equation (2), Bergman has also assumed a constant velocity of spreading.

### 2.3 Lateral bias model

The lateral bias model is based upon the potential difference appearing between the 'on' and the 'off' regions, laterally across the device. Immediately after the device is switched on locally, the centre junction of the 'on' region is forward biased whereas that of the 'off' region remains in reverse bias. As the total voltage drop across the device at this moment is only a few volts, charges in the base regions redistribute themselves. The result of this is that the bias on the emitter junctions <sup>goes</sup> ~~is~~ from forward to reverse and the centre junction has a much lower reverse bias. A ~~very~~ large lateral potential difference thus appears across the device from the 'on' to the 'off' region. The direction of this electric field aids the flow of majority carriers from the 'on' to the 'off' region, resulting in a rapid spread of plasma.

As this spread is a consequence of the electric field acting upon the charge carriers, it would lose its significance when the active 'on' region is conductivity-modulated and the carriers are in an ambi-<sup>the</sup>

polar state. The region in which this field is effective, usually referred to as the transition region, is only a small distance from the edge of the active region. The width of the transition region,  $l$ , was found by Bergman (31) to be

$$l = v_s \cdot t_r \text{ - - - - - (3)}$$

where  $v_s$  is the spreading velocity of the plasma and  $t_r$  is the rise-time of the load current pulse. Ruhl (27) has estimated  $l$  to be within the range 6 to 18 thousandths of an inch (150 $\mu$ m to 460 $\mu$ m).

This lateral biasing effect on plasma spread was described by Gentry (36), Somos (10,32) and Gerlach (28). However, for some years not much attention was paid to the mode of spreading based on this effect. Detailed analysis of this model was not published until 1970 when Ruhl (25) and Somos and Piccone (32) gave accounts of their work.

Having assumed the spreading velocity to be a linear function of the lateral hole current and the lateral field in the transition region to be a constant; Ruhl arrived at the expression

$$v_s = \frac{A m k T}{q} \ln \left( \frac{J_e}{J_0} + 1 \right) + C' \text{ - - - - - (4)}$$

where  $v_s$  is the spreading velocity

$A$  is an unspecified function independent of  $J_e$  and temperature

$m$  is a multiplier dependent on current density,  
 recombination trap density and energy level  
 $k$  is the Boltzmann's constant  
 $T$  is the absolute temperature  
 $q$  is the electronic charge  
 $J_e$  is the instantaneous emitter current density  
 at the edge of the active 'on' region  
 $J_0$  is the p-base n-emitter junction reverse  
 saturation current density  
 $C'$  is an unspecified function independent of  $J_e$

He then modified equation (4) such that it would  
 still be applicable even at low current densities. The  
 final equation was

$$V_s = \frac{AmkT}{q} \ln \left( \frac{J_e}{J_0} + K \right) + C \text{ ----- (5)}$$

where  $K$  is a constant of value usually near 1  
 $C$  is a function of the change in sensitivity  
 of the inactive region to gate current.

#### 2.4 Experimental work relating to the plasma spreading models

In 1966, Dodson and Longini (29) carried out  
 a number of experiments to observe the dependence of  
 spreading velocity upon other parameters such as load  
 current, p-base width, temperature etc. Their results

showed some deviations from the theory of Longini and Melngailis. It was concluded that some of the deviations might have resulted from neglecting the lateral field appearing in the p-base region.

The experiments were performed on rectangular devices as shown in figure 2. The n-emitter was etched off at one end of the device for gate connection. Islands through the n-emitter layer were also made along the device whereby tungsten probes could be lowered down to make contact with the p-base. Arrival of the 'on' plasma at a particular island was detected by reverse-biasing the island and observing the reverse-bias current. The times taken for the plasma to reach the islands were recorded by photographing traces on the oscilloscope. Spreading velocities were then calculated by dividing the distance between two islands by the time taken for the plasma to spread from one to the other. The results obtained for spreading velocities were found to lie within the range from  $0.02\text{mm}/\mu\text{sec}$  to  $0.5\text{mm}/\mu\text{sec}$ . In summary, the results and conclusions that Longini and Melngailis presented are as follows;

- (a) At low currents, the spreading velocity  $v_s$  is proportional to the load current  $I$ , whereas at high load currents,  $v_s$  is proportional to  $I^n$  where the value of  $n$  varies between 2 and 6.
- (b) The prediction that the spreading velocity decreases as the distance from the gate contact increases, was

not always true. This was considered to be the effect of the asymmetrical geometry, e.g. the non-uniform base thickness, of the device<sup>not shown in fig.2.</sup> Some of the deviations might be due to differences in load current rise-time as they had a tendency to occur more frequently at high current levels.

(c) Spreading velocity increases as base width decreases. As predicted by Longini and Melngailis, different values of base width change the spreading velocity because there is a resultant change in the carrier density present in the 'on' region, and thus affects the carrier concentration gradient from the 'on' to the 'off' region.

(d) The spreading velocity increases with temperature at low load current levels and stays independent of temperature at high currents, in accordance with the theory of Longini and Melngailis.

(e) The spreading velocity is independent of anode-to-cathode voltage across the device prior to triggering.

(f) If a gap were to appear across the entire emitter of the device, the plasma would still spread across it. This was attributed to the difference in emitter junction bias between the 'on' and 'off' region. The higher forward bias at the 'on' emitter region would set up a lateral potential difference between the 'on' and 'off' regions which would cause the n emitter in the 'off' region, near the gap, to inject carriers into the p-base thereby turning on the device at that point. A certain delay in plasma spreading would certainly occur when it reached the gap. The delay period would depend upon the value

of load current.

In the same year as Dodson and Longini published their experimental work on plasma spreading, Gerlach (30) also published measurements on spreading velocity employing similar techniques. Having a similar device structure, Gerlach obtained the time delay of plasma arriving at individual islands by measuring the increase of voltage at the probes. The probe voltage gives the value of forward bias across the emitter p-n junction together with the voltage drop due to the transverse path resistance of the p-base. This emitter junction potential would rise as plasma approached, and, at high current densities it could reach a value of about 1 volt. Voltages appearing at other probes where the device is still 'off' were prevented from rising by the high lateral resistance in the p-base.

Gerlach's photographs of probe voltages showed an initial negative value before rising to the final voltage. This was due to the fact that although the whole of the device was not turned-on, the anode and cathode metallisation caused the bias across the device to be the same in both 'on' and 'off' regions. Charge redistribution occurred at the region where the device was 'off'. The cathode p-n junction capacitor charged up while that of the central p-n junction discharged. The consequence of this was a reverse bias on all three junctions. The negative probe voltage recorded before the plasma spread to the probe was due to this reverse bias on the emitter p-n junction. The value of spreading velocity varied from

0.033mm/ $\mu$ sec to 0.074mm/ $\mu$ sec. Also, spreading velocity values for currents lower than 10 A could not be accurately determined as the plasma did not spread far enough.

Gerlach's results showed good agreement with Bergman's theory at low currents. However, at high currents, as the load current rise-time remains unchanged with the load current employed, the experimentally-obtained spreading velocity values were much higher than the theoretically calculated ones. The discrepancy becomes greater at the highest current densities, where the diffusion constant drops and results in a decreased theoretical value. Also the results do not support Bergman's theory for the influence of temperature on the spreading velocity. Assuming the current rise time to be independent of temperature and the diffusion constant to be proportional to  $T^{-3/2}$ , the theoretically-calculated spreading velocities over the temperature range  $-20^{\circ}\text{C}$  to  $140^{\circ}\text{C}$  were lower than those determined experimentally.

Gerlach suggested that the differences between the theoretical diffusive model and experimental results for the variation of spreading velocity with respect to load currents were due to the neglect of the lateral bias present between the 'on' and 'off' regions. The lateral bias, which increases with increasing load current would enhance the plasma spread. He also suggested that the increase in experimentally measured spreading velocity with temperature was due to

to the lower triggering current required to switch the device on.

Ruhl (27) also made his measurements on spreading velocities by observing the delay in the rise of the n-emitter-p-base junction voltage along his devices. Instead of rectangular experimental structures as used by Dodson and Longini and by Gerlach, he employed circular amplifying-gate devices with emitter shorting dots. Contacts to the p-base were made by probing down to the demetalized shorting dots.

His results showed that;

(1) For a given 'on' area current density, the spreading velocity remains fairly constant, independent of radial position, once the plasma had spread beyond 0.1cm. of the gate contact. For the Longini and Melngailis theory, Dodson and Longini rewrote equation (1) as

$$V_s = G_1 \frac{I}{S} - G_2 \frac{S}{I}$$

where S is the peripheral length.

The spreading velocity is a function of the peripheral length which in turn is a function of the radial distance.

(2) The spreading velocity is a linear function of the logarithm of the 'on' area current density as predicted by the lateral bias model.

(3) The p-base width affects the spreading velocity significantly. A thinner p-base increases the value of

$\alpha_{npn}$  and thus enables the device to be more sensitive

to triggering current. Also a thinner p-base would normally have a higher lateral resistance which would impose a higher bias across the emitter p-n junction for a given lateral p-base current.

(4) No first order correlation between n-base width and spreading velocity was found.

(5) Emitter shorts acting as a parallel shunt to the emitter p-n junction would lower the active area current density. The consequence of this would be a reduction in spreading velocity.

(6) Devices made without gold doping gave faster spreading than gold-doped devices of similar structure. Without shorting dots, devices without gold doping showed a speed of spreading about five times faster than gold-doped devices. The presence of gold in the p-base lowers the minority carrier lifetime and hence the transport efficiency and the current gain. This means a drop in sensitivity of the device to gate triggering current or the sensitivity of 'off' region to the lateral p-base current. The plasma spreading velocity would thus be lowered.

\*  $t_v$  is given by (approximately),  $2 \sqrt{\frac{t_1 t_2}{\alpha_{pnp} + \alpha_{npn} - 1}}$

where  $t_1$  is the carrier transit time of n-base

$t_2$  is the carrier transit time of p-base.

## CHAPTER 3

### EXPERIMENTAL DETAILS

#### 3.1. Specimen Structure

Devices used for the experiments in this project were specially prepared rectangular devices having structure as shown in figure 3. Structural details of each of the four batches of devices used are shown as in Table 1. Since the use of connections to the inner p-base of the device, in spreading velocity measurements, by probing through tiny little 'windows' in the cathode with micromanipulators could be tedious, six gold/boron gate dots surrounding the cathode as shown in figure 3 were made. Each of these dots could be used individually as the gate of the device or for direct measurements of arrival of plasma in the plasma spreading velocity measurements described in the subsequent section. Silver wires were soldered onto these dots and cathode for electrical connections. Fluxless solders were used in order to avoid contamination and Baker's fluid was used to facilitate soldering. Soldering was done by first applying solder onto the dots and a point on the cathode of the device which was already placed on a hotplate. The temperature of the hotplate was just high enough to wet the solder. The end of the silver wire where it was to be soldered onto the device was coated with solder by using a soldering iron. The wire was then carefully brought down to the

appropriate dot or cathode where solder was applied and the temperature of solder was then raised to its melting point by using a very fine soldering iron. Extreme care and steadiness of hand were required when making these soldered joints, otherwise the device could easily be damaged.

All devices used were supplied by Westinghouse Brake-English Electric Co. Ltd., Wiltshire, England.

### 3.2 Measurement Techniques

One aim of the work in this thesis was to relate the small signal a.c. alpha values of the equivalent transistor sections inside the device to the spreading velocities of the switched-on plasma. The experimental work was in two stages; firstly to measure the spreading velocity of the plasma, and, secondly, the measurement of the small signal a.c. current gains.

The technique for measuring plasma spreading velocities used here was similar to that described by Dodson and Longini (29), Gerlach (30) and by Bassett, Hogarth and Newman (39). The spread of plasma was observed by recording the voltage rise, with respect to the cathode, at the various 'gate' dots along the device. Time taken for the plasma to spread from one dot to the other was recorded by photographing voltage traces on an oscilloscope. The distance between dots was measured from centre to

centre of the dots. Spreading velocities were then calculated by dividing the distance covered by the plasma spread by the time taken.

The circuit used for this measurement is as shown in figure 4. The apparatus was as set up as shown in Plate 1.

Operation of the circuit can best be described by analysing it into three parts; viz., parts (a), (b), and (c) as shown in figure 4.

Part (a) is a half -wave rectifying circuit. The use of the transformer and variac as shown made possible the choice of a particular voltage to be imposed across the device. The diodes conduct in the positive half cycle of the a.c. voltage thus allowing the LC circuit of part (b) to charge up. During the negative half cycle, the diodes ceased to conduct and prevented the capacitors from discharging. The resistor and capacitor used in this part of the circuit acted as an output filter for ripple reduction. The value of the resistor used was thus chosen to be much higher than the impedance of the capacitor.

Part (b) is an LC transmission line. When the test device was triggered, the capacitors discharged with a time constant governed by the inductance and capacitance values. A current pulse width of desired duration could

thus be obtained by having different numbers of LC sections and combinations of inductance-capacitance values. The inductors used were air-cored and the capacitors were oil-filled. Insulated copper wires were used for winding the inductors. The number of turns required for each inductor were estimated by calculating the inductance value needed for the desired current pulse length, about 600  $\mu$ sec for the test devices, together with the diameters of the copper wire and the inductor to be made. Oil-filled capacitors were used because of the high voltage and large capacitance values required in this circuit. The oil-filled capacitors used were 240  $\mu$ F, 600 V d.c. working.

Part (c) is the output circuit which includes a liquid load, the test device, d.c. voltmeter, gate pulse generator, oscilloscope with a four-channel plug-in unit, a Polaroid camera mounted on the oscilloscope and a 0.023 $\Omega$  coaxial shunt.

The liquid load, consisting of 1 ml. of 98% sulphuric acid added to 699 ml. of water and immersed in a water bath at room temperature, was used as an accurate, non-inductive resistor while providing adequate cooling for high load currents. As sulphuric acid is aqueous, care was taken to ensure that the acid itself did not

absorb enough moisture to lead to any noticeable dilution. A mark was thus made on the side of the beaker to indicate the correct level of the solution when freshly made up. Acid levels raised above this mark would subsequently mean a dilution of the acid as a result of absorbing moisture from the ambient. A fresh solution would then be made up.

The test device, unencapsulated and having the structure shown in figure 3, was held down by a clamp for electrical connections. The arrangement is as shown in Plate 2, details of which are as shown in figure 5. One of the gate dots at the end of the device was used for gate triggering. Four of the remaining seven, located at different distances from the gate triggering dot were chosen to observe the spread of the 'on' plasma. Each of these four chosen dots are connected to an individual channel of the four-channel plug-in unit of the oscilloscope. The 'common' terminal of the oscilloscope was connected to the silver wire that was soldered to the cathode of the device. The reason for making this connection instead of directly connecting the 'common' terminal of the oscilloscope to the cathode rod, which was connected to the cathode of the device, was because at high load currents, the series resistance of the cathode rod with the stray resistance could lead to a voltage drop as high as 0.5 volt. This could lead to the rise of the cathode p-n junction voltage, indicating the arrival of plasma and of the order of 1 volt, picked

up by other silver wires not being clearly observed.

The test device was triggered by a single-shot gate pulse operated manually from a gate-pulse generator, the circuit of which is as shown in figure 6. The pulse from the gate pulse generator has a sharp leading edge and a value high enough for immediate triggering of the device when applied. The oscilloscope used was a Tektronix type, and the four channel plug-in unit was tektronix type 1A4. The controls, time base 'A', single sweep, d.c. input, positive d.c. external trigger synchronised to the gate pulse generator, were used on the oscilloscope. All channels that were to be displayed on the oscilloscope were chopped. Photographs of traces of the four channels were taken with a Polaroid camera. After a number of trials, an oscilloscope beam intensity of 4.5 and scale illumination of 8 were found to give the best results.

When taking photographs of the traces, the shutter of the camera was held open before triggering the device. Photographs of the plasma spread, load current pulse and voltage decay across the device were taken. The scale of the time base used for these photographs, though it might vary between batches, was the same for a single device so as to simplify the analysis of the results subsequently.

When taking photographs of the load current pulse, one channel on the oscilloscope was used. The oscilloscope

pick-up probe was connected across the co-axial line. The voltage thus observed divided by the resistance of the co-axial line, i.e.  $0.023\Omega$ , gave the value of the load current.

One channel of the oscilloscope was also used when photographing traces of anode-to-cathode voltage decay across the devices. In order to display the trace adequately on the oscilloscope for analysis, a  $10\text{ M}\Omega$  resistor in series with an oscilloscope pick-up probe of x10 attenuation was used to give x20 attenuation of anode-to-cathode voltages.

Typical photographs taken by the use of these techniques are shown in figure 7.

Methods of measuring small signal a.c. alphas were described by Fulop (28), Crees and Hogarth (41), and by Raderecht and Hogarth (42). The technique used here was as previously published by Fulop, Fong Yan, Joadat-Ghassabi and Hogarth (43) and was based on the fact that the current gain of the p-n-p and n-p-n transistor sections cut off at different frequencies. Thus measuring the 'common-gate' a.c. current gain  $\alpha_c\left(\frac{h_{21}}{h_{12}}\right)$  of the device as a function of frequency could be used to separate out the n-p-n and p-n-p alpha values.

A typical plot of  $\alpha_c$  versus frequency is as shown in figure 8. The first drop in the plot is due to the

alpha cut-off of the p-n-p transistor section whereas the second drop is due to alpha cut-off of the n-p-n transistor section.

Considering the two-transistor analogue of a thyristor as shown in figure 1, it is clearly shown in the diagram that

$$(1 - \alpha_{pnp}) i_a = \alpha_{npn} i_k$$

Thus,

$$\alpha_e = \frac{i_a}{i_k} = \frac{\alpha_{npn}}{1 - \alpha_{pnp}} \text{----- (6)}$$

Assuming a frequency variation of  $\alpha_{npn}$  and  $\alpha_{pnp}$  to be

$$\alpha_{npn} = \frac{\alpha_{npn0}}{1 + j \frac{f}{f_{npn}}} \text{----- (7)}$$

$$\alpha_{pnp} = \frac{\alpha_{pnp0}}{1 + j \frac{f}{f_{pnp}}} \text{----- (8)}$$

where  $\alpha_{npn0}$  and  $\alpha_{pnp0}$  are the low frequency current gains of the n-p-n and p-n-p transistor sections  $f_{npn}$  and  $f_{pnp}$  are the alpha cut off frequencies of the n-p-n and p-n-p transistor sections and  $j$  is the imaginary number,  $\sqrt{-1}$ .

Putting equations (7) and (8) into (6), we have

$$\alpha_e = \frac{\frac{\alpha_{npn0}}{1 + j \frac{f}{f_{npn}}}}{1 - \frac{\alpha_{pnp0}}{1 + j \frac{f}{f_{pnp}}}} \text{----- (9)}$$

at low frequencies where  $f \ll f_{pnp} \ll f_{nnp}$ ,

$$\alpha_e = \frac{\alpha_{nnp_0}}{1 - \alpha_{pnp_0}}$$

this is the first plateau value of the plot in figure 8.

At  $f = f_{pnp}$ ,

$$\alpha_e = \frac{\alpha_{nnp_0}}{1 - \frac{\alpha_{pnp_0}}{1+j}} \approx \frac{\alpha_{nnp_0}}{1 - 0.707\alpha_{pnp_0}}$$

At frequencies where  $f_{pnp} \ll f \ll f_{nnp}$ ,

$$\alpha_e = \frac{\alpha_{nnp_0}}{1 - \frac{\alpha_{pnp_0}}{1+j\frac{f}{f_{pnp}}}} \approx \alpha_{nnp_0}$$

At  $f = f_{nnp}$ ,

$$\alpha_e = \frac{\alpha_{nnp_0}}{1+j} = 0.707 \alpha_{nnp_0}$$

Thus a plot of  $\alpha_e$  as a function of frequency could give the knowledge of small-signal, low frequency, a.c. alpha values and alpha cut-off frequencies of the two equivalent transistor sections in a thyristor.

The circuit used in obtaining this plot is as shown in figure 9. The filter network shown was used to filter out any noise, ripples and unwanted a.c. signals from the high-tension stabilised power supply. The signal generator that feeds an a.c. signal into the gate of the thyristor was coupled in parallel with the direct gate current power supply through a coupling capacitor in order to avoid direct current flowing through the output circuit of the generator. Identical values of  $r_a$  and  $r_k$  were used to facilitate direct measurements of  $\alpha_e$  as

$$\alpha_e = \frac{i_a}{i_k} = \frac{i_a \cdot r_a}{i_k \cdot r_k} = \frac{V_a}{V_k} \quad \text{if } r_a = r_k$$

Low resistance values of  $r_a$  and  $r_k$  were used to minimise feedback which could give a false measured alpha value. A resistance of  $5.7\Omega$  was chosen entirely because of the availability of components. Five high-stability carbon resistors connected in parallel were used for each of the two resistors to minimise drifts in resistance values. The absolute values of the resistors were measured on a bridge. Carbon resistors were chosen to avoid any change in impedance with variation of frequency which would probably occur in wire-wound resistors. The same reason explains why  $v_a$  and  $v_k$  were measured to give the  $\alpha_e$  values, instead of directly measuring the a.c. anode and cathode currents as most a.c. ammeters have built-in inductive components which would again lead to false readings of the a.c. circuit current resulting from changes in circuit impedance with frequency. Measurements of <sup>voltages across</sup>  $r_a$  and  $r_k$  were made using an a.c. valve-voltmeter covering the entire experimental frequency range, doubly-checked by using an oscilloscope. Noise generated in the circuit and equipments were kept to a minimum by using a single common point, and coaxial screened cables were used <sup>where</sup> as appropriate. The whole experimental arrangement is as shown in Plate 3.

During the early stages of this experiment when proving the suitability of the circuit, considerable

effort was spent in finding the best combination of equipments and components. Testing of the circuit was carried out with over 30 Westinghouse production samples of various sizes and structures, having power handling capabilities that ranged from low power to high power. In general, the circuit proved to be reliable and adequate except at very high frequencies, depending on the device dimensions, when positive feedback was observed.

At high frequencies, values of which depended upon the geometry of individual devices, the  $\alpha_e$  versus frequency plots <sup>showed</sup> ~~show~~ an increase as shown in figure 10. This effect was found to be due to positive feedback from the output circuit into the input circuit via the reverse biased  $V_{BO}$  junction capacitance, analogous to the Miller effect. An alternating anode current that was fed back into the gate circuit enters the device again and effectively increases the input gate current resulting in a higher output anode current. The consequence of this is a higher a.c. anode-to-cathode current ratio, i.e. a higher  $\alpha_e$ . At still higher frequencies, the impedance of the  $V_{BO}$  capacitance drops, leading to a more severe feedback thus pushing the measured  $\alpha_e$  value even higher. This capacitance feedback effect is significant for the test devices as most of them have a large cathode area which would yield a high  $V_{BO}$  capacitance value.

Despite the fact that positive feedback occurring in this mode did not, for all but a few devices, set in until the second drop of the plot, and thus would not interfere in the measurements of  $\alpha_{pnp}$  or  $\alpha_{npn}$ , an attempt was made to reduce this unwanted feedback. The principle of a tuned circuit was employed whereby a variable inductance was connected between the gate and anode connections of the device as shown in figure 11.

The capacitance, C, was connected in series with the variable tuning inductor to isolate any d.c. voltage and/or current that appeared in the anode circuit from the input gate circuit. When the inductance value of the variable inductor L was varied such that the series combination of L and C connected in parallel with the junction capacitance,  $C_j$ , of the device resonates at a particular frequency, the tuned circuit would appear to have infinite impedance to any a.c. signals of that frequency. In other words, a.c. signals in the anode circuit was prevented from feeding back into the gate circuit by the resonating tuned circuit.

Experiments conducted in this manner showed the second drop determined by  $\alpha_{npn}$  quite neatly. However, on some devices, this drop had a different slope other than the 6 dB per octave as expected in transistors. This effect could be accounted for by the loading effect of the gate-cathode input capacitance of the device on the tuned circuit, which indicates the  $\alpha_{npn}$  drop. The validity

of this to tune out stray capacitance which would cause positive feedback from anode to gate, was tested on a range of devices of different geometrical structures. Plots of  $\alpha_e$  against frequency were measured on devices with and without inductance tuning. It was found that inductance tuning affected the  $\alpha_e$  value only for frequencies above 100 kHz. Below 100 kHz, the plots were the same whether the tuned circuit was used or not. This meant that the feedback capacitance did not cause a low enough impedance to introduce positive feedback for the devices tested.

As mentioned above, as inductance tuning would give an incorrect  $\alpha_{npn}$  drop, hence giving a false  $\alpha_{npn}$  cut-off frequency, the use of inductance tuning was kept to a minimum. In fact, it was used only when the second plateau did not show up properly, such as in curves (3) and (4) shown in figure 10. By using inductance tuning on devices that exhibited plots similar to curves (3) and (4) in figure 10, the second plateau of the plot could normally be seen, though after the n-p-n transistor section began to cut-off, the loading effect of the gate-to-cathode capacitance on the tuned circuit gave a false  $\alpha_e$  value. As the aim of this experiment was to obtain the alpha values of the two transistor sections in the device, i.e. the two plateau values of  $\alpha_e$ , the knowledge of the  $\alpha_{npn}$  cut-off frequency, though useful was not essential. After the circuit was proved to be suitable for the experiments, the specially-made

experimental devices described previously were measured. Plots were made at all contacts to the devices that were involved in the spreading velocity measurements. In order to simulate the device during the spread, alpha measurements at a particular dot were made at an anode-to-cathode voltage equivalent to that observed on the photograph as the plasma spread to that dot. Different d.c. anode current levels were used so as to allow extrapolation of the alpha values obtained to the point of switching. The values at the point of switching were then used to relate to the spreading velocity values.

## CHAPTER 4

### RESULTS

#### 4.1. Introduction

The results of the experimental work are shown in two parts. The first shows the results of spreading velocity measurements whereas the second gives the results of current gain measurements. Four batches of specially-prepared rectangular devices as shown in figure 3 were used. Details of their design are quoted in Table 1.

#### 4.2. Results of spreading velocity measurements

Typical photographs recorded in this experiment are shown in figure 7. Figure 7(a) shows the gate current triggering pulse, figure 7(b) shows the load current pulse when the device is triggered, figure 7(c) shows the probe voltages during the passage of the plasma spreading, and figure 7(d) shows the anode-to-cathode voltage decay after the device is triggered. All devices were triggered at an anode-to-cathode voltage of 350 volts. The load current pulse widths, when the current had dropped to 90% of its maximum value was 600  $\mu$ sec. The spreading times between the voltage probes were taken as the time difference for the voltages at the probes to reach 90% of their final values. Table 2 gives a summary of the results. The spreading velocity values shown

in Table 2 are the average values obtained in each batch. The number of devices used in each batch varied from four to six.

#### 4.3. Results of current gain measurements

##### 4.3.1. Results showing the positive feedback effect of the $V_{B0}$ junction capacitance

Figure 12 and figure 13 show plots of effective current gain ( $\alpha_e$ ) against frequency for two test devices. Table 3 gives the design details of the two devices which, unlike the devices of Table 1 and Table 2, were encapsulated production devices and were merely used to test the circuit used for current gain measurements. As shown in the plots, both devices showed peculiar readings at high frequencies (dotted lines). However, inclusion of a tuning inductor as described in Chapter 3, and varying it at each frequency to give a minimum value of effective current gain, gave a drop as shown by the solid lines. This enables the second plateau to be seen adequately. However, the slope of the drops in effective current gain values thus obtained deviates from the 6 dB per octave drop as given by classical transistor theory for current gain cut-off. This is due to the loading effect of the tuning inductor on the diffusion capacitance of the n-p-n transistor section which governs the current gain cut-off of that section. Inclusion of the inductor in the measurements of current gain values would thus give a false reading on the n-p-n transistor current

gain cut-off frequencies. The only advantage of using the inductor is that it would show up the second plateau more clearly.

#### 4.3.2. Results on experimental rectangular devices

In obtaining these results, the tuning inductor was not used as all devices showed the second plateau adequately although the current gain values can be seen to rise at high frequencies. Typical results obtained are shown in Table 4, Table 5 and Table 6. The plotted values are as shown in figure 14, figure 15 and figure 16. The current gain values of the n-p-n transistor section are given by the effective current gain value of the second plateau and the p-n-p transistor section current gain values are calculated as follows, as

$$\alpha_{e_0} = \frac{\alpha_{npn_0}}{1 - \alpha_{pnp_0}}$$

therefore,

$$\alpha_{pnp_0} = \frac{\alpha_{e_0} - \alpha_{npn_0}}{\alpha_{e_0}}$$

i.e. the difference in effective current gain values of the two plateaux is divided by the low frequency, initial plateau, current gain value.

Current gain measurements at each dot, or probe, were performed at an anode-to-cathode voltage as observed in the spreading velocity measurements when the probe voltage reached 90% of its maximum value.

This scheme was adopted because it was believed that the operative current gain should be measured at a voltage across the device while it is being turned-on, which is the particular device voltage when that portion of the device near the probe in question turns on. Thus it seems appropriate to measure the current gain at the particular device voltage when, or just before, that portion of the device turns on rather than at the off state voltage of the device.

With the anode-to-cathode voltage chosen as described, current gain versus frequency plots were obtained at each probe with increasing steps of direct anode current until the maximum measurable anode current value nearest the point of switching was reached. The n-p-n and p-n-p transistor section current gain values were then deduced from the plots and plotted against the anode current values. The plots were then extrapolated to the point of switching, estimated by recording the anode current value at which the device switches, which yields the current gain values at which that <sup>particular</sup> portion of the device switches. The average current gain values for an n-p-n transistor section obtained for the experimental batches of devices are as shown in Table 7.

Owing to some unknown reasons, plots on batch N208S4 devices were not satisfactory. The current gain values fell off continuously after the first drop and no second plateau was observed.

**PAGE  
NUMBERS  
CUT OFF  
IN  
ORIGINAL**

## CHAPTER 5

### DISCUSSIONS

#### 5.1. Device designs affecting the spread of plasma

##### 5.1.1 The values of current gains of the n-p-n and the p-n-p transistor sections

The values of current gains of the two transistor sections in a thyristor are important in governing the speed of turning on as well as the plasma spreading velocity of thyristors. As described in Chapter 2, plasma spreads in thyristors as a consequence of the turned-on region contributing enough carriers to the neighbouring 'off' region so that the sum of the current gain values of the n-p-n transistor section and the p-n-p transistor section equals to unity. From this one would expect thyristors having high current gain values when it is 'off', will have high plasma spreading velocity values when it is turned on. Devices are normally made with much higher current gain values in the n-p-n transistor section, notwithstanding the influence of the shorting dots which at low current levels depress the  $\alpha_{n-p-n}$  values, because of the much shorter minority carrier transit time in the p-base layer. This is desirable because gate triggering currents are normally applied to the p-base, so a high value of current gain of the n-p-n transistor section would mean that the device can be switched 'on' by a much smaller current, i.e. the device is more sensitive.

In order to obtain high current gain values of the n-p-n transistor section, the following points have to be noted,

a) p-base layer width and impurity doping

The width of the p-base layer should be made thin in order to reduce the minority carrier transit time thus leading to a good base transport factor. Also the p-base layer should not have too high an impurity doping level in order to have a good emitter efficiency.

b) gold doping

Devices are normally doped with gold to obtain a fast turn-off time by 'killing' the minority carrier lifetime. However, <sup>this</sup> ~~it~~ reduces the value of the current gains of the two transistor sections by shortening the diffusion length of carriers thus resulting in a lowered plasma spreading velocity. Also, it will give a higher forward voltage drop across the device because of the increased resistances of the p and n layers. The increased resistance would result in a higher emitter junction voltage, causing higher carrier injection across the junction, and thus enhance the spread of plasma.

### 5.1.2. Emitter shorts

Emitter shorts are incorporated in the cathode of the device primarily for better  $dv/dt$  capabilities as described in Chapter 1. It would also shorten the turn-off time of the device by shunting excess carriers

out of the p-base layer when the device is turning off. However, emitter shorts would impede the spread of plasma by shunting excess carriers out of the p-base layer while the device is turning on. A careful design of emitter shorting patterns should therefore be required to compromise between these effects. Also, as detailed in Chapter 6, careful design of emitter shorting patterns can lead to an increased initial turn-on area which is important for good  $di/dt$  capabilities.

## 5.2. Discussion of results

As described in the previous section, devices with high values of current gain in the n-p-n transistor section ( $\alpha_{npn}$ ) should lead to a higher plasma spreading velocity. However, from Table 2 and Table 7, no clear correlation can be obtained between these two parameters. Devices of batch R393S6, although having lower values of current gain in the n-p-n transistor section than those of devices from batch N5S4 and batch N6S7, have a value of spreading velocity higher than that of the other batches. This does not confirm the argument described in section 5.1.1. The fact that n-p-n transistor section current gain values ( $\alpha_{npn}$ ) of devices from batch R393S6 are so low, although they were not doped with gold, could be explained in two ways.

- 1) The p-n-p transistor section current gain values ( $\alpha_{pnp}$ ) of not-gold-doped devices are higher than those of devices doped with gold. As devices will switch on when the sum of their p-n-p and n-p-n transistor section current gain

value reaches unity, devices having a higher value of current gain in the p-n-p transistor section would, at the point of switching, have a lower value of the n-p-n transistor section current gain.

2) There might be some "frauds" in the processing of this batch of devices such as having been alloyed at a temperature which was too high. For alloy-diffused devices, if the alloying temperature is too high, gold from the gold/antimony foil will diffuse excessively into the p-base layer and act as recombination and trapping centres. This will result in a lowered value of current gain in the n-p-n transistor section. In the worst case, gold will diffuse appreciably across the p-base from the gold/antimony foil and short circuit the central p-n junction (  $V_{BO}$  junction ).

The fact that devices of batch R393S6 still have a relatively higher value of spreading velocity, for a much lower value of n-p-n transistor section current gain values, might be explained by the density of unwanted gold diffusion just described. Gold diffused from the gold/antimony foil should not have a density as high as in devices from batches N6S7 and N5S4 which were deliberately doped with gold. This might first appear to argue against the explanation just given for the low n-p-n transistor current gain values of devices from batch R393S6. However, as can be seen from Table 1, devices of batch N6S7 and N5S4 were alloyed with a much thicker gold/antimony foil to

give a much thinner p-base in order to maintain the n-p-n transistor section current gain values at a reasonably high level. Thus the above argument for a low n-p-n transistor section current gain value for devices of batch R393S6 can still be maintained. The much lower density of gold in the p-base of devices from batch R393S6 means that these recombination and trapping sites will be filled up quickly by excess carriers when the plasma is spreading across the device. Once these sites are saturated, the influence of them on the spread of plasma will be minimal and the plasma will spread much faster. The values of the plasma spreading velocity shown in Table 2 are the average velocities of spread between the measuring probes and, in keeping with the argument just mentioned, devices of batch R393S6 have a slightly higher value than those of batch N6S7 and N5S4. Also, assuming the argument is to be valid, the alloying temperature for alloying not-gold-doped devices is much more critical than that of gold doped devices. This may explain why no clear correlation can be found between the n-p-n transistor section current gain values and the values of plasma spreading velocity.

The low spreading velocity values observed were due to

a) The low 'on' current density of typically  $75 \text{ A/cm}^2$  when the device was completely 'on' during measurements. This low current density in the 'on' region will result

in a low excess carrier concentration gradient from the 'on' to the 'off' region in the base layers. This will thus lead to the low spreading velocity values observed. At the lower current densities in the 'on' region, plasma sticking will occur because the lateral current that flows into the 'off' region will not be high enough to cause switching. This is referred to as the 'static spread'.

b) The emitter shorts that were incorporated into the test devices. As emitter shorts will short out any lateral current in the base  $\bar{a}$  layer that arrives in their vicinity, they will hinder the spread of plasma and thus lead to a low value of spreading velocity.

Although the current density inside the device during plasma spreading is an important factor affecting the spreading velocity, small signal current gain measurements were not performed at the current densities observed during spreading because of the difficulties in simulating this dynamic process. Perhaps this is another reason for not being able to correlate the current gain measurements to the spreading velocities observed.

## CHAPTER 6

### THEORETICAL DEVELOPMENTS

#### 6.1. Introduction

Present theories concerning the evaluation of the spreading velocity of the turned-on region in thyristors, either the diffusion model or the lateral bias model, have paid little attention to the area of the initially turned-on region. The diffusion model describes the plasma spread by lateral diffusion of excess carriers down their concentration gradients in the base layers while the lateral bias model relates the spreading velocity to the load current density that is to flow through the device while the plasma spreading takes place. As the excess carrier concentration, the current density inside the device and the carrier concentration gradient are all functions of both the load current that will flow through the device and the area of the initially turned-on region, a knowledge of the initial turned-on area of the device seems imperative in the calculations of the spreading velocity of the 'on' plasma and the evaluation of power dissipation in the initial stage of the 'on' cycle.

#### 6.2. Assumptions made in evaluating the initial turned-on area

In the evaluation of initial turned-on area

in thyristors shown in section 6.3, the following assumptions were made;

- 1) Effective base resistance looking in from the gate contact is only the lateral resistance of the p-base material between the gate contact and the first ring of emitter shorting dots. Thus negligible gate current is assumed to flow past the first ring of emitter shorts.
- 2) p-base thickness is much smaller than the lateral length of the cathode p-n junction. Thus the base resistance looking in from the gate contact is high and will cause varying injection along the cathode p-n junction.
- 3) The thickness of the p-base layer is very much smaller than the diffusion length of minority carriers.
- 4) The depletion layer spread at the  $V_{BO}$  junction (central p-n junction) occurs primarily in the n-base side of the junction because of the difference in doping of the two regions.
- 5) No recombination of carriers that constitute the gate current occurs in the p-base layer; i.e. the gate current remains constant.

Assumptions (1) to (4) can readily be seen to be reasonable assumptions. Validity of assumption (5) can be proved as follows;

Figure 17 shows a two dimensional representation of the device. The variation of gate current with  $y$  can be obtained by considering the line equations of

its flow in the  $p_2$  layer.

We assume  $I_g$  to be the gate current flowing into the device,

$\alpha_2$  to be the common base current gain of the  $n_2-p_2-n_1$  transistor section of the device,

$J_K$  to be the cathode current density,

$L$  to be the width of the device in the  $z$  direction as illustrated in figure 17,

and also that  $\alpha_2$  is independent of  $y$ .

Thus,

$$\frac{\partial I_g}{\partial y} = - (1 - \alpha_2) J_K L \quad (10)$$

Equation (10) is a general equation which covers finite values of  $J_K$  and  $\alpha$ . If we consider the limiting case for which  $\frac{\partial I_g}{\partial y} \rightarrow 0$  when  $J_K$  will also tend to zero. If we consider  $J_K=0$  so that there is no injection and the only minority carriers are generated thermally leading to a recombination current, then  $\alpha$  must equal zero in the absence of cathode current and equation (10) remains valid.

Differentiating equation (10) with respect to  $y$ ,

$$\frac{\partial^2 I_g}{\partial y^2} = - (1 - \alpha_2) L \frac{\partial J_K}{\partial y} \quad (11)$$

As, assuming current flow is due to diffusion only,

$$J_K = q D_n \frac{n_{p_2}}{w_{p_2}} = q D_n \frac{n_{p_2 0}}{w_{p_2}} \left[ \exp \frac{q V_{p_2 n_2 y}}{k T} - 1 \right]$$

where  $D_n$  is the diffusion constant of electrons  
 $n_{p_2}$  is the excess minority carrier concentration  
in the  $p_2$  layer  
 $w_{p_2}$  is the width of the  $p_2$  layer  
 $V_{p_2n_2y}$  is the voltage across the cathode p-n  
junction and is a function of  $y$   
 $q$  is the electronic charge  
 $k$  is the Boltzmann constant  
 $T$  is the absolute temperature

therefore,

$$\frac{\partial J_K}{\partial y} = \frac{q}{kT} J_K \frac{\partial V_{p_2n_2y}}{\partial y}$$

Also, putting

$$\partial V_{p_2n_2y} = -I_g \frac{\rho_{p_2}}{w_{p_2} L} \partial y$$

equation (11) becomes (44)

$$\frac{\partial^2 I_g}{\partial y^2} + \frac{q \rho}{kTL w_{p_2}} I_g \frac{\partial I_g}{\partial y} = 0 \quad (12)$$

The boundary conditions to equation (12) are,

$$\text{at } y = 0, \quad I_g = I_g(0) = \lambda$$

where  $\lambda$  is the input gate current

at  $y = y_s$ ,

$$\frac{\partial I_g}{\partial y} = 0$$

because  $J_K = 0$  for  $y > y_s$

Let  $\frac{q \rho}{kTL w_{p_2}}$  be  $A$  and integrating equation (12) gives,

$$\frac{\partial I_g}{\partial y} + \frac{A}{2} I_g^2 = K \quad (13)$$

where  $K$  is the constant of integration.

Separating variables and integrating,

i.e. 
$$\int_{\lambda}^{I_g} \frac{dI_g}{K - \frac{1}{2} A I_g^2} = \int_0^y dy$$

$$\frac{1}{2\sqrt{K}} \int_{\lambda}^{I_g} \left( \frac{1}{\sqrt{K} + \sqrt{\frac{A}{2}} \cdot I_g} + \frac{1}{\sqrt{K} - \sqrt{\frac{A}{2}} \cdot I_g} \right) dI_g = y$$

$$\frac{1}{\sqrt{2AK}} \left[ \log \frac{\sqrt{K} + \sqrt{\frac{A}{2}} I_g}{\sqrt{K} - \sqrt{\frac{A}{2}} I_g} \right]_{\lambda}^{I_g} = y$$

$$\therefore \frac{1}{\sqrt{2AK}} \left\{ \log \frac{\frac{\sqrt{K} + \sqrt{\frac{A}{2}} I_g}{\sqrt{K} - \sqrt{\frac{A}{2}} I_g}}{\frac{\sqrt{K} + \sqrt{\frac{A}{2}} \lambda}{\sqrt{K} - \sqrt{\frac{A}{2}} \lambda}} \right\} = y$$

$$\frac{\sqrt{K} + \sqrt{\frac{A}{2}} I_g}{\sqrt{K} - \sqrt{\frac{A}{2}} I_g} = \frac{\sqrt{K} + \sqrt{\frac{A}{2}} \lambda}{\sqrt{K} - \sqrt{\frac{A}{2}} \lambda} e^{\sqrt{2AK} \cdot y}$$

Let

$$B = \frac{\sqrt{K} + \sqrt{\frac{A}{2}} \lambda}{\sqrt{K} - \sqrt{\frac{A}{2}} \lambda}$$

Since  $\sqrt{\frac{2K}{A}}$  is expected to be only a little larger than  $\lambda$  then clearly  $B \gg 1$ .

$$\therefore \sqrt{K} + \sqrt{\frac{A}{2}} \cdot I_g = (\sqrt{K} - \sqrt{\frac{A}{2}} \cdot I_g) B \exp(\sqrt{2AK} \cdot y)$$

or

$$I_g = \sqrt{\frac{2K}{A}} \left( \frac{B e^{\sqrt{2AK} \cdot y} - 1}{B e^{\sqrt{2AK} \cdot y} + 1} \right) \quad (14)$$

Equation (13) can be proved to be valid by substituting the boundary conditions, thus

$$\begin{aligned} \text{at } y = 0, \quad I_{g_0} &= \lambda = \sqrt{\frac{2K}{A}} \left( \frac{B-1}{B+1} \right) \\ \text{at } y = y_s, \quad I_{g_{y_s}} &= \sqrt{\frac{2K}{A}} \cdot \left( \frac{B e^{\frac{2AK}{A} \cdot y_s} - 1}{B e^{\frac{2AK}{A} \cdot y_s} + 1} \right) \\ \text{if} \quad B e^{\sqrt{2AK} \cdot y_s} &\gg 1, \\ I_g(y_s) &\approx \sqrt{\frac{2K}{A}} \end{aligned}$$

Also, from equation (13), substituting the boundary conditions,

$$\text{at } y = y_s, \quad \frac{\partial I_g}{\partial y} = 0$$

$$\therefore \frac{A}{2} I_{g_{y_s}}^2 = K$$

$$\text{or} \quad I_{g_{y_s}} = \sqrt{\frac{2K}{A}} \quad \text{-----} \quad (15)$$

at  $y = 0$ , equation (13) becomes

$$\frac{\partial I_{g_0}}{\partial y} = K - \frac{1}{2} A \lambda^2 \leq 0$$

case 1) for  $\frac{\partial I_{g_0}}{\partial y} = 0$  which means negligible recombination,

$$K = \frac{1}{2} A \lambda^2$$

or

$$\lambda = \sqrt{\frac{2K}{A}}$$

recalling that  $\lambda$  is the input gate current  $I_{g_0}$ , and comparing it with equation (15), it gives

$$I_{g_0} = I_{g_{y_s}}$$

Hence, current supplied to the gate contact flows out completely through the first emitter shorting dot without being reduced by recombination along its path.

case 2) for  $\frac{\partial I_{g_0}}{\partial y} < 0$

$$\text{i.e. } K - \frac{1}{2} A \lambda^2 < 0$$

$$\therefore \lambda > \sqrt{\frac{2K}{A}}$$

Again, comparing this with equation (15) means

$$I_{\epsilon_0} > I_{\epsilon_{y_s}}$$

In this case, as is clearly understood, recombination of gate current carriers is taken into account. Hence, gate current appearing at the first shorted emitter dot,  $y_s$  has a value smaller than that of the input gate current.

In order to show that whether the gate current can be approximated to a constant, independent of  $y$ , i.e., negligible recombination, equations (10) and (13) were used,

$$\text{i.e. } \left. \frac{\partial I_g}{\partial y} \right|_{y=0} = K - \frac{1}{2} A \lambda^2 = -(1 - \alpha_2) J_K(0) \cdot L$$

$$\text{as } \lambda = I_{g_0} \quad \text{and} \quad \sqrt{\frac{2K}{A}} = I_{g_{y_s}}$$

$$\therefore \frac{A}{2} (I_{g_{y_s}}^2 - I_{g_0}^2) = -(1 - \alpha_2) L J_K(0)$$

or

$$\frac{A}{2} (I_{g_{y_s}}^2 - I_{g_0}^2) = (1 - \alpha_2) L q D_n \frac{n_{p_2_0}}{w_{p_2}} \exp \frac{q V_g}{k T}$$

$$I_{g_0}^2 - I_{g_{y_s}}^2 = \frac{2k T L^2}{e} D_n (1 - \alpha_2) n_{p_2_0} \exp \frac{q V_g}{k T} \quad \text{--- (15a)}$$

As a means of testing the general validity of equation (15a), reasonable numerical values for device N5S4 were substituted.  $D_n$  was taken to be  $30 \text{ cm}^2 \text{ sec}^{-1}$ , the resistivity  $\rho$  of the base layer was set as 1 ohm-cm, and  $\alpha_2$  was the value estimated just before switching and was taken as 0.776. It was found for devices having  $I_{\epsilon_0} = 40 \text{ mA}$ , that  $I_{\epsilon_{y_s}}$  had dropped to 99.7% of

the value of  $I_{g_0}$  for  $V_g = 0.6$  V, and to 96.4% of  $I_{g_0}$  for  $V_g = 1$  V. This justifies the assumption previously made that  $I_{g_y}$  may be approximated as a constant from the gate contact to the first emitter shorting dot. For values of  $V_g$  less than 0.6 V the approximation is very close indeed.

### 6.3. Evaluation of the initial turned-on area

The initial turned-on area can be estimated by first examining the profile of the voltage across the cathode p-n junction of the device. We shall consider initially a commonly used thyristor. This normally incorporates a particular pattern of emitter shorts. Direct gate current will flow from the gate electrode to the cathode metallization via the emitter shorting dots. These will impose a varying bias across the cathode p-n junction in a manner similar to the emitter fringing effect in transistors. With reference to figure 17, voltage drop across the cathode p-n junction is given by

$$V_J(y) = V_{J_0} - \int_0^{y_s} I_g(y) \frac{\rho_{p_2}}{A_{p_2}} dy \quad (16)$$

where  $V_{J_0}$  is the voltage across the cathode p-n junction at  $y = 0$

$\rho_{p_2}$  is the resistivity of the  $p_2$  region

$A_{p_2}$  is the cross-sectional area of the  $p_2$  layer, looking in from the gate contact.

Using assumption (5) as stated in section 6.2, i.e.  $I_g$  constant, equation (16) can be written as

$$V_J(y) = V_{Jc} - I_g \frac{\rho_{p_2}}{A_{p_2}} y \quad (17)$$

As it was assumed that all input gate bias drops between the input and the first emitter shorting dots situated at  $y = y_s$ , the voltage across the junction at  $y_s$  is thus equal to zero. Substituting this condition into equation (17) yields

$$I_g = \frac{V_{Jc} A_{p_2}}{\rho_{p_2} y_s}$$

Equation (17) would first appear to give a linear variation of bias across the cathode junction up to the first ring of emitter shorts. However, at higher voltages across the junction, say above 0.7 volt, a comparatively high injection level occurs across the emitter junction, with consequent conductivity modulation of the  $p_2$  layer. Schematic plots of equation (17) are shown in figure 18.

The slope of  $V_J$  versus  $y$  plot, i.e.

$$\frac{dV_J}{dy} = - I_g \frac{\rho_{p_2}}{A_{p_2}}$$

is proportional to  $\rho_{p_2}$ . As  $\rho_{p_2}$  is a function of  $V_J$ , at higher  $V_J$  values because of the conductivity modulation of the  $p_2$  layer, the schematic plots show a non-linear variation for higher  $V_J$  values. To a first approximation, a linear variation of  $V_J$  with  $y$  was assumed for all bias voltages across the junction. As will be shown later, the calculations used in obtaining the initial turned-on area is, in part, based on the voltage across the cathode p-n junction,

this approximation would lead to a slightly smaller predicted initial turned-on area.

The varying bias across the cathode p-n junction as given in equation (17) will induce non-uniform carrier injection along the junction. The current density flowing through the p-n junction is related to the bias voltage by the equation

$$J_k = J_0 \left( \exp \frac{q V_j}{n k T} - 1 \right) \quad (18)$$

where  $J_0$  is the saturation current density

and  $n$  is a number having a value of either 1 or 2.

If the switching "on" condition of the device can be described by the cathode current density, which is a function of  $y$ , the initial turned-on area can be calculated. This can be done by comparing the cathode current density with the device breakover current density in two terminal operation and which is the minimum value of cathode current density for the device to switch on. In two-terminal operation, as the cathode current is equal to the anode current, the cathode breakover current density is equal to the breakover current divided by the area of the device. Thus,

$$J_{k_B} = \frac{I_{B_0}}{A_K} \quad (19)$$

where  $J_{k_B}$  is the cathode breakover current density

$I_{B_0}$  is the breakover current

$A_K$  is the area of the cathode

in practice, not the whole of the device turns on uniformly,

$$\therefore J_{k_B} = \frac{I_{B_0}}{A}, \quad \text{where } A < A_K$$

It will be assumed that only that part of the cathode junction area for which  $J_K(y) \geq J_{K_B}$  will switch on and this in fact will be defined as the initial turned-on area. Because of the very much higher cut-off frequency of the n-p-n transistor section compared to the p-n-p transistor, it will further be assumed that any part of the  $J_K(y)$  profile including that exceeding  $J_{K_B}$  has time to establish itself before the device switches on. Figure 19 shows schematic plots of  $J_K$  versus  $y$ . Intersection of the plot with the breakover current density value ( $J_{K_B}$ ) defines the boundary of the 'on' area.

Comparing equations (18) and (19), the boundary of the initial 'on' area is at  $J_K = J_{K_B}$ , hence

$$J_0 \left( \exp \frac{q V_{Jc}}{nkT} - 1 \right) = \frac{I_{B0}}{A_K}$$

$$\therefore V_{Jc} = \frac{nkT}{q} \ln \left( \frac{J_{K_B}}{J_0} + 1 \right) \quad (20)$$

Equation (20) gives the critical cathode junction voltage where the cathode current density is just high enough to switch the device on. Combining equations (17) and (20), the boundary of the initial 'on' area appears at

$$y_{on} = \frac{A_{P2}}{I_g \rho_{P2}} \left\{ V_{J_0} - \frac{nkT}{q} \ln \left( \frac{J_{K_B}}{J_0} + 1 \right) \right\} \quad (21)$$

Thus, the device will turn on initially from  $y = 0$ , i.e. gate contact, to  $y = y_{on}$ .

The initial turned-on area for circular devices with circular emitter short patterns is  $\pi (y_{on}^2 - r_2^2)$ , where  $r_2$  is the radius of the outer edge of the gate isolation ring, see fig. 17a, and  $y_{on}$  is the radius of the edge of the initial turned-on region. For the specially prepared rectangular devices used in this work, the initial turned-on area is, to a first approximation,  $y_{on} L$ , where  $L$  is the width of the device.

From equations (17) and (21), expressing  $y_{on}$  in terms of  $y_s$ ,

$$\frac{y_{on}}{y_s} = 1 - \frac{n k T}{q V_{J_0}} \ln \left( \frac{J_{KB}}{J_0} + 1 \right)$$

or

$$y_{on} = \left[ 1 - \frac{n k T}{q V_{J_0}} \ln \left( \frac{J_{KB}}{J_0} + 1 \right) \right] \cdot y_s \quad (22a)$$

alternatively, from equation (21)

$$y_{on} = y_s - \frac{A_{P_2}}{I_g P_2} \cdot \frac{n k T}{q} \ln \left( \frac{J_{KB}}{J_0} + 1 \right) \quad (22b)$$

$I_g$  is assumed to be of sufficiently high value for  $y_{on}$  to be finite and positive.

As can be seen from both equations (22a) and (22b), the only external influences on the initial turned-on area are the input gate biases. For higher gate bias voltages, the initial turned-on area will be larger. Thus, as is well known, overdriving the gate improves the di/dt capability of devices. Also, from equations (22a) and (22b), the turned-on area will be determined

by the parameters of the individual device such as breakover current, the cathode area and shape of the device, the saturation current density, the emitter short geometry, the resistivity and geometry of the p-base layer.

#### 6.4. Comparison of diffusion models of plasma spread as proposed by Bergman and by Longini and Melngailis.

The previous sections described the calculation of the initial turned-on area when switching on the thyristor, which is an important factor governing the total time required for the 'on' plasma to spread across the device. Another factor which is equally, if not more, important is the velocity of plasma spread. Chapter 2 outlined the two categories of theories on the plasma spreading velocity, viz. the diffusion model and the lateral bias model, each of which has its own merits. A complete theory that can accurately describe the mechanism of plasma spread, which includes both the effects of carrier diffusion and lateral bias, is not known. However, it appears to the author that the consideration of carrier diffusion throughout the spreading process is essential while the influence of the lateral bias is important only in the initial period of plasma spread when the lateral field is high and the carriers are not yet in the ambipolar state. A theoretical investigation will not be attempted here; however it would be interesting to show that the diffusion model proposed by Longini

and Melngailis can be merged into that proposed by Bergman.

As described in Chapter 2, Longini and Melngailis expressed the spreading velocity, based on the diffusion of carriers down their concentration gradient, as given in equation (1), i.e.

$$v_s = \frac{F}{N_0} - \frac{N_0}{F} \left( \frac{D}{\tau} + \frac{\pi^2 D^2}{a} \right)$$

and Bergman expressed the spreading velocity in terms of load current rise-time as given in equation (2), i.e.

$$v_s = 1.48 \sqrt{\frac{D}{t_r}}$$

These two equations can, however, be proved to be identical. Consider a thyristor which has just been turned on, with the plasma not yet having spread appreciably. We shall further assume an exponential decay of excess carriers from the 'on' to the 'off' region as shown in figure 20 with the carrier concentration in the 'on' region taken to be uniform. Thus, the carrier concentration anywhere in the 'on' region is  $N_0$ , where  $N_0$  has the significance defined by Longini and Melngailis. Also, from the 'on' to the 'off'

region, excess carrier concentration is described by the equation,

$$n_p = N_0 \exp - \frac{y}{L}$$

Lateral diffusion current density flowing from the 'on' to the 'off' region is therefore given by,

$$J = q D^* \frac{\partial n_p}{\partial y} = - \frac{q D^*}{L} n_p$$

where  $D^*$  is the ambipolar diffusion constant and is

$$\text{equal to } \frac{2D_n D_p}{D_n + D_p}$$

and  $L$  is the diffusion length.

As the boundary between the 'on' and the 'off' region is defined at  $y = 0$ , i.e.  $n_p = N_0$ , lateral diffusion current density flowing from the 'on' to the 'off' region should thus be written as,

$$J = - \frac{q D^*}{L} N_0$$

Taking absolute values, flux of carriers flowing from the 'on' to the 'off' region is thus

$$\frac{J}{q} = \frac{D^*}{L} N_0$$

This is in fact referred to in the Longini and Melngailis paper as  $\frac{2F}{\pi}$ . Therefore, on the assumption that the co-ordinate system used by them may be seen to provide a linear approximation,

$$\frac{2F}{\pi} = \frac{D^*}{L} N_0$$

or

$$F = \frac{D^*}{L} N_0 \frac{\pi}{2}$$

alternatively,

$$\frac{F}{N_0} = \frac{\pi D^*}{2L}$$

The ratio  $\frac{F}{N_0}$  can readily be evaluated to be of the order of  $10^3$  cm/sec. Comparing the first term and the second term of equation (1), the first term is, as described, of the order of  $10^3$  cm/sec whereas the second term is of the order of  $10^2$  cm/sec. Therefore the spreading velocity given by equation (1) is mainly described by the first term. Thus approximating,

$$\begin{aligned} v_s &\approx \frac{F}{N_0} \\ &= \frac{\pi D^*}{2L} \end{aligned} \quad \text{-----} \quad (23)$$

Bergman defined  $v_s t_r$  as the fall from 90% to 10% of the excess carrier concentration from the 'on' region to the 'off' region.

At 90% of the excess carrier concentration gradient,

$$n_p = 0.9 N_0 = N_0 \exp -\frac{y}{L}$$

$$\therefore y = -L \ln 0.9$$

At 10% of the excess carrier concentration gradient,

$$n_p = 0.1 N_0 = N_0 \exp -\frac{y}{L}$$

$$\therefore y = -L \ln 0.1$$

$$\therefore v_s t_r = -L (\ln 0.1 - \ln 0.9)$$

$$= 2.2L \quad \text{-----} \quad (24)$$

Putting equation (24) into equation (23),

$$v_s = \frac{\pi}{2} \cdot \frac{D^*}{v_s t_r} \quad (2.2)$$

$$v_s^2 = \frac{2.2\pi}{2} \cdot \sqrt{\frac{D^*}{t_r}}$$

$$\therefore v_s = 1.86 \sqrt{\frac{D^*}{t_r}}$$

Comparing this with Bergman's expression, i.e.

$$v_s = 1.48 \sqrt{\frac{D^*}{t_r}},$$

the difference between the two expressions is in the numerical coefficient. As we have ignored the second term in Longini and Melngailis equation in the above derivation, a slightly higher value of spreading velocity is expected for the model proposed by Longini and Melngailis. Inclusion of a correction factor of value  $\frac{1.48}{1.86}$  or 0.796 in the approximated equation of the Longini and Melngailis model, i.e.

$$v_s = (0.796) \left(\frac{\pi}{2}\right) \left(\frac{D^*}{L}\right)$$

simplifies their model to that of Bergman's. Also,

from the derivation of the model of Longini and Melngailis to that of Bergman just shown, it can be concluded that the key point in the diffusive model is to obtain the tail of the exponential decay. If one can obtain an estimate of  $L$ , one could dispense with the rise-time of the load current pulse which might be difficult to measure.

## REFERENCES

- 1) P.S. Raderecht  
M. Tech. Dissertation, Brunel University.
- 2) J. L. Moll, M. Tanenbaum, J. M. Goldey and N. Holonyak  
"P-N-P-N Transistor Switches", Proc.I.R.E. 1956,  
pp. 1174 - 1182.
- 3) I. M. Mackintosh  
"Three terminal P-N-P-N Transistor Switches"  
I.E.E.E. Trans. on Electron Devices, Jan. 1958, pp.10-12.
- 4) I. M. Mackintosh  
"The Electrical Characteristics of Silicon P-N-P-N  
Triodes"  
Proc. I.R.E. June 1958, pp. 1229 - 1235.
- 5) A. K. Jonscher  
"Notes on the theory of four-layer semiconductor  
switches"  
Solid State Electronics Vol.2, 1961, pp. 143 - 148.
- 6) A. K. Jonscher  
"P-N-P-N Switching Diodes"  
J. Electronics and Control, 1957, vol.14, pp. 481 - 498.
- 7) T. Misawa  
"Turn-on Transient of P-N-P-N Triode"  
J. Electronics and Control, Dec. 1959, vol.7, pp.523-533.
- 8) V. A. Kuzmin  
"Theory of voltage-current characteristics of  
p-n-p-n semiconductor devices"  
Radio and Elect. Phys. 1963, vol.8, pp.309 - 310.

- 9) V. A. Kuzmin  
"Volt-ampere characteristics of p-n-p-n type  
semiconductor devices in the 'on' condition"  
Radio Engineering and Electronic Physics, Jan. 1963,  
vol.8, no. 1, pp. 150 - 156.
- 10) I. Somos  
"Switching characteristics of silicon power-controlled  
rectifiers, I - Turn-on action"  
Communications and Electronics, July 1961, pp.320-326.
- 11) I. Somos  
"Switching characteristics of silicon power-controlled  
rectifiers, II - Turn-off action and dv/dt self-  
switching"  
I.E.E.E. Conference Paper no. CP 63 - 1010, April 1963.
- 12) D. R. Muss and C. Goldberg  
"Switching Mechanism in the p-n-p-n Silicon Controlled  
Rectifier"  
I.E.E.E. Trans. on Electron. Devices, May 1963,  
pp. 113 - 120.
- 13) Gentry, Gutzwiller, Holonyak and Von Zastrow.  
"Semiconductor Controlled Rectifiers. Principles  
and Applications of p-n-p-n Devices"  
1965, Prentice - Hall Inc., Englewood Cliffs, N.J.
- 14) R. W. Aldrich and N. Holonyak Jr.  
"Multi-terminal p-n-p-n switches"  
Proc. I.R.E., vol.46, 1958, p.1236
- 15) A. Herlet  
"The maximum Blocking Capability of Silicon Thyristors"  
Solid State Electronics 1965, vol.8, pp.655 - 671.

- 16) B. V. Cordingley  
"Improving the turn-on performance of high power thyristors"  
J. of Science and Technology, vol.38, no.1, pp.2-7, 1971.
- 17) P. G. Dermenzhi and Yu. A. Yevseyev  
"The problem of turning on large area p-n-p-n structures with the control current"  
Radio Engineering and Electronic Physics, 1970, vol.15, no.7, pp. 1266 -1268.
- 18) W. H. Dodson and R. L. Longini  
"Skip turn-on of thyristors"  
I.E.E.E. Trans. on Electron. Devices, Vol. ED-13, no.7, July 1966, pp. 598 - 604.
- 19) D. I. Gray  
"This SCR is not for burning"  
Electronics, Sept. 1968, pp.96 - 100.
- 20) N. Mapham  
"Overcoming turn-on effects in silicon controlled rectifiers"  
Electronics vol. 35, pp. 50-51, Aug.17 1962.
- 21) K. Oakman and J. Smallbone  
"Regenerative gate thyristors"  
Electronic Components, 19 March 1971, pp.241-242.
- 22) S. Ikeda and T. Araki  
"The di/dt capability of thyristors"  
Proc. I.E.E.E., vol.55, no.8, August 1967, pp.1301-1305.
- 23) D. E. Piccone and I.Somos  
"Are you confused by high di/dt SCR ratings?"  
Electron. Eng., vol.28, Jan 1969.

- 24) K. Huber, M. Melehy and R.L. Biesele  
"Uniform turn-on in four-layer diodes"  
I.R.E. Trans., Nov. 1961, vol. ED-8, pp. 461-464.
- 25) P. S. Raderecht  
"A review of the shorted emitter principle as  
applied to p-n-p-n silicon controlled rectifiers"  
Int. J. Electronics, vol. 31, no. 6, pp. 541-564,  
1971.
- 26) B. V. Cordingly  
"An acoustic technique for studying thyristors  
turn-on action and di/dt capability"  
Proc. I.E.E.E. Jan. 1970, pp. 139-140.
- 27) H. J. Ruhl, Jr.  
"Spreading velocity of the active area boundary  
in a thyristor"  
I.E.E.E. Trans. on Electron Devices ED-17, no. 9,  
Sept. 1970, pp. 672-680.
- 28) W. Fulop  
"Three terminal measurements of current amplification  
factors of controlled rectifiers"  
I.E.E.E. Trans. on Electron Devices, vol. ED-10,  
May 1963, pp. 120-133.
- 29) W. H. Dodson and R. L. Longini  
"Probed determination of turn-on spread of large  
area thyristors"  
I.E.E.E. Trans. on Electron Devices, vol. ED-13,  
no. 5, May 1966, pp. 478-484.

- 30) W. Gerlach  
Telefunken-Zeitung, Jg.39 (1966), no. 3/4, pp.301-314.
- 31) I. Somos and D.E. Piccone  
"Behaviour of thyristors under transient conditions"  
Proc. I.E.E.E., vol.55, no.8, August 1967, pp.1306-1311.
- 32) R. L. Longini and J. Melngailis  
"Gated turn-on of four-layer switch"  
I.E.E.E. Trans. on Electron Devices, May 1963,  
pp.178-185.
- 33) G. D. Bergman  
"The gate triggered turn-on process in thyristors"  
Solid State Electronics, 1965, vol.8, pp.757-765.
- 34) I. Somos and D.E. Piccone  
"Plasma spread in high power thyristors under  
dynamic and static conditions"  
I.E.E.E. Trans. on Electron Devices, ED17, no.19,  
pp.680-687, Sept.1970.
- 35) E. F. Burtsev, I.V. Grekhov, N. K. Kryukova and  
V. G. Sergeev  
"Investigation of the switching process in a p-n-p-n  
structure"  
Soviet Physics Semiconductors, vol.3, no.11, pp.1377-1382,  
1970.
- 36) I.V. Grekhov and V.G. Sergeev  
"Propagation of the turned-on state in a p-n-p-n  
structure"  
Soviet Physics Semiconductors, vol.4, no.7,  
pp.1191-1192, Jan. 1971.

37) Yoshio Terasawa

"Observation of turn-on action in a gate triggered thyristor using a new microwave technique"

I.E.E.E. Trans. on Electron Devices, vol. ED-20, no. 8, August 1970.

38) F. E. Gentry

"Recent advances in p-n-p-n devices"

I.E.E.E. Conference Paper no. CP 63-430.

39) R. J. Bassett, C. A. Hogarth and J. P. Newman

"An investigation into the mode of switching of inverse gate thyristors"

Int. J. Electronics, 1971, vol. 31, no.5, pp.453-465.

40) I. Somos and D. E. Piccone

"Some observations of static and dynamic plasma spread in conventional and new power thyristors"

Power Thyristors and Their Applications,

I.E.E. Conference Publication no.53, part 1, pp.1-7.

41) D. E. Crees and C. A. Hogarth

"Current gain in p-n-p-n silicon controlled rectifiers"

J. Electronics and Control, 1963, vol. 14, p.481.

42) P. S. Raderecht and C. A. Hogarth

"The temperature variation of the parameters of silicon controlled rectifiers"

Journal of Electronics and Control, August 1964, vol. 17, no. 2, p.145.

43) W. Fulop, W. Fong Yan, M.R. Joadat-Ghassabi and C.A. Hogarth

"Three-terminal current gain measurements of high power thyristors"

Int. J. of Electronics, 1972, vol.33, no.6, pp.601-609.

44) An equation of similar form has been derived by  
M. R. Joadat-Ghassabi, Ph.D. thesis, Brunel University,  
1975.

Silicon General Characteristics	Crystal No.	Diffusion No.	Gold Dope Condition	Gettering No.	Gallium Diffusion Depth (inch)	Surface Resistivity ( $\Omega$ - cm)	Main Cathode Au/S6 Thickness (inch)
0.018" thick, 1.45" diameter 90-140 cm, N type	Monsanto D1088	N6S7	838°C 35 min.	-	0.0023	0.45	0.0014
0.018" thick, 1.45" diameter 90-140 cm, N type	Monsanto D1074	N5S4	836°C 35 min.	-	0.00288	0.33	0.0019
0.018" thick, 1.45" diameter 80-120 cm, N type	Dow Corning F2130874	R393S6	-	D230	0.00275	0.43	0.00115
0.012" thick, 1.45" diameter 39-65 cm, N type	Monsanto D3516	N208S4	840°C 46 min.	-	0.00237	0.39	0.0015

TABLE 1: Four Batches of Silicon Used in Preparing Rectangular Thyristors

Devices with Diffusion Batch No.	Average Spreading Velocity Between Probes*	
	2 and 3	3 and 4
	(mm/ $\mu$ sec)	(mm/ $\mu$ sec)
R393 S6	0.0313	0.029
N5 S4	0.0234	-
N6 S7	0.0285	-
N208 S4	0.0478	0.023

\* see figure 3 for numbering of probes

TABLE 2: Summary of Plasma Spreading Velocity Results

Device No.	Silicon Thickness	Gold Doping	Cathode Diameter
1	0.018 in.	None	1.19 in.
2	0.007 in.	Heavy	0.35 in.

**TABLE 3:** Design Details of the Test Devices that Shows Positive Feedback of the  $V_{BO}$  Junction Capacitance

TABLE: 4a

Device K393S6 (6)

Probe No: 2

Voltage across the device = 7 volts

Frequency KHz	a.c. current gain = $i_a/i_k$			
	d.c. anode current			
	3 mA	5 mA	7 mA	10 mA
0.3	0.38	0.496	0.608	0.77
0.4	0.378	0.492	0.603	0.762
0.5	0.375	0.491	0.6	0.76
0.6	0.373	0.49	0.6	0.753
0.7	0.37	0.488	0.597	0.757
0.8	0.365	0.485	0.593	0.753
0.9	0.362	0.483	0.59	0.75
1	0.361	0.48	0.587	0.743
2	0.328	0.44	0.54	0.693
3	0.29	0.392	0.47	0.63
4	0.257	0.352	0.443	0.57
5	0.23	0.318	0.407	0.517
6	0.21	0.29	0.373	0.497
7	0.19	0.27	0.35	0.443
8	0.172	0.252	0.327	0.417
9	0.165	0.24	0.31	0.393
10	0.16	0.23	0.297	0.375
15	0.142	0.191	0.253	0.32
20	0.122	0.178	0.237	0.297
30	0.119	0.168	0.223	0.28
40	0.119	0.168	0.223	0.28
50	0.12	0.171	0.228	0.283
60	0.122	0.172	0.23	0.287
70	0.125	0.175	0.235	0.293
80	0.128	0.181	0.238	0.3
90	0.13	0.183	0.245	0.3
100	0.13	0.185	0.245	0.303
$\alpha_{npn0}$	0.119	0.168	0.223	0.28
$\alpha_{pnp}$	0.686	0.66	0.63	0.633

TABLE: 4b

Device R393S6 (6)

Probe No: 3

Voltage across the device = 7 volts

Frequency KHz	a.c. current gain = $i_a/i_k$			
	d.c. anode current			
	1 mA	2 mA	3 mA	4 mA
0.3	0.45	0.66	0.78	0.87
0.4	0.45	0.66	0.775	0.866
0.5	0.45	0.655	0.775	0.866
0.6	0.44	0.652	0.772	0.86
0.7	0.44	0.65	0.77	0.86
0.8	0.435	0.643	0.768	0.852
0.9	0.43	0.642	0.765	0.848
1	0.425	0.635	0.758	0.845
2	0.376	0.573	0.692	0.781
3	0.32	0.51	0.621	0.707
4	0.28	0.45	0.558	0.64
5	0.25	0.405	0.5	0.58
6	0.225	0.368	0.46	0.532
7	0.21	0.34	0.427	0.493
8	0.19	0.318	0.4	0.465
9	0.18	0.302	0.38	0.44
10	0.17	0.29	0.362	0.425
15	0.145	0.25	0.313	0.363
20	0.136	0.235	0.295	0.34
30	0.13	0.225	0.281	0.32
40	0.13	0.225	0.281	0.32
50	0.135	0.23	0.286	0.325
60	0.14	0.235	0.292	0.335
70	0.14	0.24	0.297	0.34
80	0.145	0.24	0.3	0.343
$\alpha_{npn_0}$	0.13	0.225	0.281	0.32
$\alpha_{pnp_0}$	0.711	0.66	0.637	0.63

TABLE: 4c

Device R393S6 (6)

Probe No: 4

Voltage across the device = 12 volts

Frequency KHz	a.c. current gain = $i_a/i_k$			
	d.c. anode current			
	5 mA	7 mA	10 mA	15 mA
0.3	0.523	0.613	0.687	0.817
0.4	0.523	0.612	0.683	0.813
0.5	0.52	0.608	0.682	0.813
0.6	0.517	0.607	0.68	0.81
0.7	0.517	0.607	0.675	0.81
0.8	0.507	0.6	0.667	0.807
0.9	0.507	0.598	0.672	0.8
1	0.5	0.597	0.667	0.8
2	0.46	0.557	0.633	0.763
3	0.417	0.508	0.592	0.717
4	0.39	0.47	0.55	0.68
5	0.357	0.43	0.51	0.637
6	0.327	0.4	0.477	0.603
7	0.3	0.375	0.45	0.57
8	0.282	0.357	0.433	0.54
9	0.268	0.34	0.413	0.52
10	0.257	0.325	0.394	0.498
15	0.222	0.272	0.343	0.43
20	0.209	0.258	0.32	0.407
30	0.196	0.242	0.303	0.38
40	0.197	0.242	0.303	0.38
50	0.2	0.246	0.303	0.383
60	0.204	0.25	0.31	0.39
70	0.21	0.255	0.317	0.397
80	0.21	0.255	0.32	
90	0.213	0.26	0.323	
100	0.218	0.262		
$\alpha_{npn}$	0.196	0.242	0.303	0.38
$\alpha_{pnp}$	0.625	0.605	0.559	0.537

TABLE: 5a

Device N5S4 (6)

Probe No: 2

Voltage across the device = 10 volts

Frequency KHz	a.c. current gain = $i_a/i_k$			
	d.c. anode current			
	5 mA	7 mA	10 mA	12 mA
1	0.616	0.707	0.8	0.88
2	0.616	0.707	0.8	0.88
3	0.616	0.707	0.8	0.88
4	0.616	0.707	0.8	0.88
5	0.616	0.703	0.8	0.88
6	0.615	0.703	0.8	0.88
7	0.613	0.7	0.8	0.87
8	0.61	0.697	0.796	0.865
9	0.605	0.686	0.791	0.86
10	0.6	0.682	0.786	0.853
15	0.58	0.657	0.76	0.82
20	0.56	0.64	0.735	0.795
30	0.528	0.61	0.696	0.746
40	0.508	0.586	0.668	0.715
50	0.5	0.577	0.65	0.7
60	0.5	0.577	0.65	0.7
70	0.5	0.577	0.65	0.7
80	0.5	0.577	0.65	0.7
90	0.5	0.577	0.65	0.7
$\alpha_{npn}$	0.5	0.577	0.65	0.7
$\alpha_{pnp}$	0.188	0.184	0.1875	0.205

TABLE: 5b

Device N5S4 (6)

Probe No: 3

Voltage across the device = 10 volts

Frequency KHz	a.c. current gain = $i_a/i_k$			
	d.c. anode current			
	5 mA	7 mA	10 mA	12 mA
1	0.559	0.644	0.74	0.81
2	0.559	0.644	0.74	0.81
3	0.559	0.644	0.74	0.81
4	0.559	0.644	0.74	0.81
5	0.556	0.644	0.735	0.805
6	0.553	0.635	0.728	0.8
7	0.55	0.633	0.722	0.792
8	0.545	0.63	0.717	0.785
9	0.543	0.625	0.71	0.78
10	0.54	0.62	0.706	0.77
15	0.525	0.6	0.683	0.74
20	0.506	0.585	0.662	0.71
30	0.476	0.557	0.635	0.675
40	0.46	0.536	0.615	0.65
50	0.45	0.523	0.6	0.64
60	0.45	0.523	0.6	0.64
70	0.45	0.523	0.6	0.64
80	0.45	0.523	0.6	0.64
90	0.45	0.523	0.6	0.64
$\alpha_{npn}$	0.45	0.523	0.6	0.64
$\alpha_{ppn}$	0.195	0.188	0.189	0.21

TABLE: 5c

Device N5S4 (6)

Probe No: 4

Voltage across the device = 10 volts

Frequency KHz	a.c. current gain = $i_a/i_k$			
	d.c. anode current			
	5 mA	7 mA	10 mA	12 mA
1	0.53	0.608	0.696	0.75
2	0.53	0.608	0.696	0.75
3	0.53	0.608	0.693	0.745
4	0.53	0.606	0.688	0.74
5	0.525	0.602	0.687	0.735
6	0.52	0.6	0.685	0.732
7	0.517	0.595	0.682	0.73
8	0.515	0.59	0.68	0.725
9	0.509	0.583	0.673	0.72
10	0.505	0.575	0.67	0.715
15	0.485	0.55	0.645	0.692
20	0.467	0.533	0.62	0.67
30	0.45	0.507	0.59	0.635
40	0.436	0.496	0.57	0.61
50	0.426	0.49	0.56	0.6
60	0.423	0.486	0.56	0.6
70	0.425	0.486	0.56	0.6
80	0.426	0.49	0.56	0.6
90	0.426	0.49	0.56	0.6
$\alpha_{npn}$	0.426	0.49	0.56	0.6
$\alpha_{pnp}$	0.196	0.194	0.195	0.2

TABLE: 6a

Device R393S6 (1)

Probe No: 3

Voltage across the device = 8 volts

Frequency KHz	a.c. current gain = $i_a/i_k$			
	d.c. anode current			
	1 mA	2 mA	3 mA	4 mA
0.3	0.462	0.703	0.846	0.95
0.4	0.458	0.692	0.843	0.933
0.5	0.449	0.688	0.832	0.93
0.6	0.44	0.676	0.822	0.92
0.7	0.432	0.667	0.815	0.917
0.8	0.422	0.657	0.796	0.903
0.9	0.415	0.64	0.785	0.887
1	0.402	0.625	0.772	0.877
2	0.299	0.48	0.62	0.73
3	0.229	0.376	0.495	0.587
4	0.183	0.309	0.412	0.493
5	0.157	0.265	0.355	0.43
6	0.139	0.239	0.32	0.387
7	0.125	0.219	0.291	0.358
8	0.115	0.2	0.272	0.33
9	0.11	0.189	0.258	0.317
10	0.103	0.18	0.248	0.303
15	0.09	0.155	0.216	0.267
20	0.085	0.147	0.203	0.253
30	0.082	0.142	0.198	0.243
40	0.082	0.142	0.199	0.243
50	0.087	0.148	0.205	0.25
60	0.09	0.151	0.209	0.257
70	0.091	0.157	0.211	0.26
80	0.091	0.16	0.218	0.263
90	0.091	0.16	0.219	0.267
100	0.091	0.161	0.22	0.27
$\alpha_{npn}$	0.082	0.142	0.198	0.243
$\alpha_{pnp}$	0.823	0.798	0.766	0.744

TABLE: 6b

Device R393S6 (1)

Probe No: 4

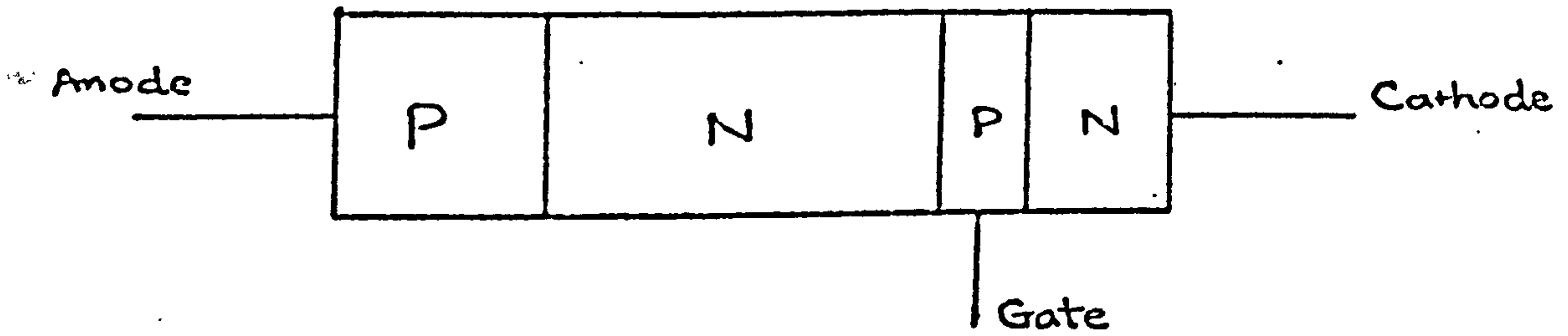
Voltage across the device = 12 volts

Frequency KHz	a.c. current gain = $i_a/i_k$			
	d.c. anode current			
	2 mA	4 mA	5 mA	6 mA
0.3	0.485	0.75	0.831	0.91
0.4	0.48	0.745	0.825	0.91
0.5	0.471	0.735	0.819	0.91
0.6	0.465	0.73	0.806	0.907
0.7	0.455	0.717	0.792	0.89
0.8	0.445	0.705	0.786	0.883
0.9	0.433	0.69	0.775	0.87
1	0.423	0.678	0.758	0.857
2	0.31	0.538	0.61	0.7
3	0.236	0.43	0.49	0.577
4	0.19	0.36	0.411	0.49
5	0.161	0.31	0.368	0.43
6	0.14	0.279	0.318	0.39
7	0.128	0.254	0.291	0.358
8	0.115	0.239	0.27	0.337
9	0.108	0.223	0.254	0.313
10	0.1	0.214	0.241	0.3
15	0.088	0.181	0.202	0.253
20	0.081	0.17	0.19	0.24
30	0.079	0.161	0.18	0.23
40	0.079	0.161	0.18	0.23
50	0.08	0.163	0.185	0.23
60	0.081	0.168	0.19	0.238
70	0.082	0.174	0.195	0.243
80	0.085	0.178	0.198	0.247
90	0.088	0.18	0.2	0.25
100	0.089	0.181	0.201	0.253
$\alpha_{npn}$	0.079	0.161	0.18	0.23
$\alpha_{pnp}$	0.837	0.785	0.784	0.747

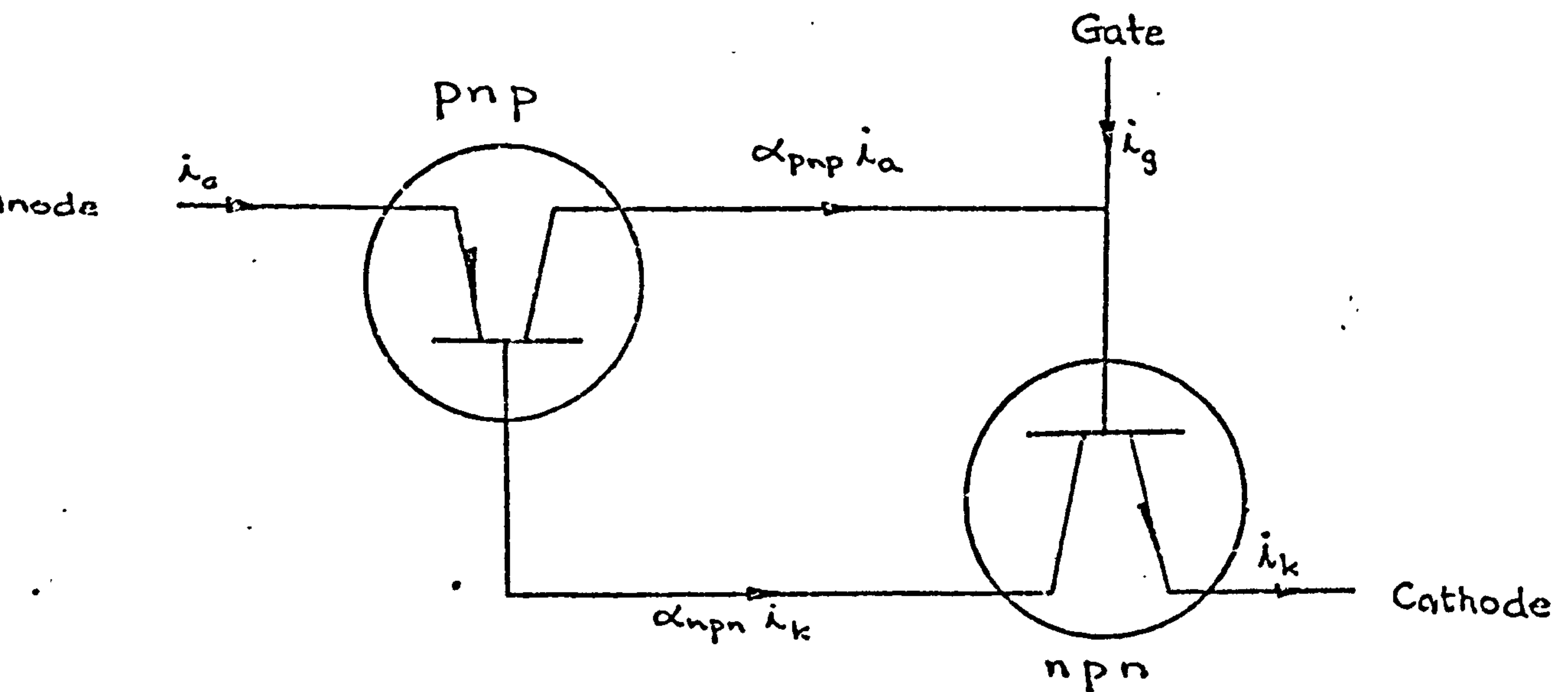
Devices with Diffusion Batch No.	Average $\alpha_{npn}$ Value Between Dots	
	2 and 3	3 and 4
R393 S6	0.345	0.319
N5 S4	0.755	0.76
N6 S7	0.778	0.77

TABLE 7: Average  $\alpha_{npn}$  Values Obtained at the Point of Switching

**TEXT BOUND  
INTO  
THE SPINE**



a) Schematic diagram of a thyristor



b) Two-transistor analogue of a thyristor

FIG. 1

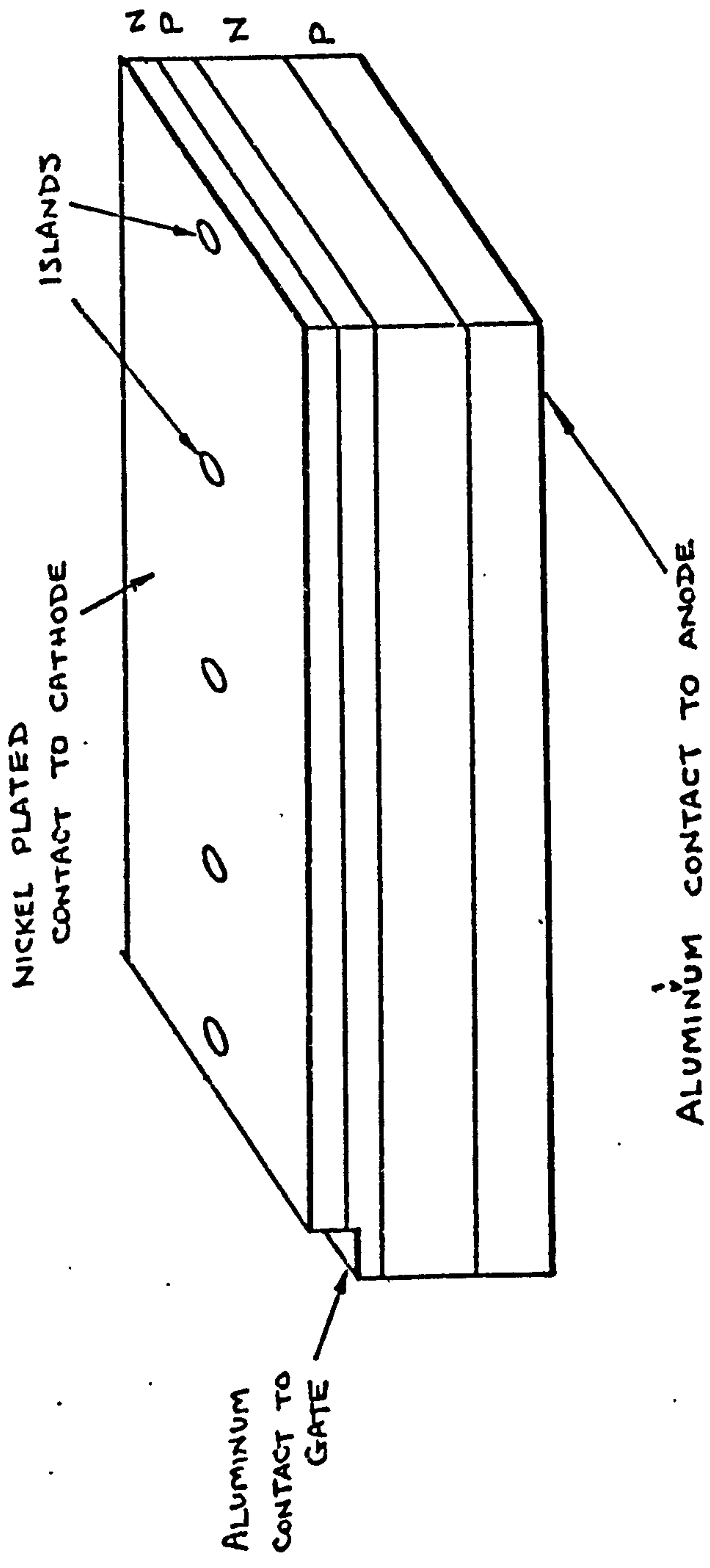


FIG. 2 Rectangular devices used by Dodson and Longini  
 (from Dodson and Longini (29))

GOLD/BORON DOTS FOR SPREADING VELOCITY  
AND CURRENT GAIN MEASUREMENTS

(2.25 mm dia., 6mm BETWEEN CENTRES)

EMITTER SHORTS

(1mm DIA. & 2mm DIA.  
3mm BETWEEN CENTRES)

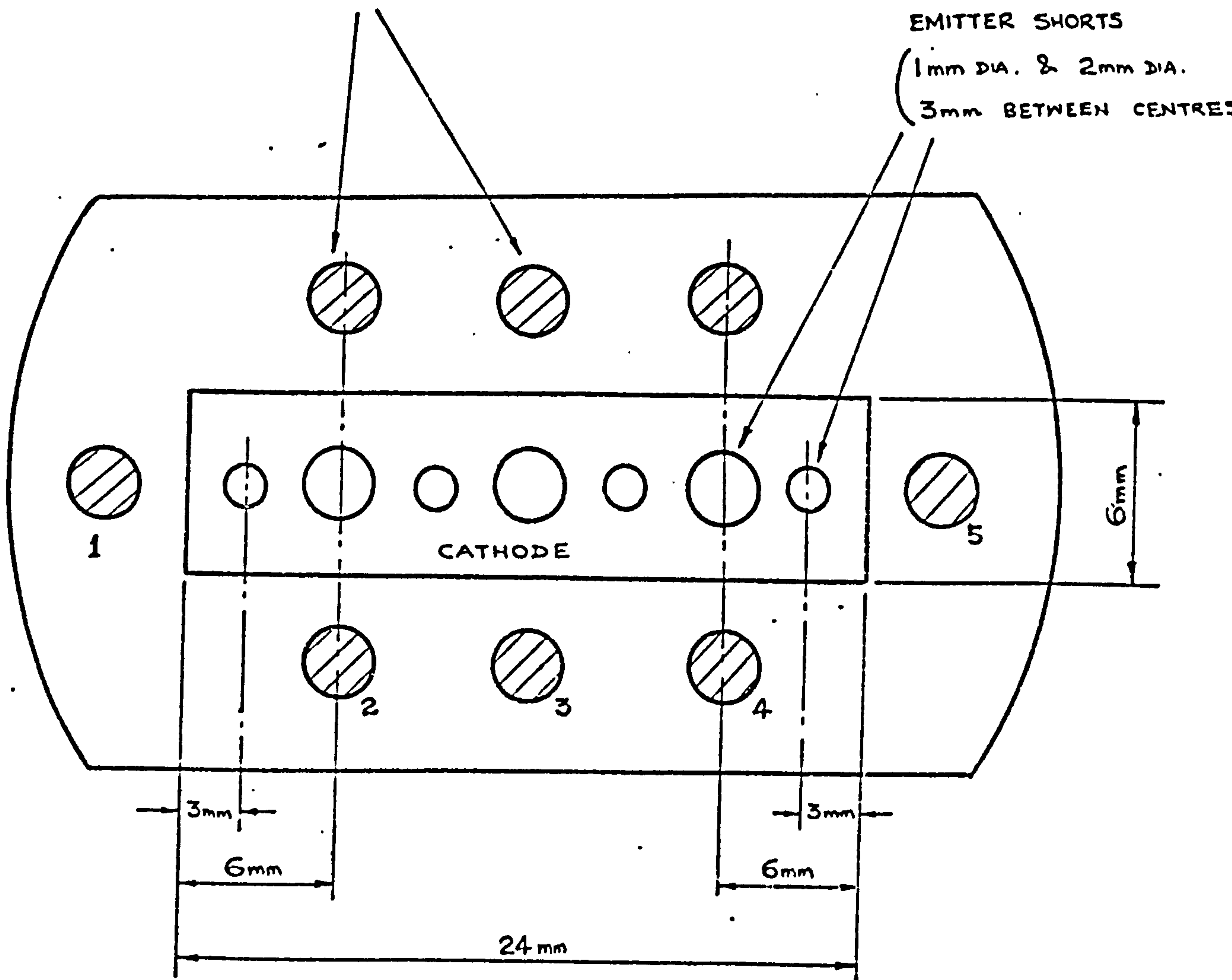


FIG. 3 SPECIALLY PREPARED THYRISTORS  
(NOT TO SCALE)

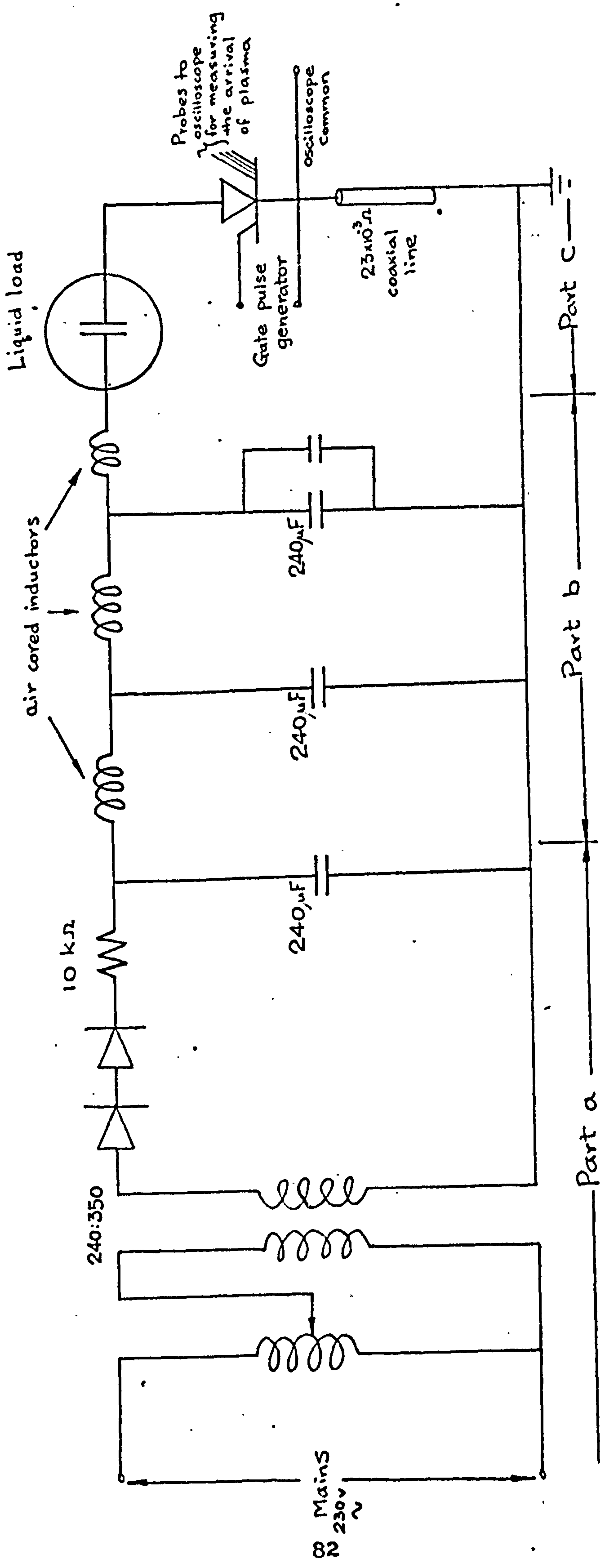
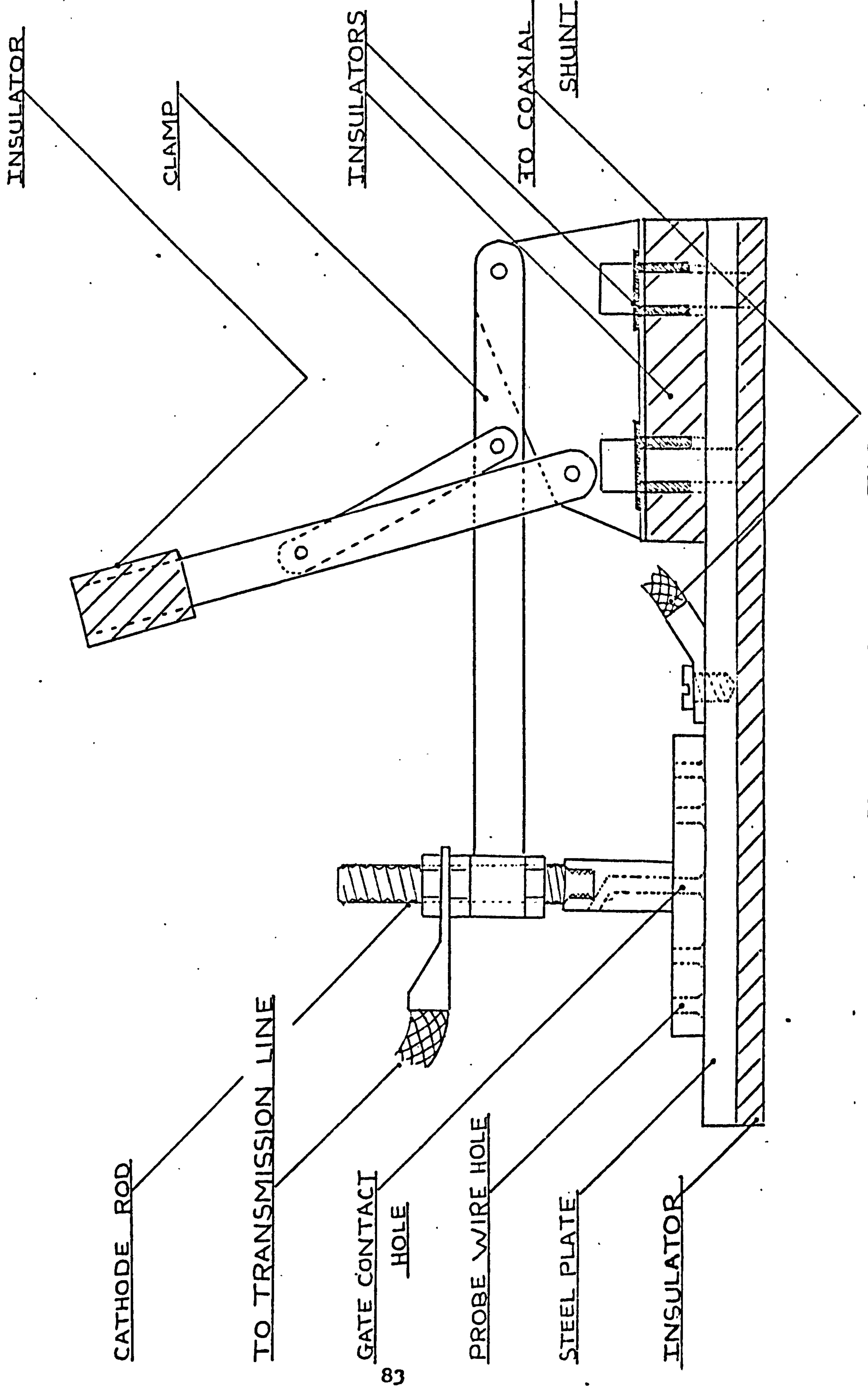
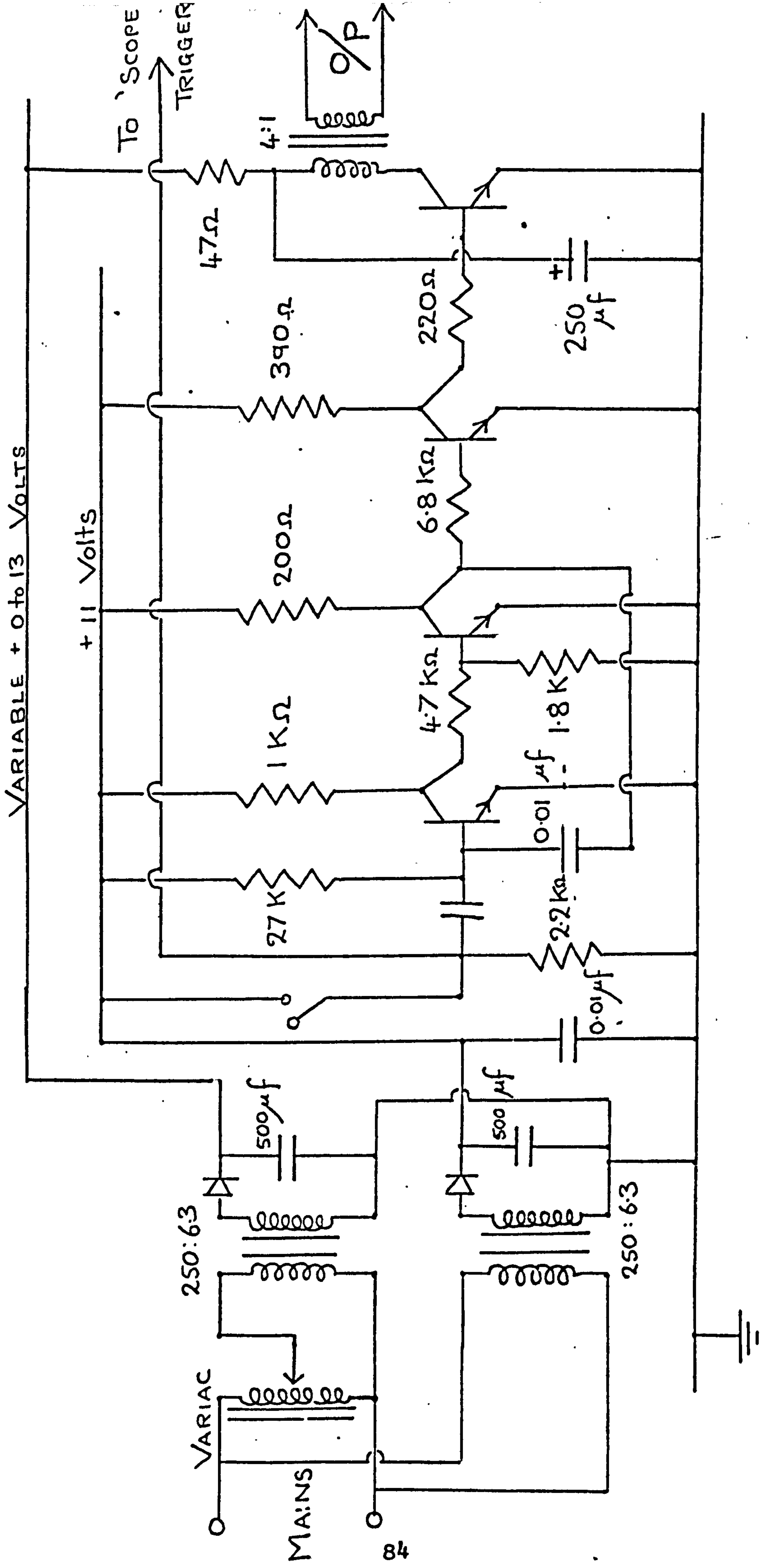


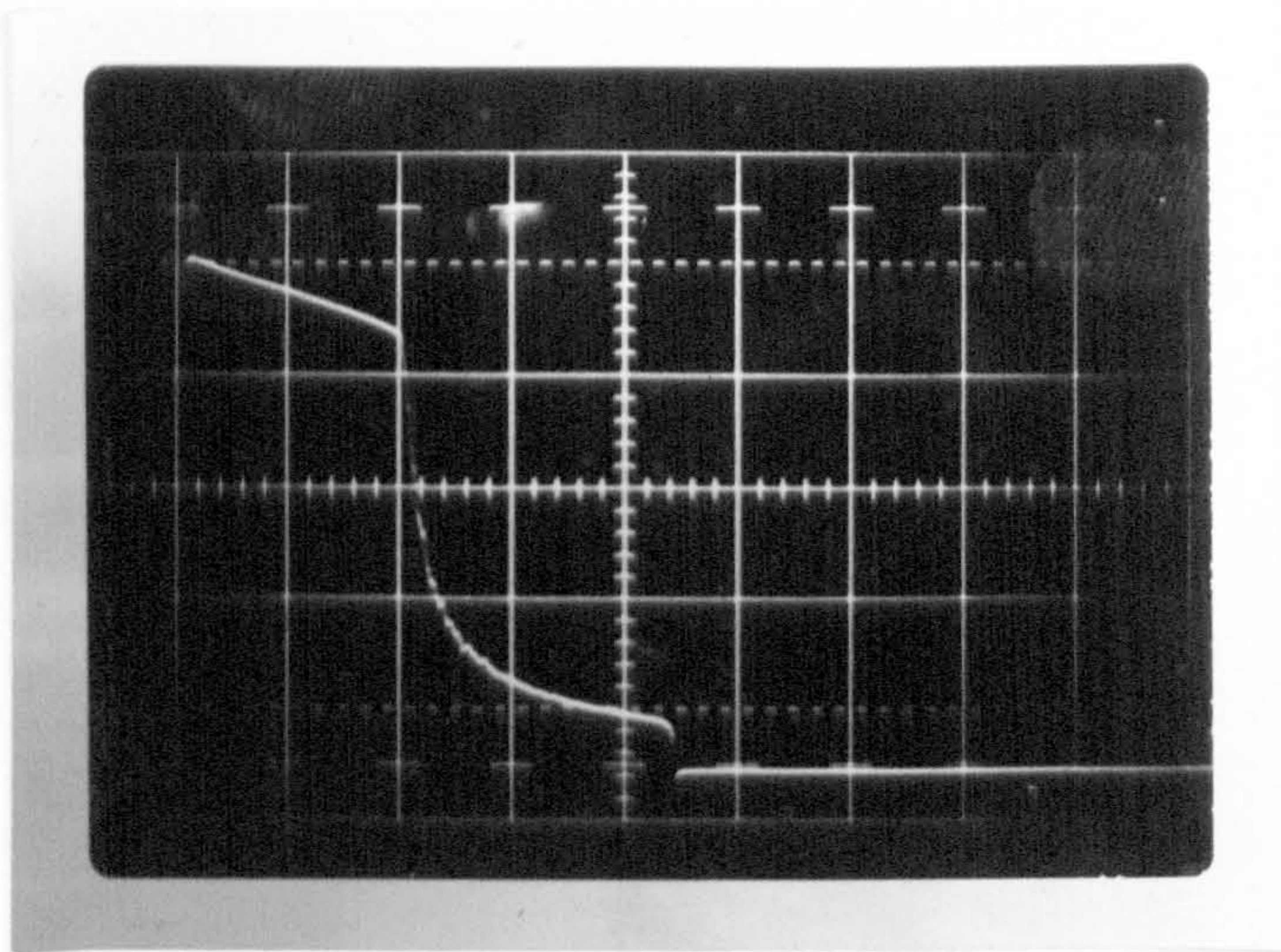
FIG. 4. Circuit used for measuring the plasma spreading velocities



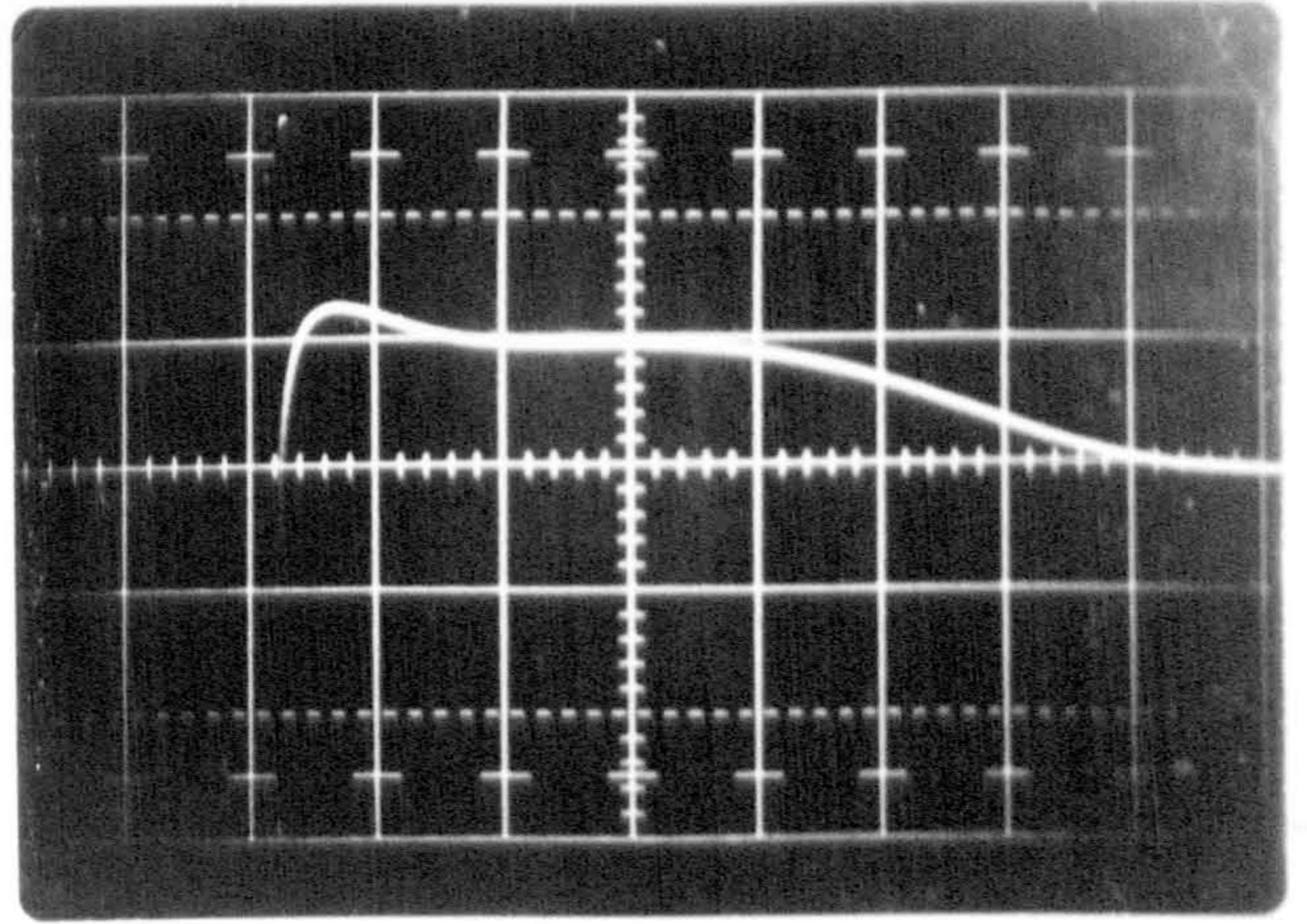
DEVICE CLAMP FIG 5



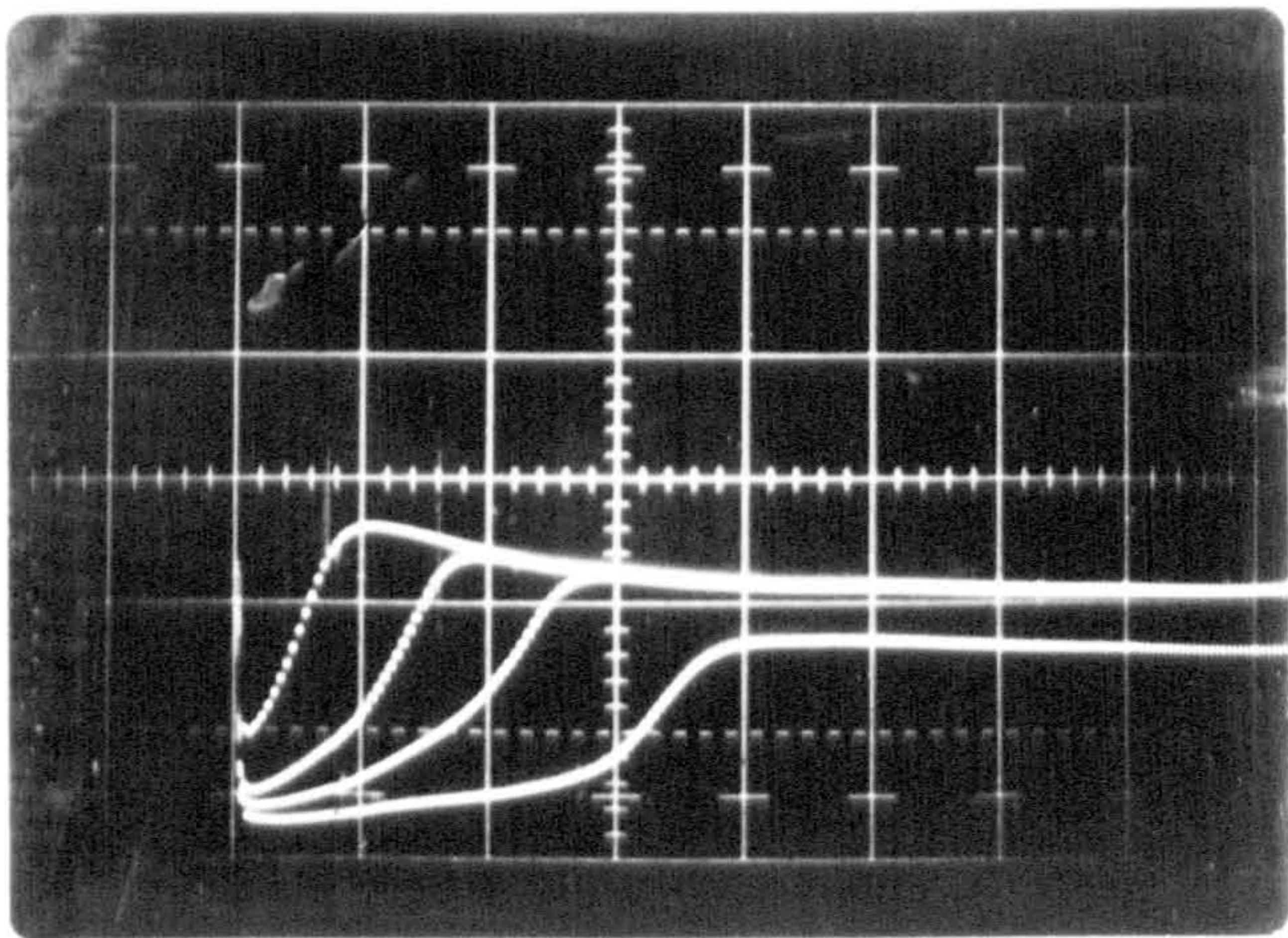
GATE PULSE GENERATING CIRCUIT FIG. 6.



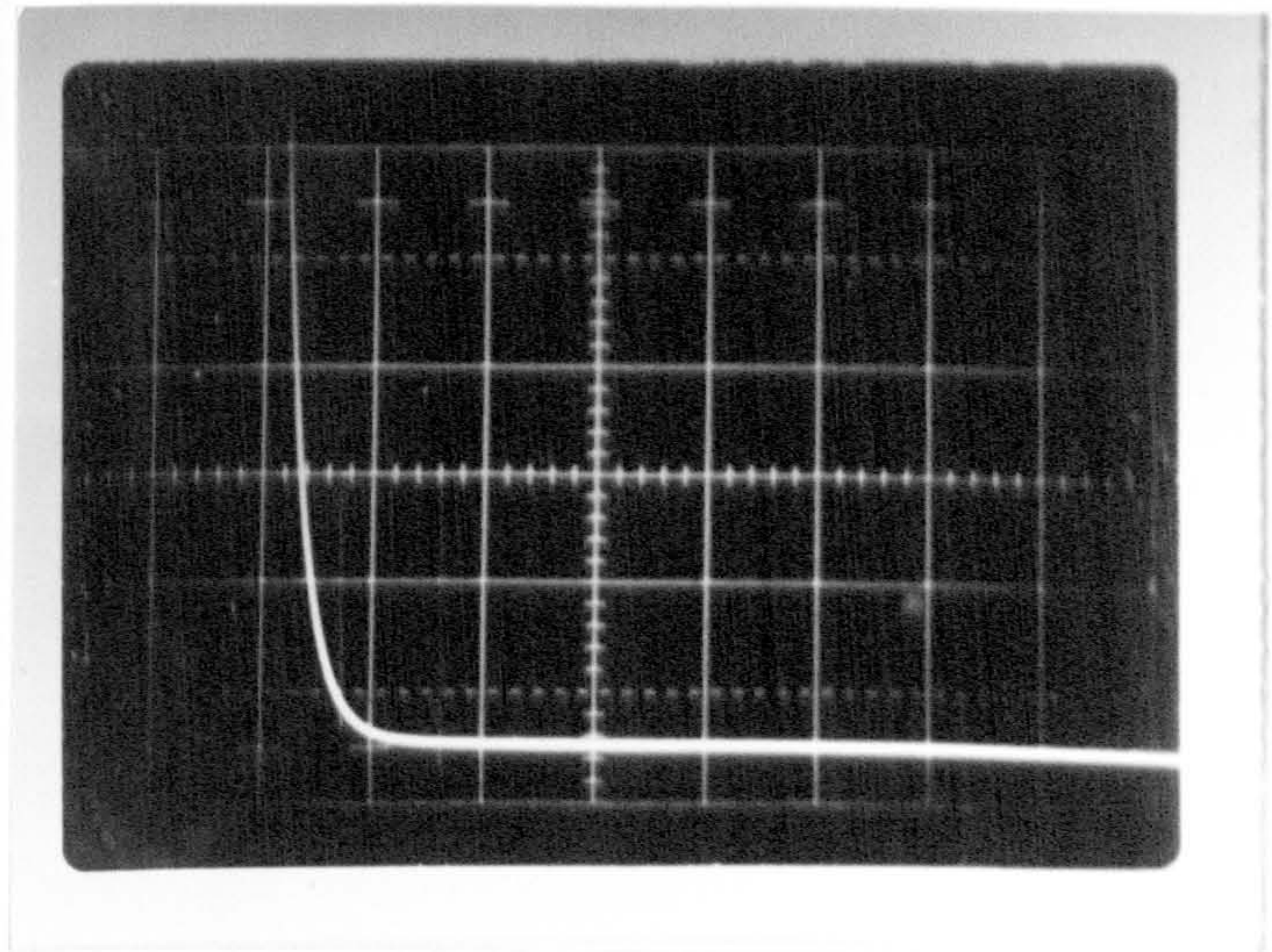
(a) Gate current trigger pulse  
 1 volt/cm. vert.  
 200  $\mu$ sec/cm. hori.



(b) load current pulse  
 0.5 volt/cm. vert. (22A/cm)  
 200  $\mu$ sec/cm. hori.



(c) probe voltages  
 0.5 volts/cm. vert.  
 200  $\mu$ sec/cm. hori.



(d) decay of device voltage  
 20 volts/cm vert.  
 200  $\mu$ sec./cm. hori.

FIG. 7 Typical photographs obtained in spreading velocity measurements.

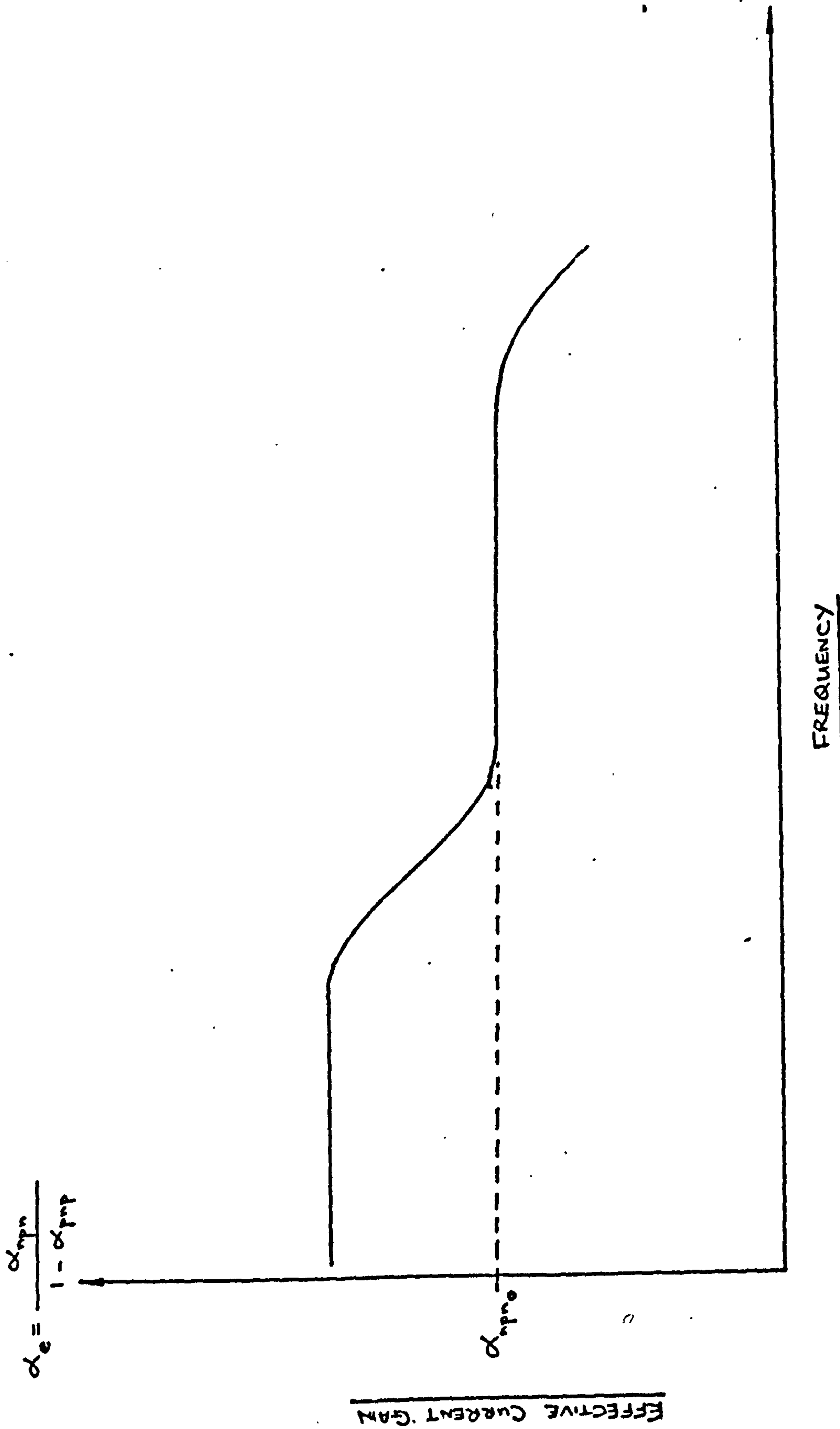


FIG. 8 Typical plot of effective current gain versus frequency

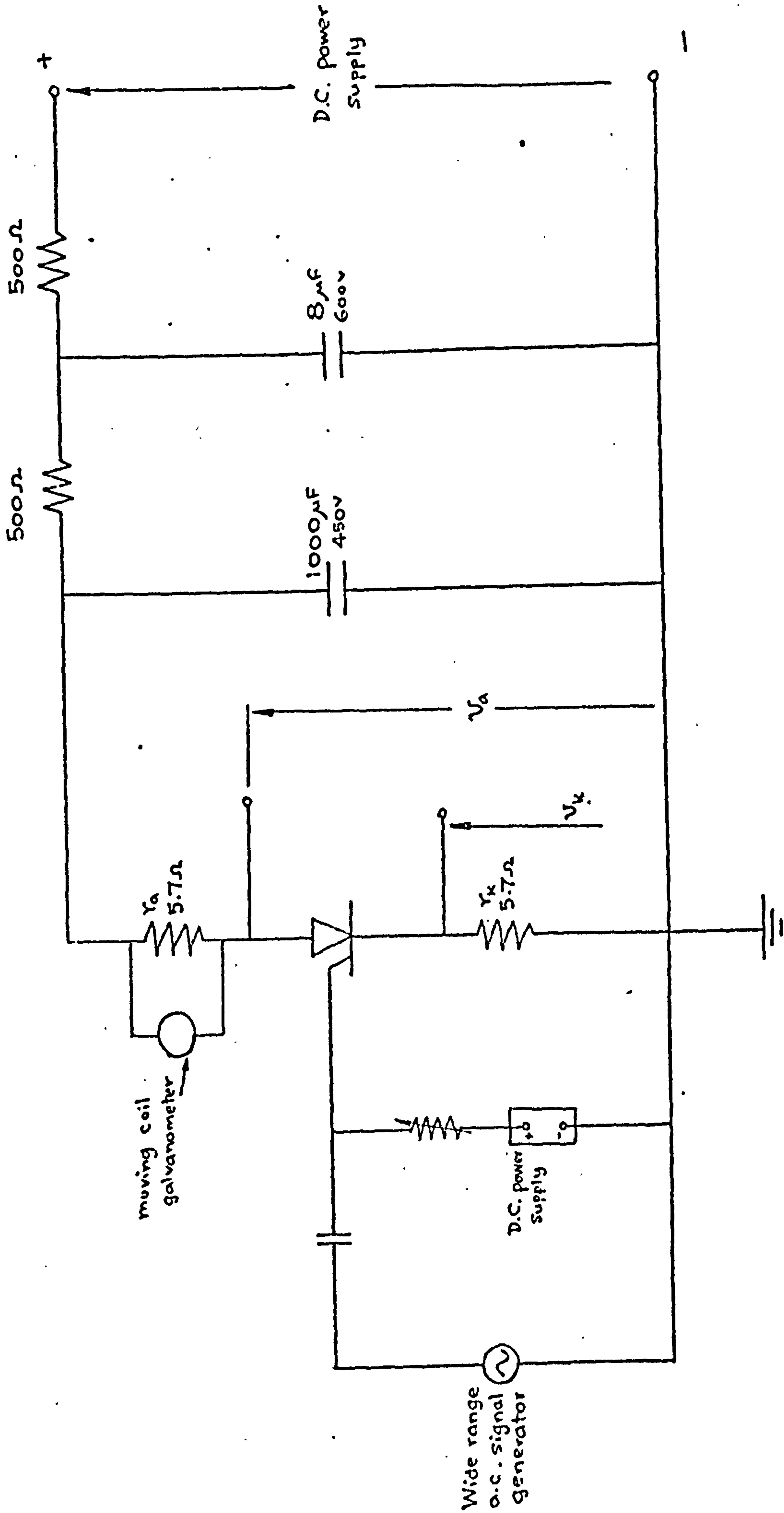


FIG. 9. Circuit for measuring the frequency variations of effective alpha values

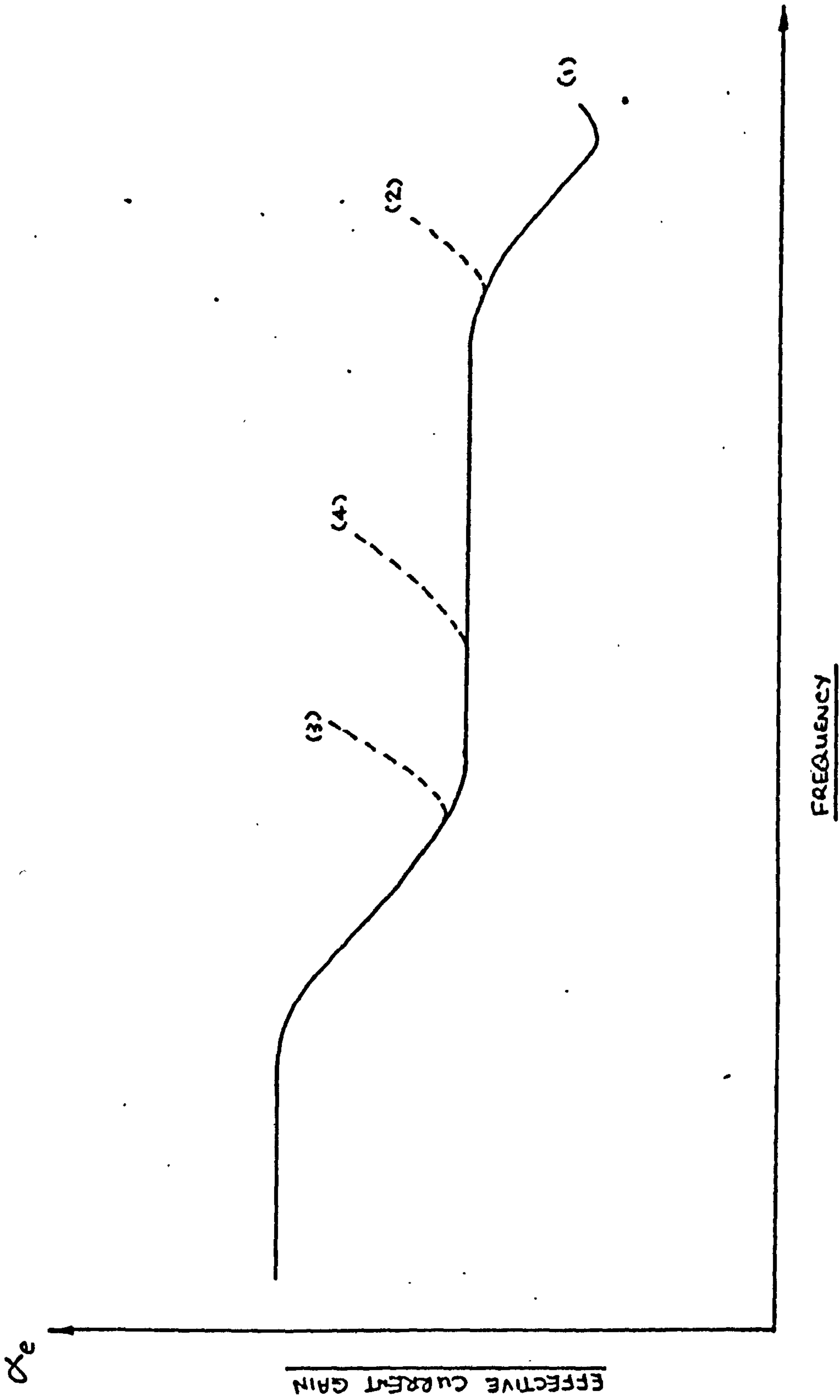


FIG. 10. Effects of feedback on current gain versus frequency plots

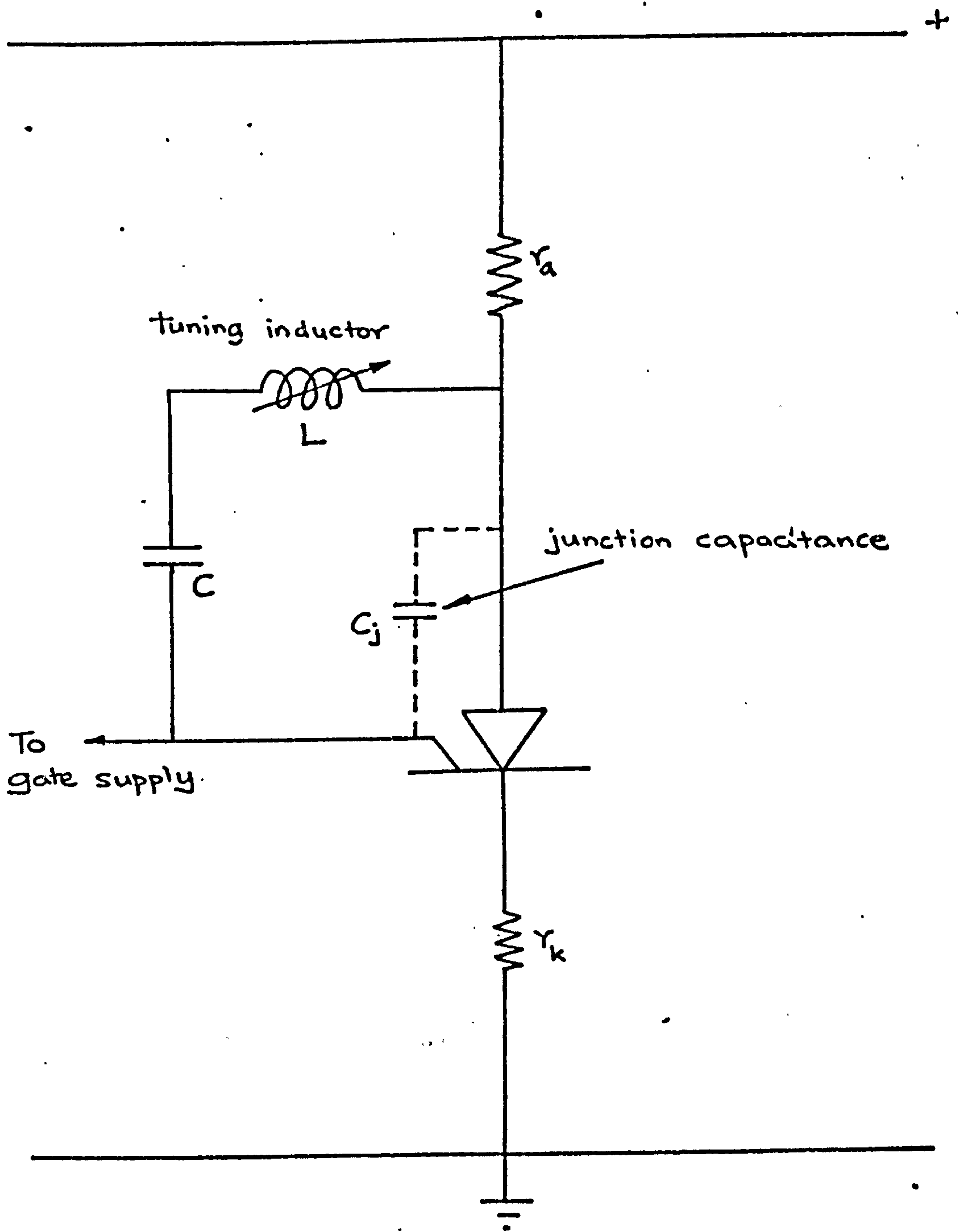
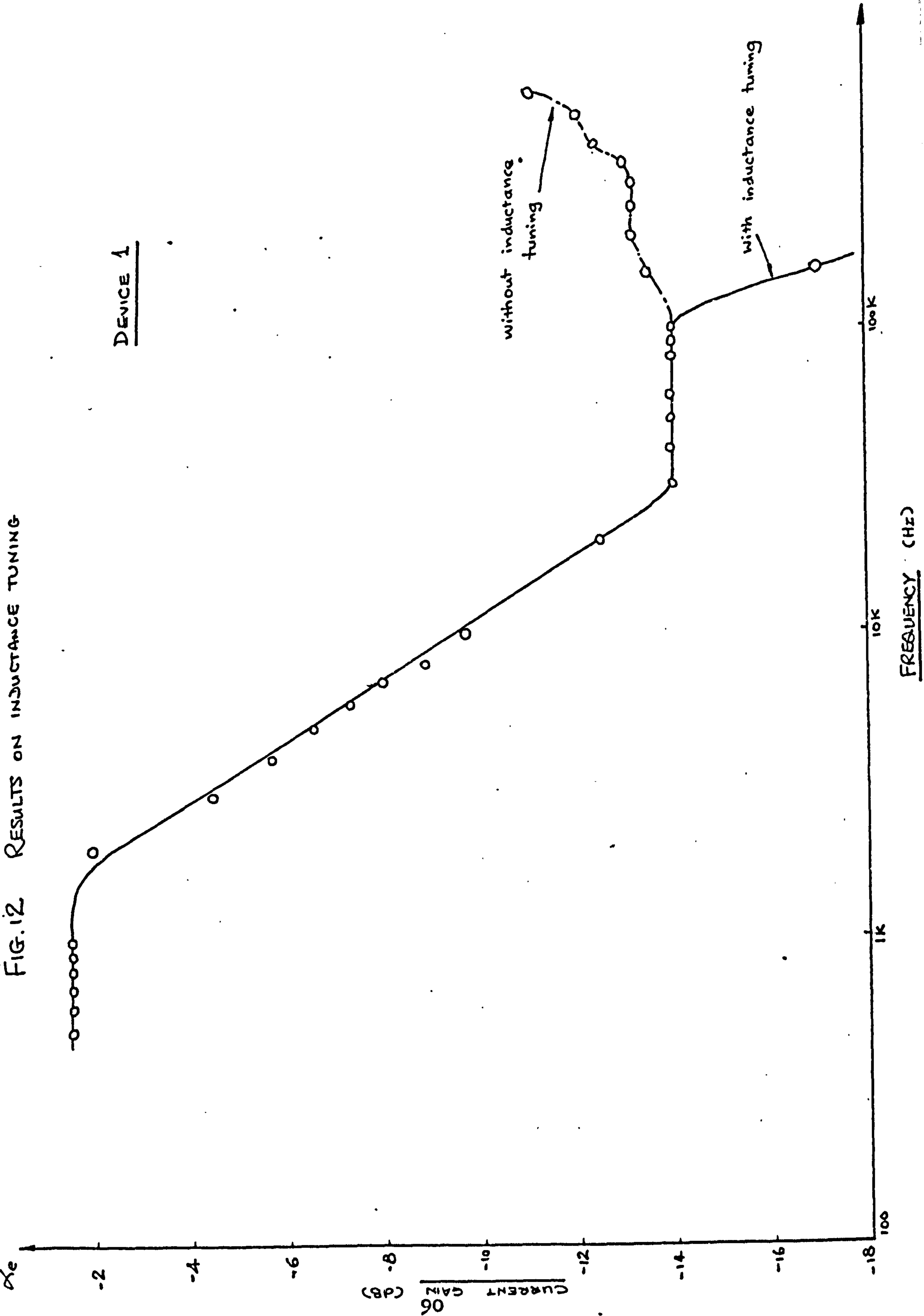


FIG. 11. Circuit used for tuning out unwanted feedback

FIG. 12 RESULTS ON INDUCTANCE TUNING

DEVICE 1



FREQUENCY (HZ)

DEVICE 2

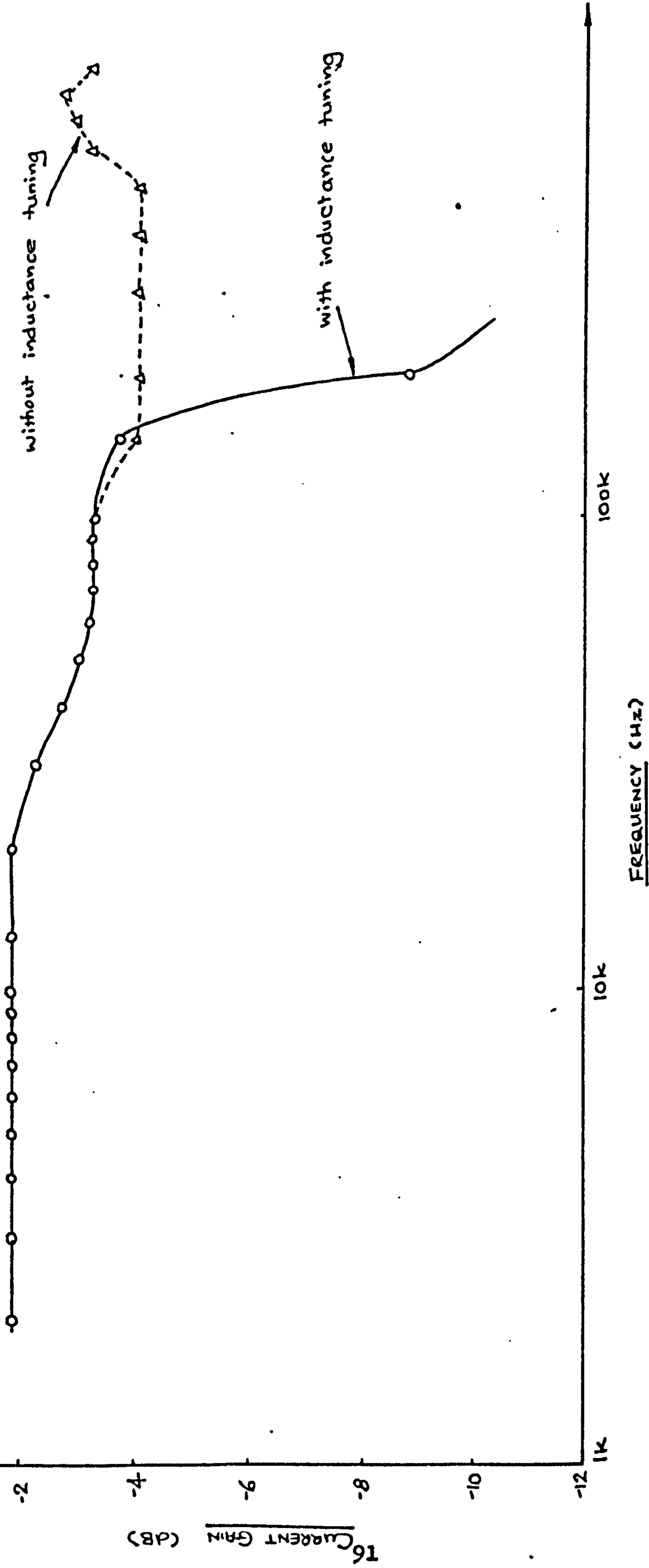
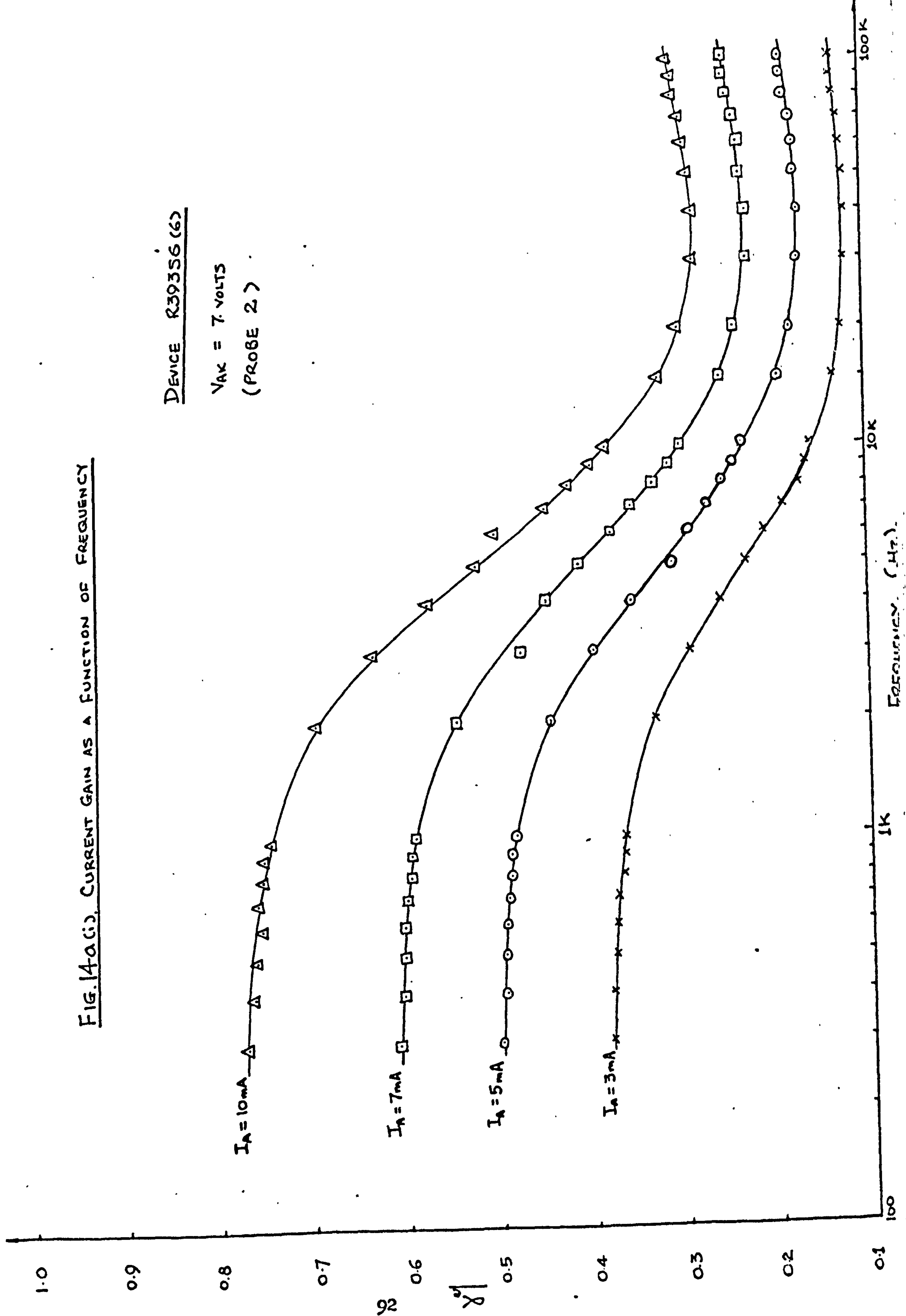


FIG. 14a(i), CURRENT GAIN AS A FUNCTION OF FREQUENCY

DEVICE R39356 (6)

$V_{AK} = 7 \text{ VOLTS}$   
(PROBE 2)



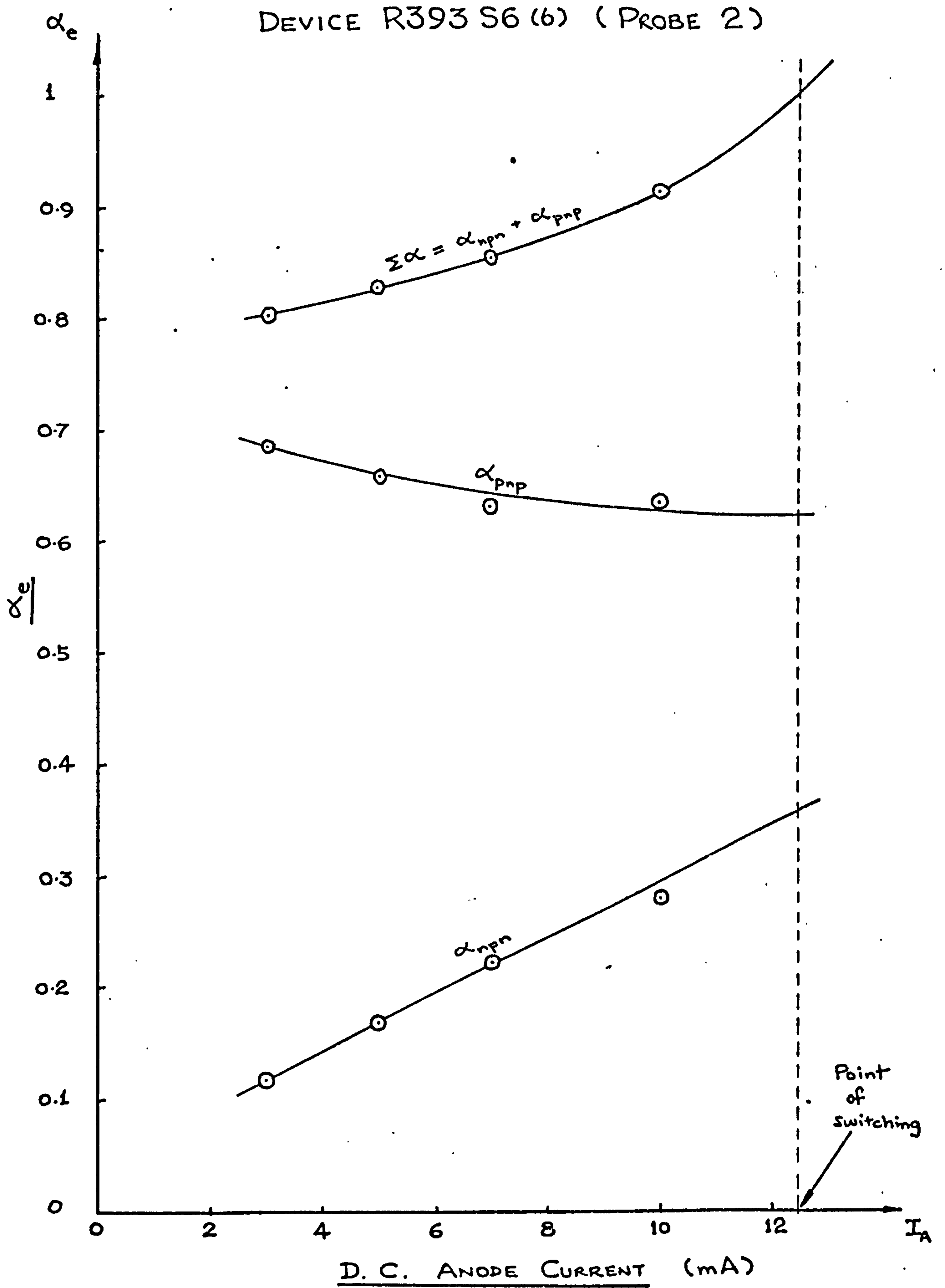
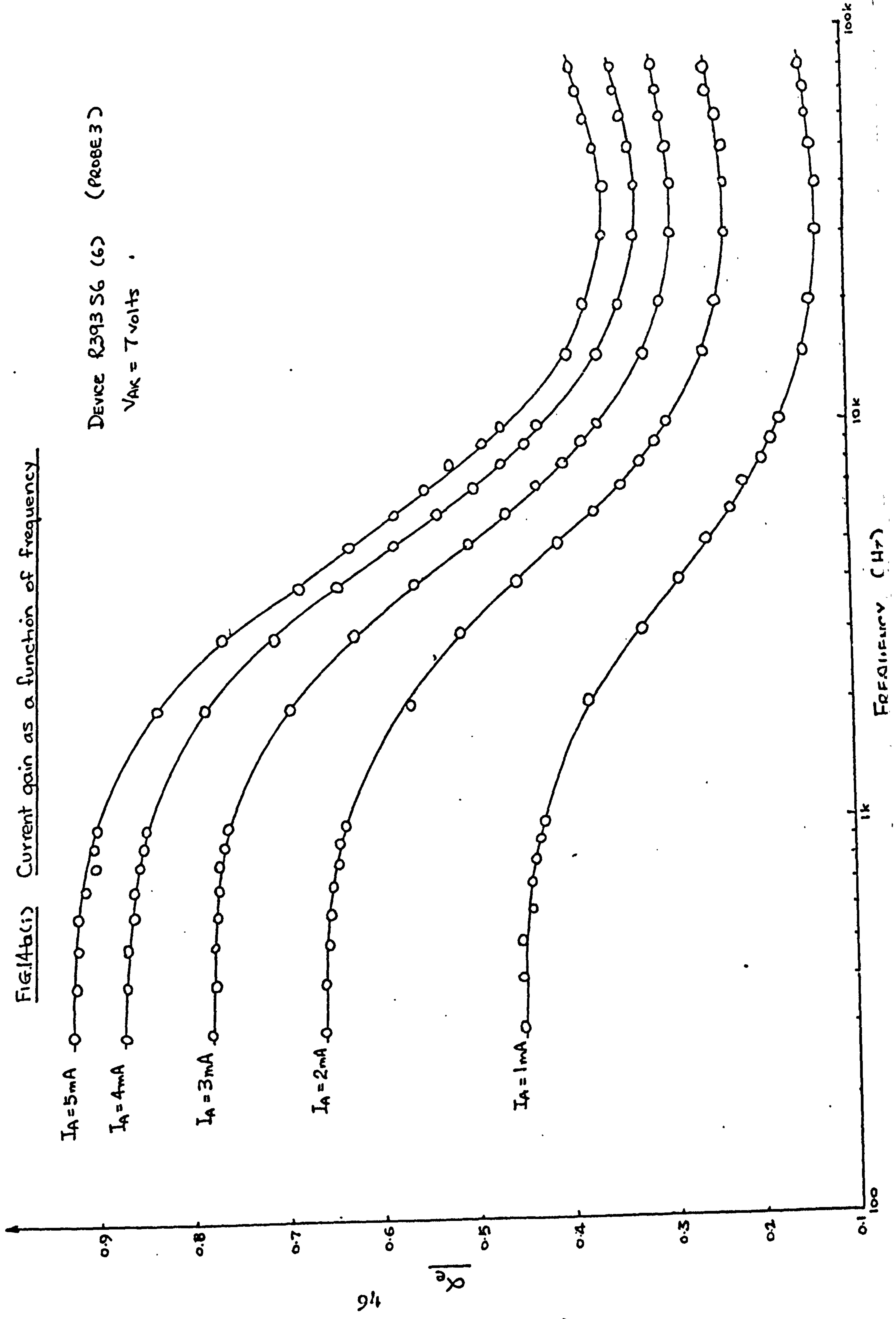


FIG.14a(ii) Current gain as a function of d.c. anode current

FIG. 14b(i) Current gain as a function of frequency

DEVICE R39356 (6) (PROBE 3)

$V_{AK} = 7 \text{ volts}$



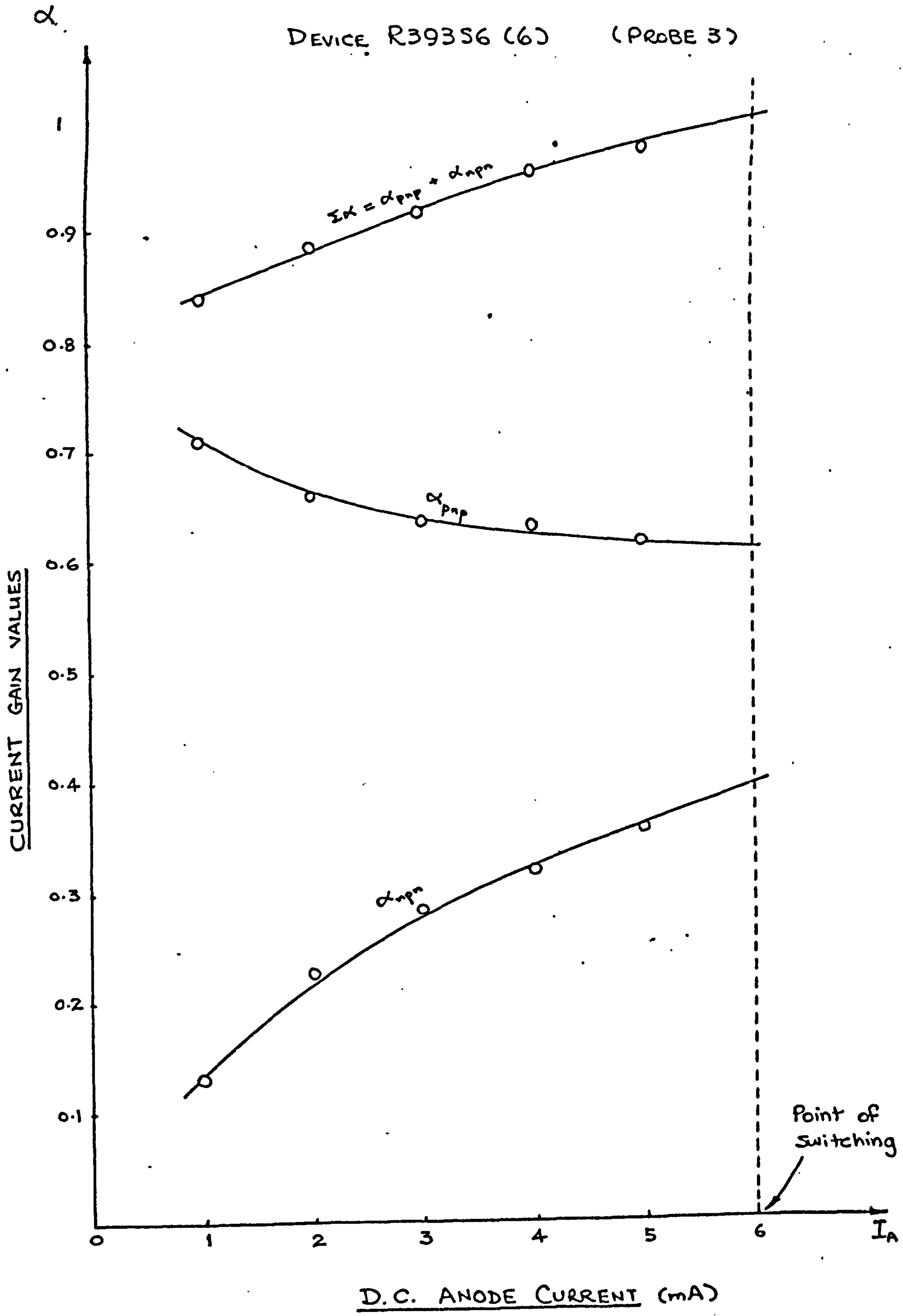
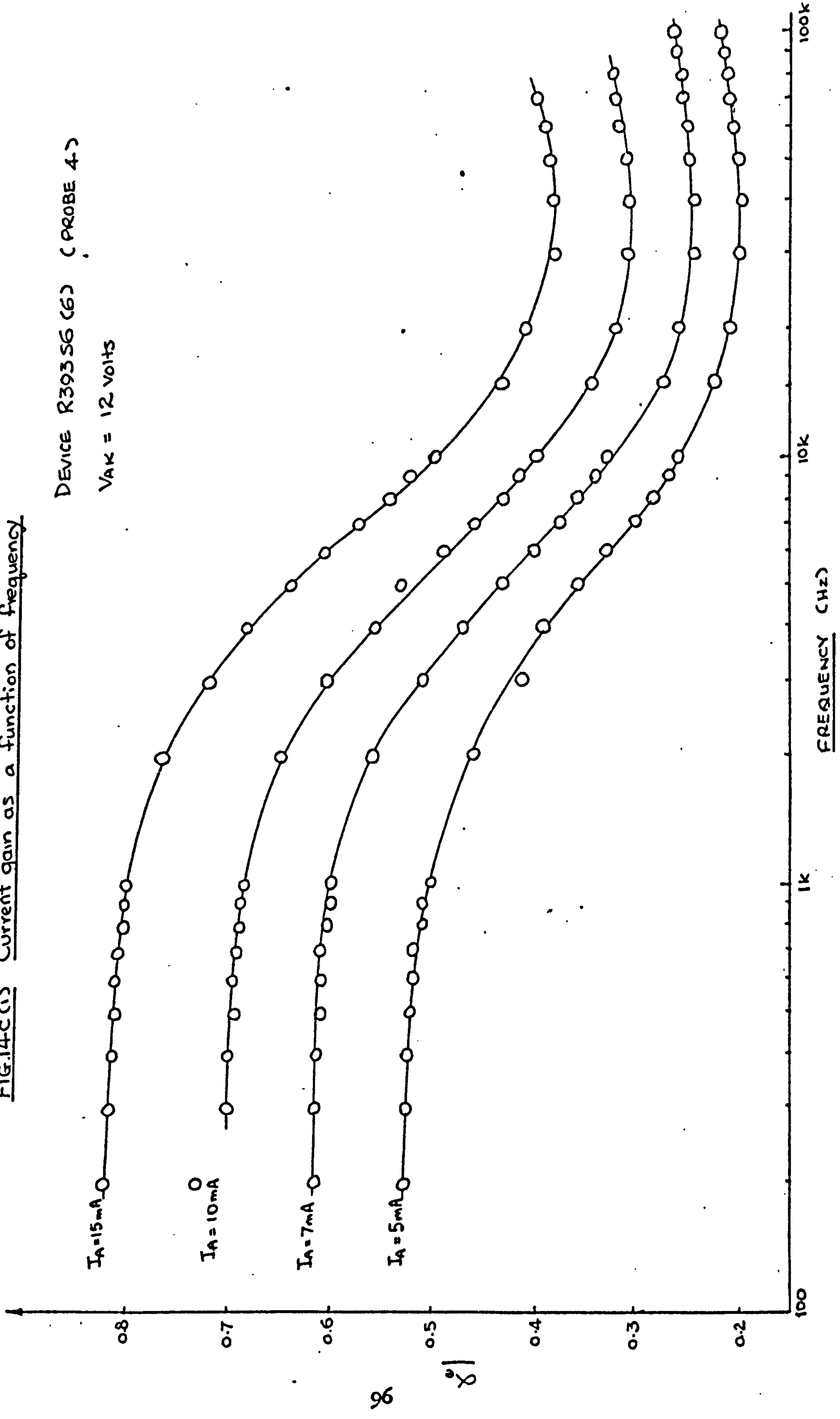


FIG.14b(ii) Current gain as a function of d.c. anode current

FIG. 14c(i) Current gain as a function of frequency

DEVICE R393S6 (6) (PROBE 4)  
 $V_{AK} = 12 \text{ volts}$



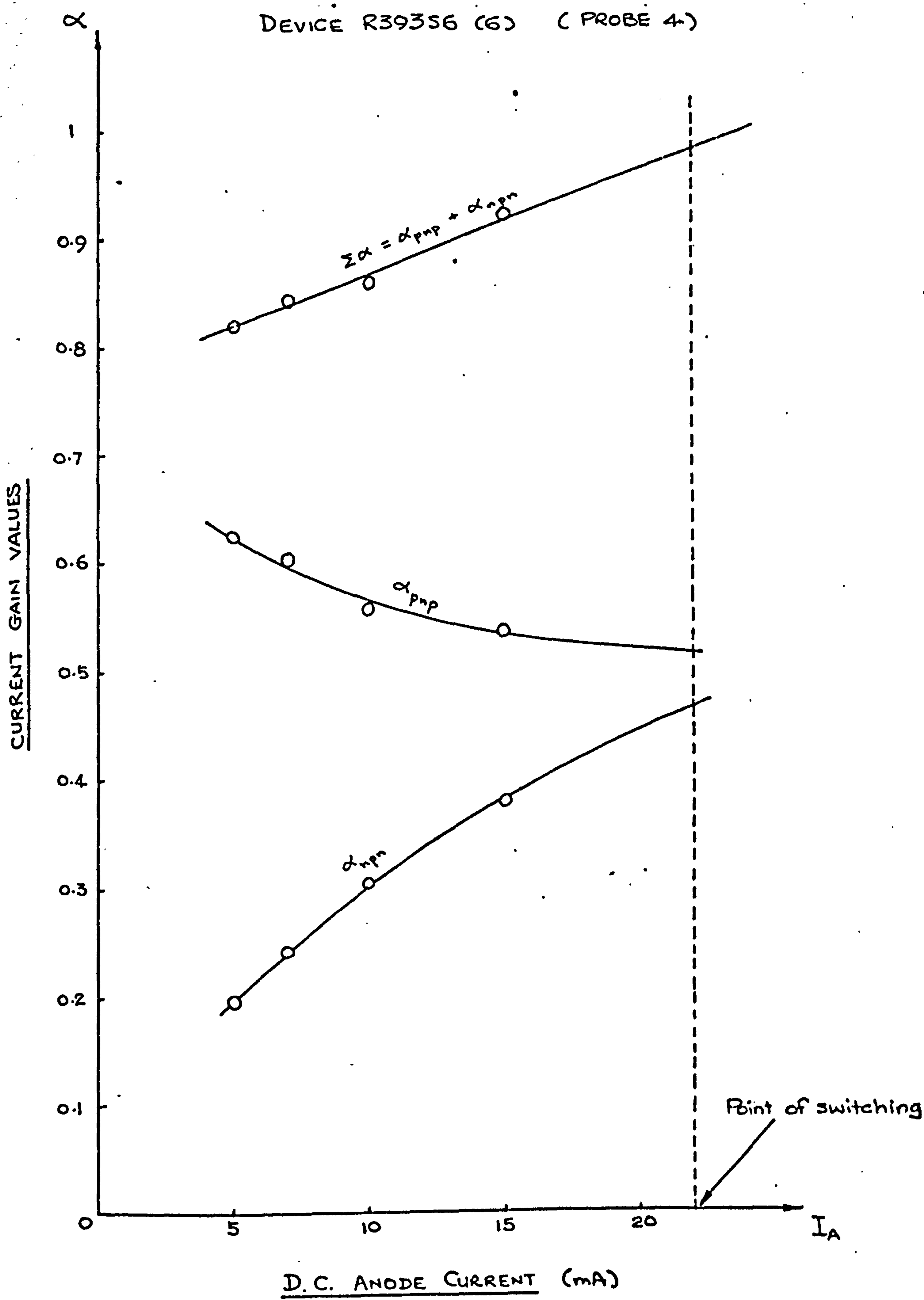


FIG.14c (ii) Current gain as a function of d.c. anode current

DEVICE NSS4 (6) (PROBE 2)

$V_{AK} = 10$  VOLTS

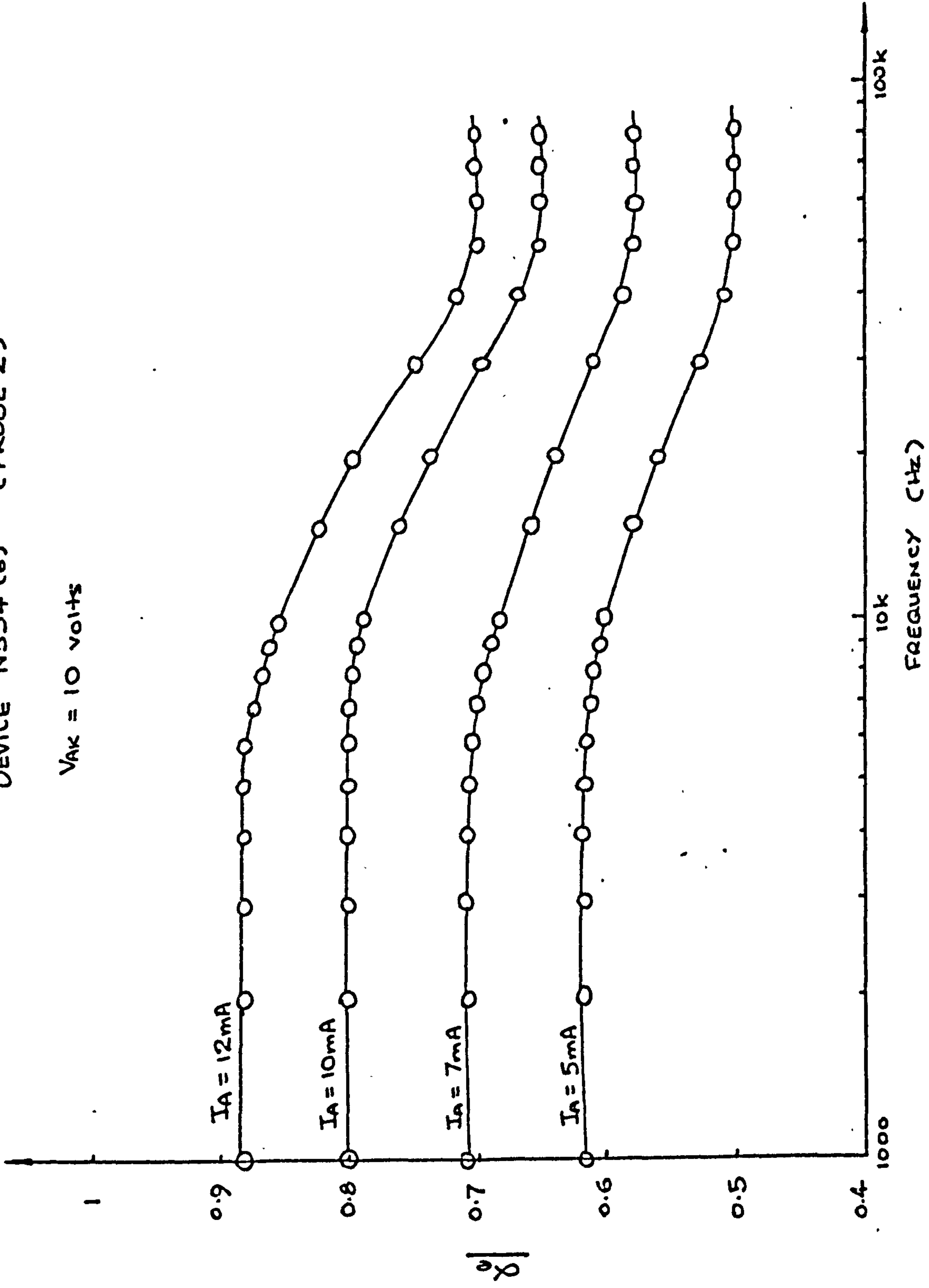


FIG15a(c) Current gain as a function of frequency

DEVICE N554 (G) (PROBE 2)

$V_{AK} = 10 \text{ volts}$

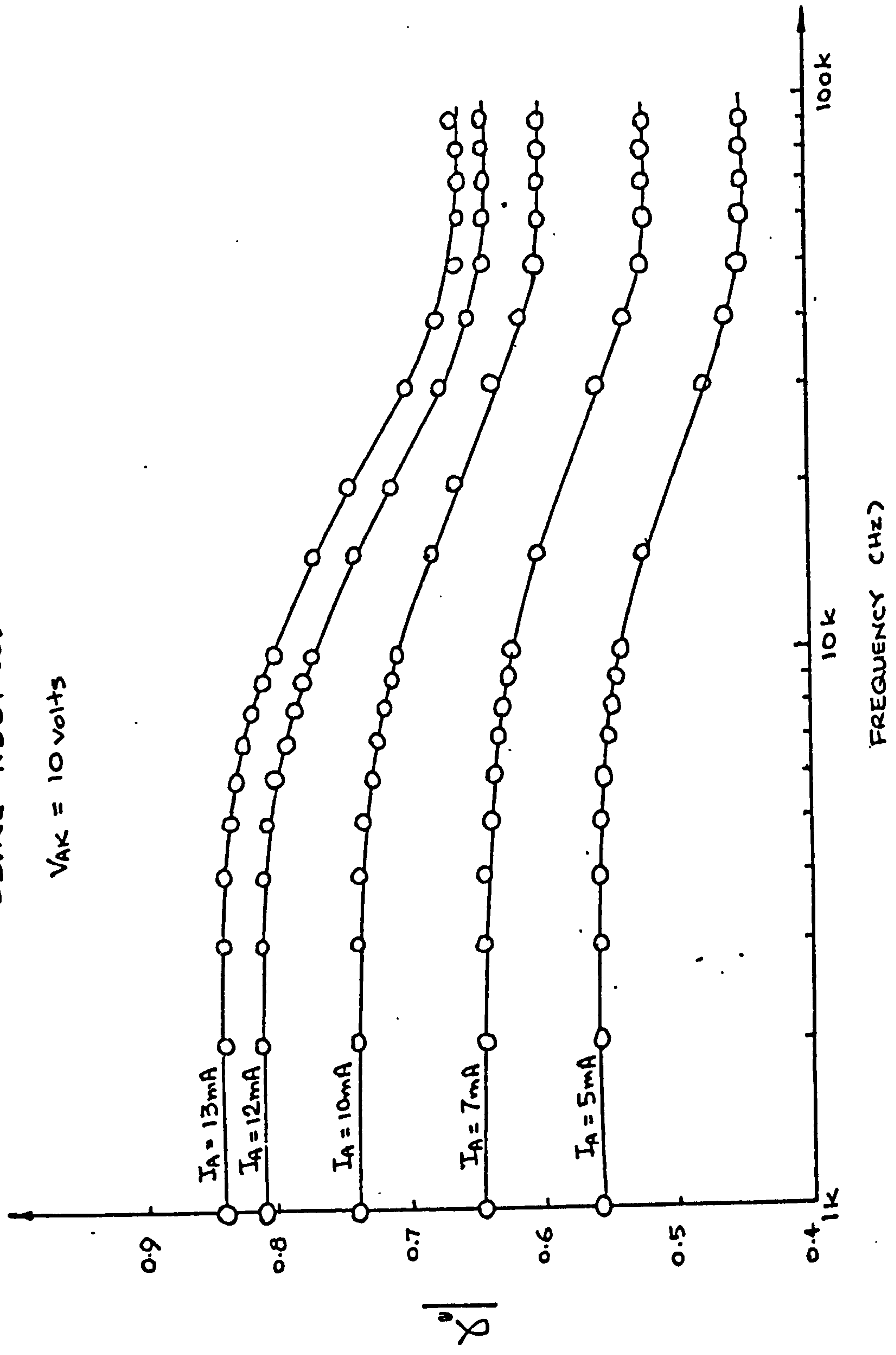
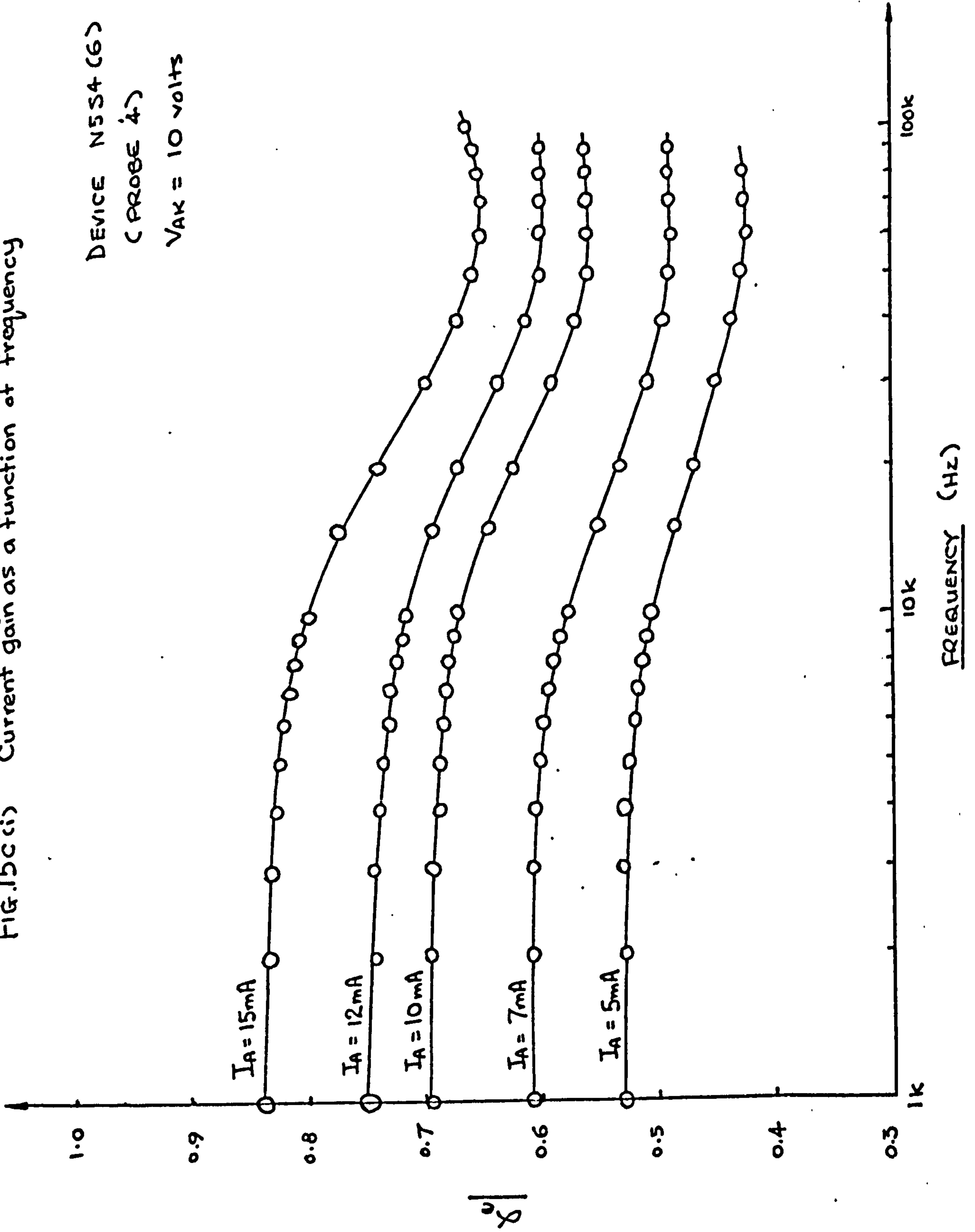


FIG.15b(i) Current gain as a function of frequency

FIG.15c(ii) Current gain as a function of frequency

DEVICE N5S4 (6)  
 ( PROBE 4)  
 $V_{AK} = 10 \text{ volts}$



DEVICE R39356. (1) (PROBE 3D)

$V_{AK} = 8$  volts

$I_A = 2mA$

$I_A = 1mA$

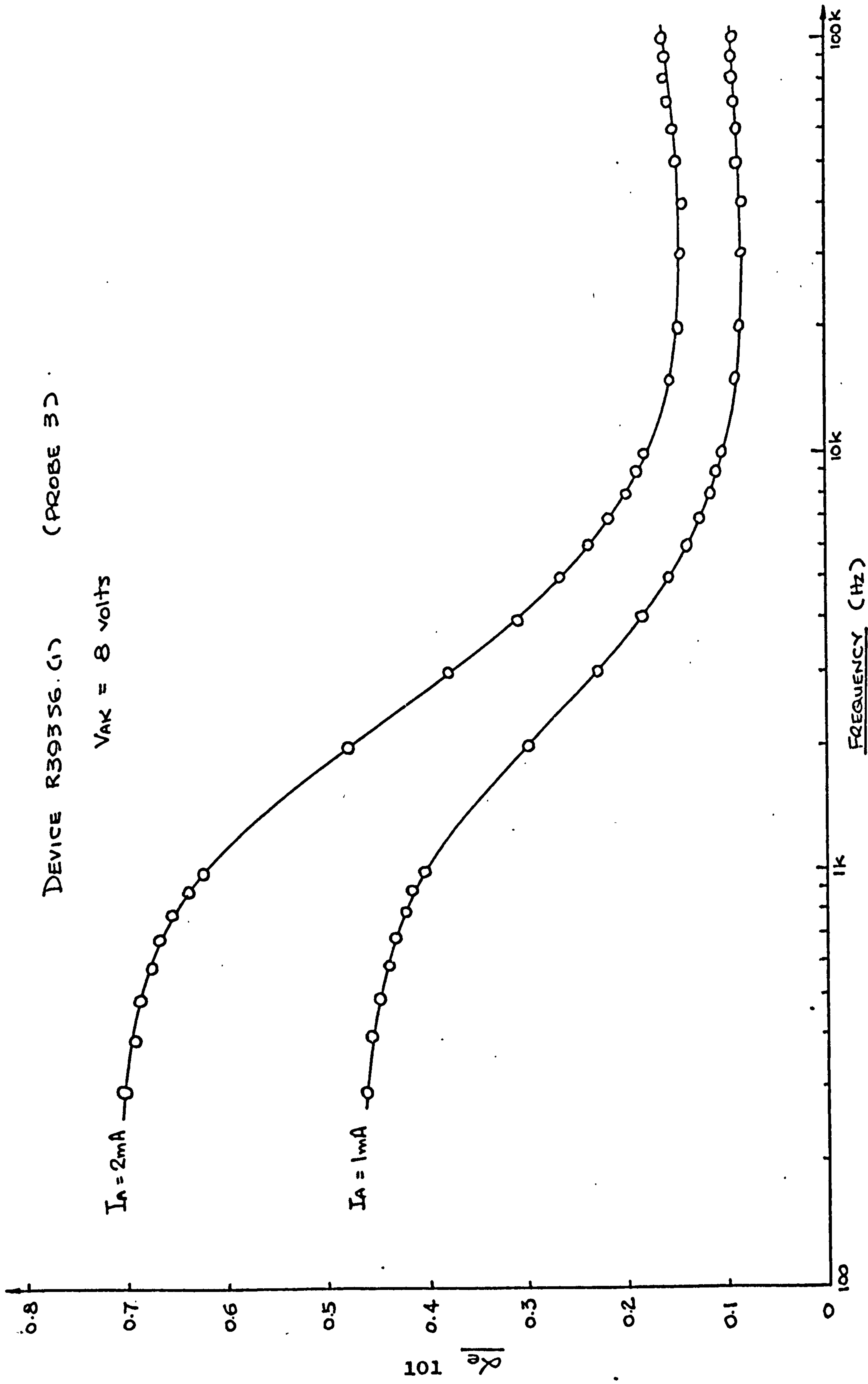


FIG.16a(c) Current gain as a function of frequency

FIG. 16(a) Current gain as a function of frequency

DEVICE R39356 (1) (PROBE 3)

$V_{AK} = 8$  volts

$I_A = 4\text{mA}$

$I_A = 3\text{mA}$

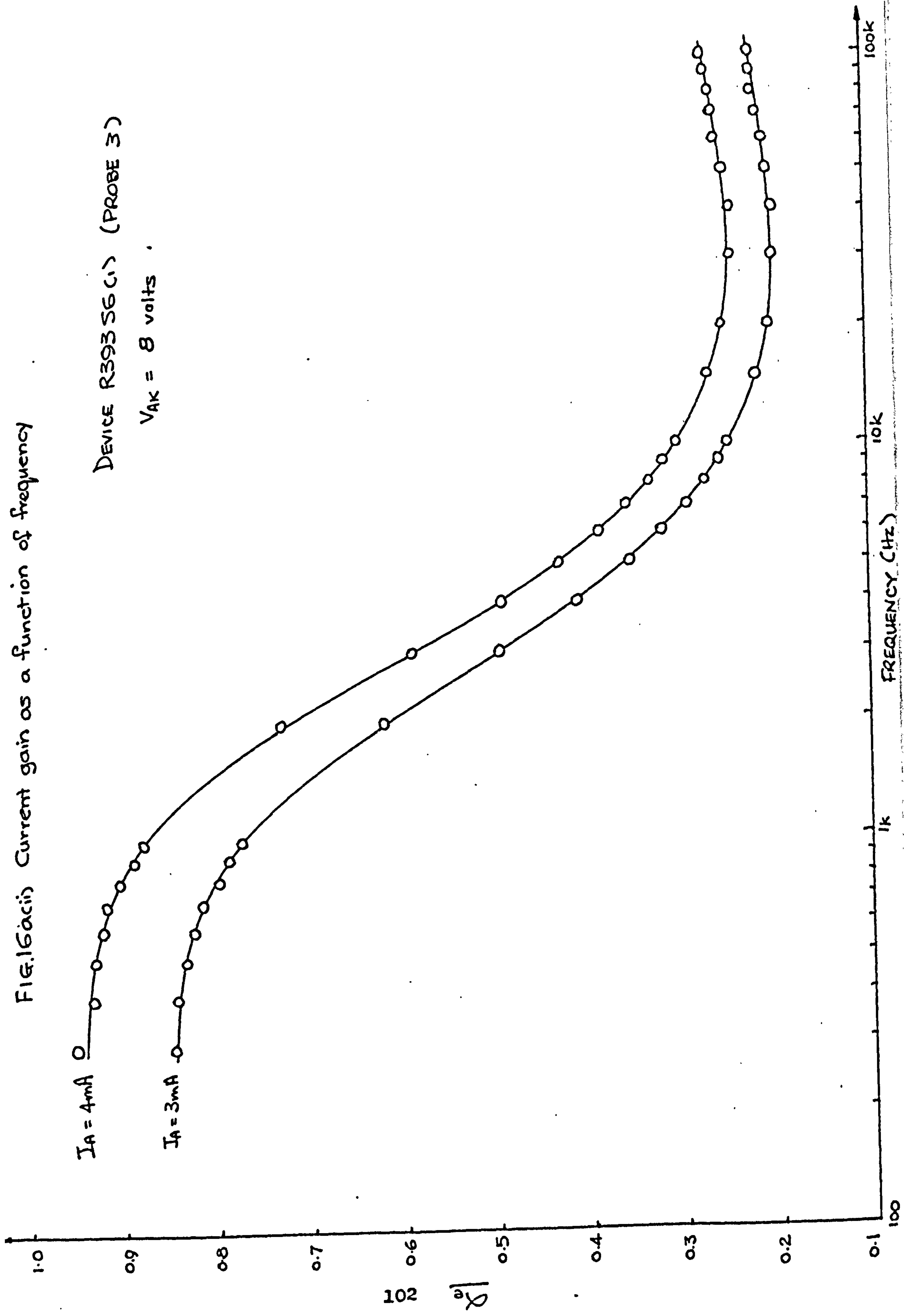


FIG.16b (i) Current gain as a function of frequency

DEVICE R30356 (1) (PROBE 4)  
 $V_{AK} = 12 \text{ volts}$

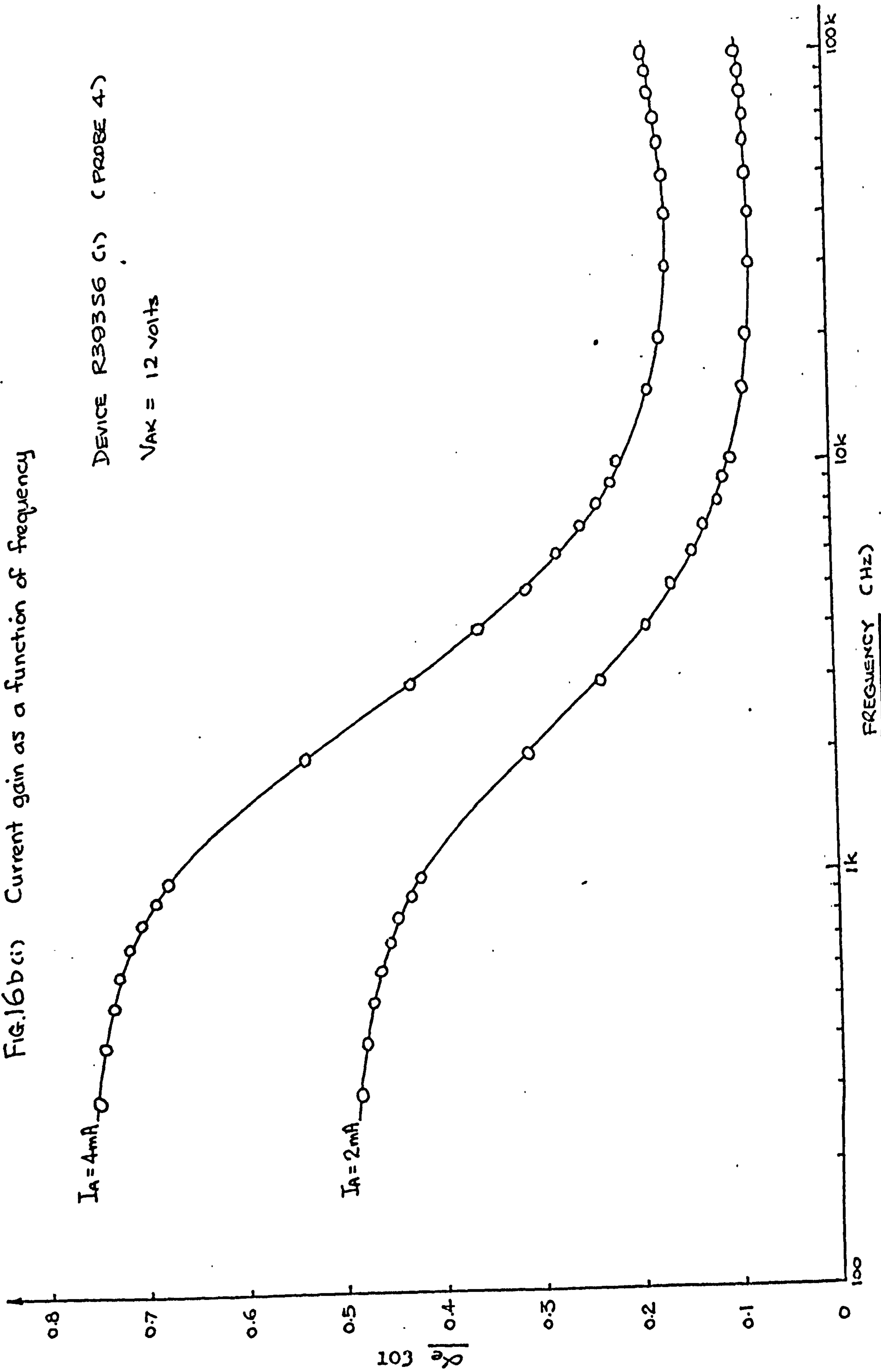


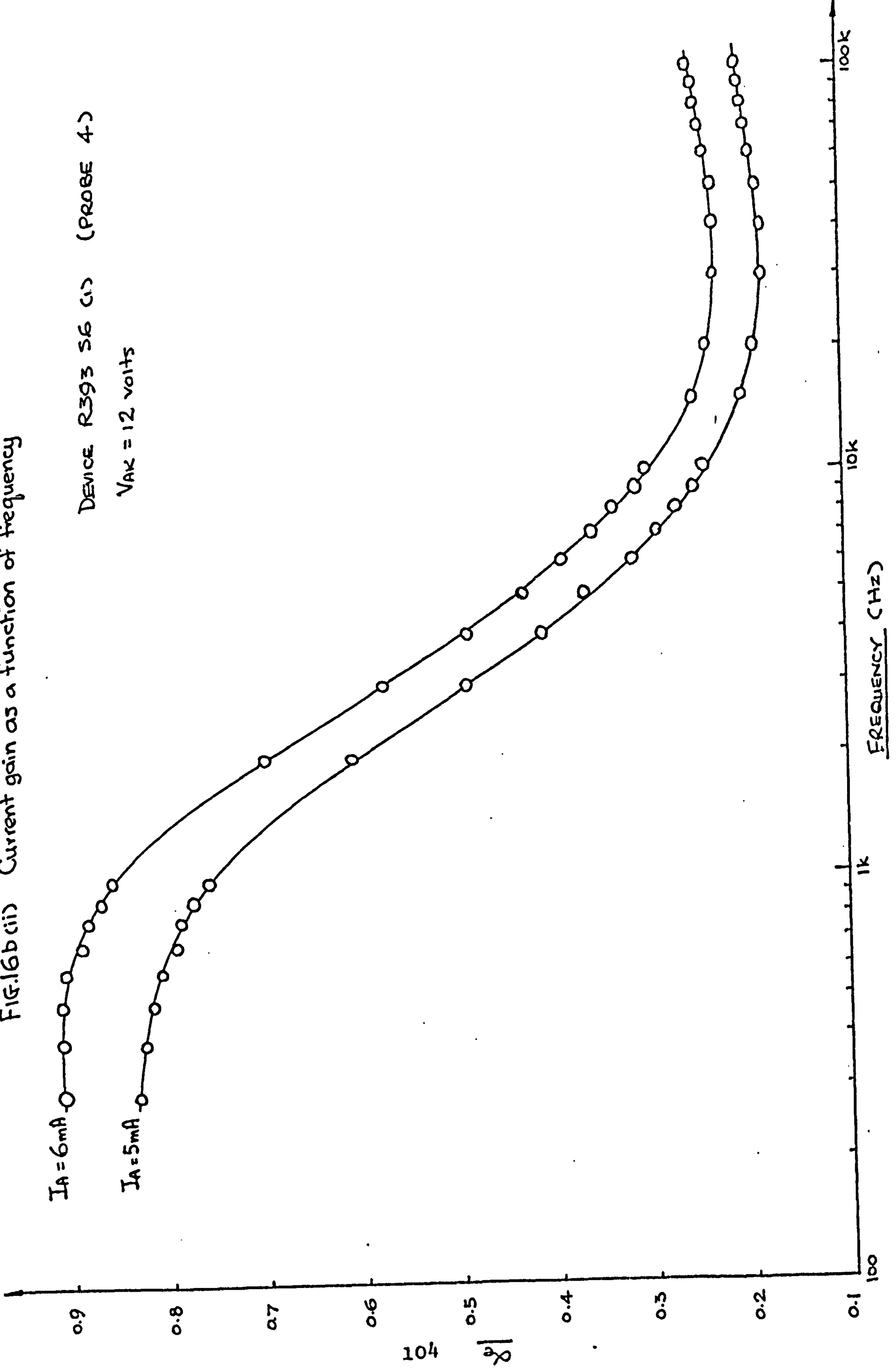
FIG.16b(ii) Current gain as a function of frequency

DEVICE R393 S6 (1) (PROBE 4)

$V_{AK} = 12$  volts

$I_A = 6$  mA

$I_A = 5$  mA



GATE ISOLATION RING  
(ISOLATING THE GATE - CATHODE JUNCTION  
FROM BEING METALLISED.)

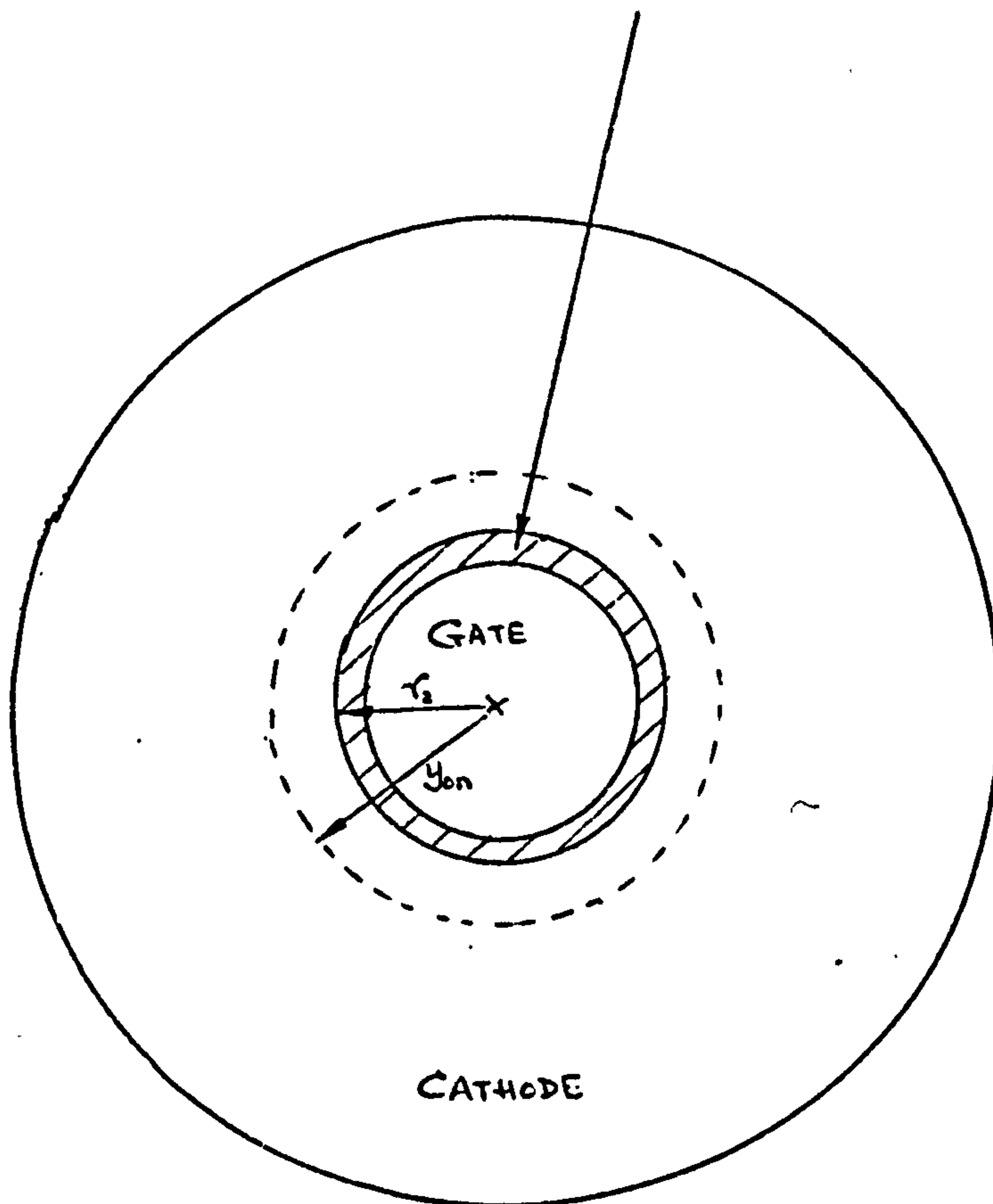


FIG. 17a. ILLUSTRATION OF GATE ISOLATION RING.

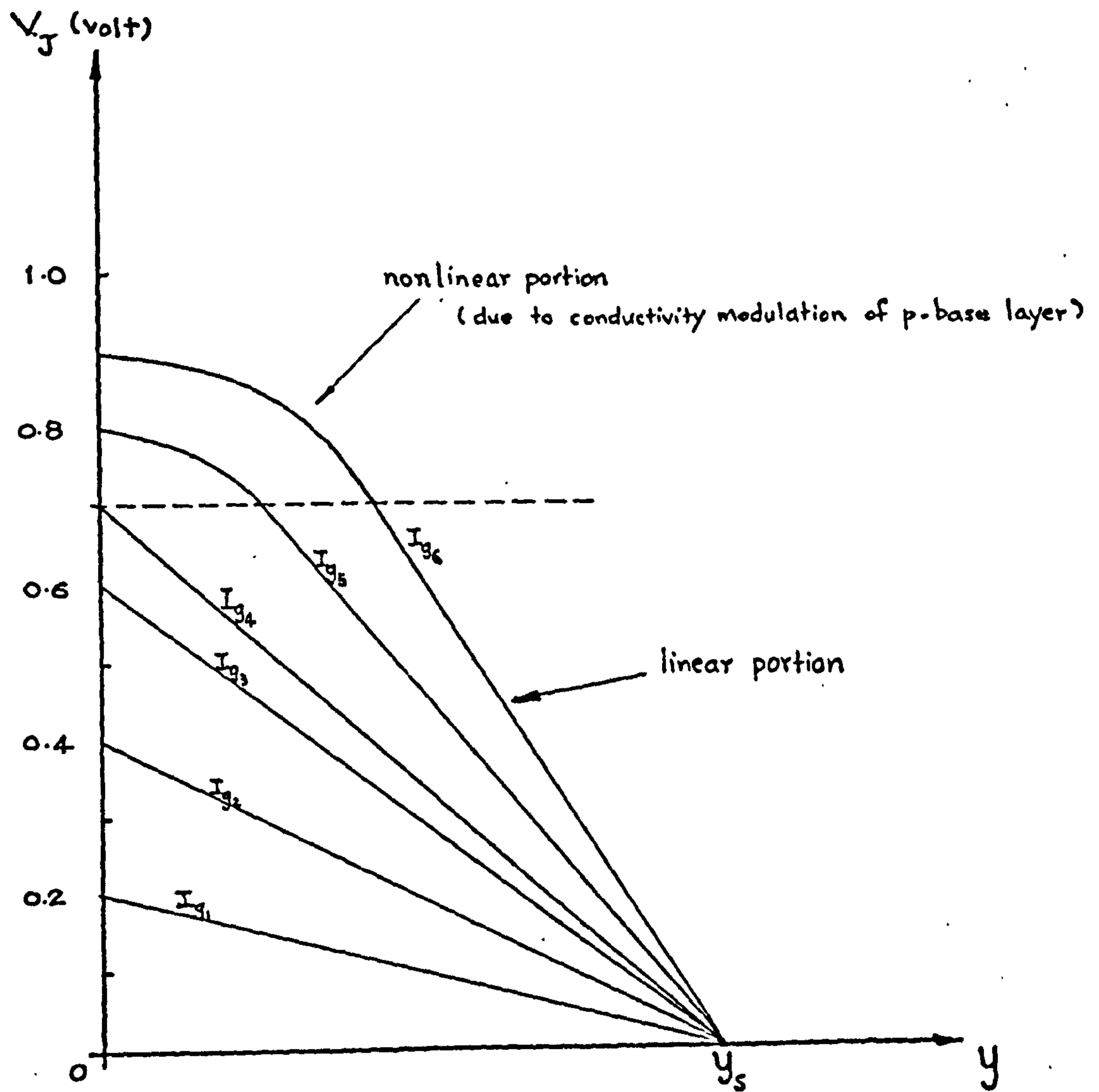


FIG. 18 Schematic plots of  $V_J(y) = V_{J_0} - I_g \frac{\rho_{p_2}}{A_{p_2}} \cdot y$

$$I_{g_6} > I_{g_5} > I_{g_4} > I_{g_3} > I_{g_2} > I_{g_1}$$

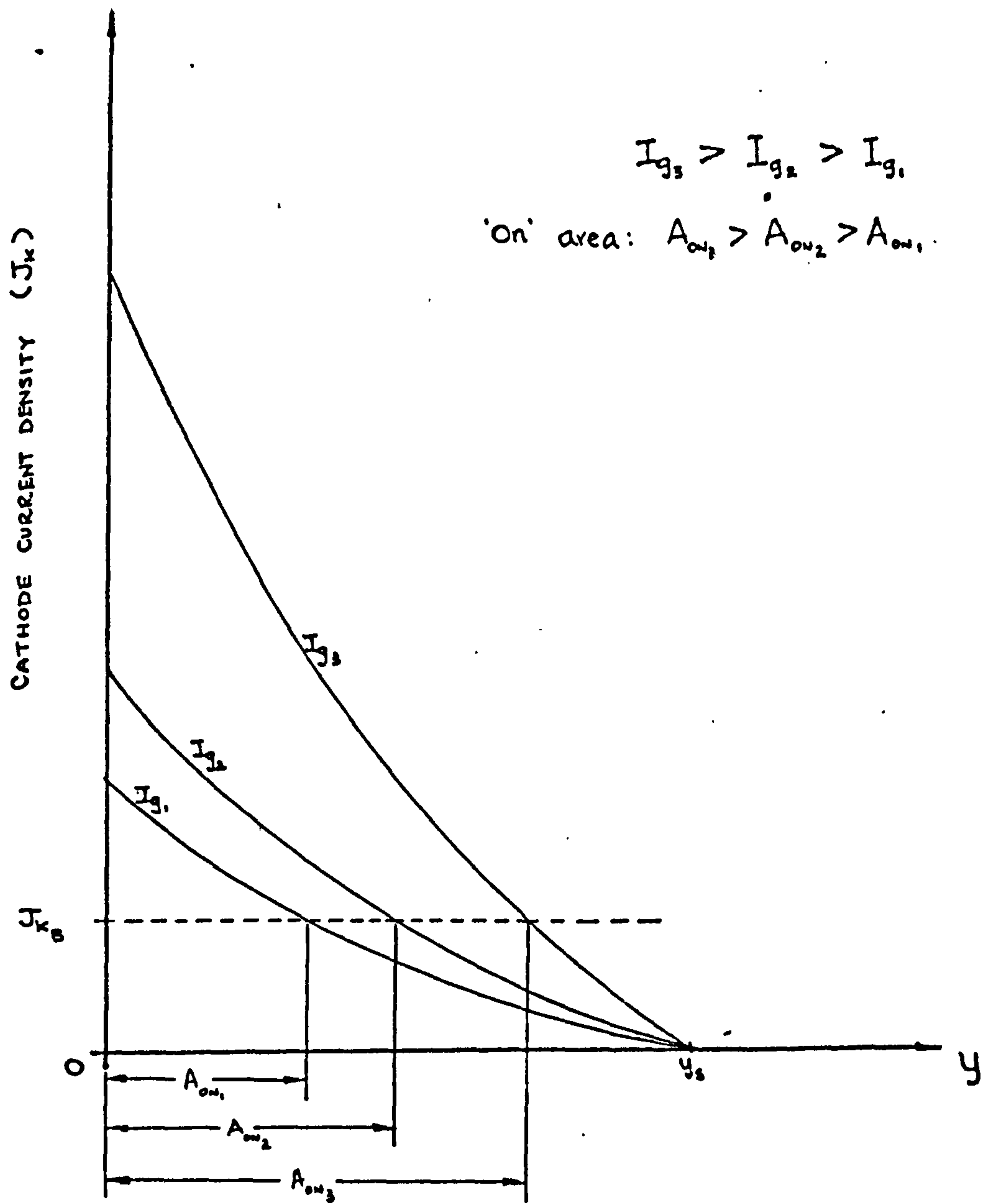


FIG. 19 Schematic plots of  $J_k$  versus  $y$ , illustrating the extend of the initial turned - on area.

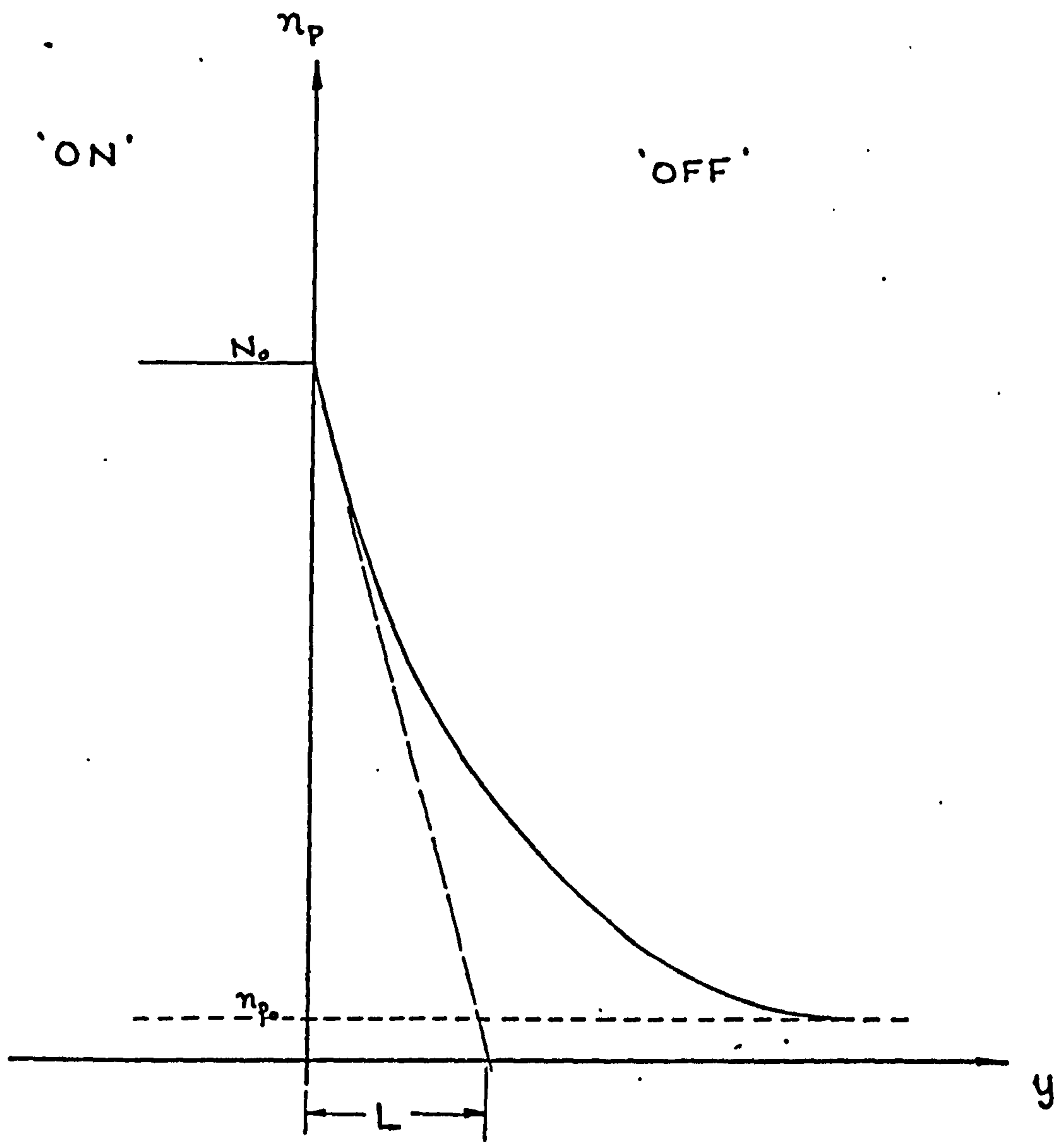


FIG. 20. Assumed exponential decay of excess carriers from the 'on' to the 'off' region.

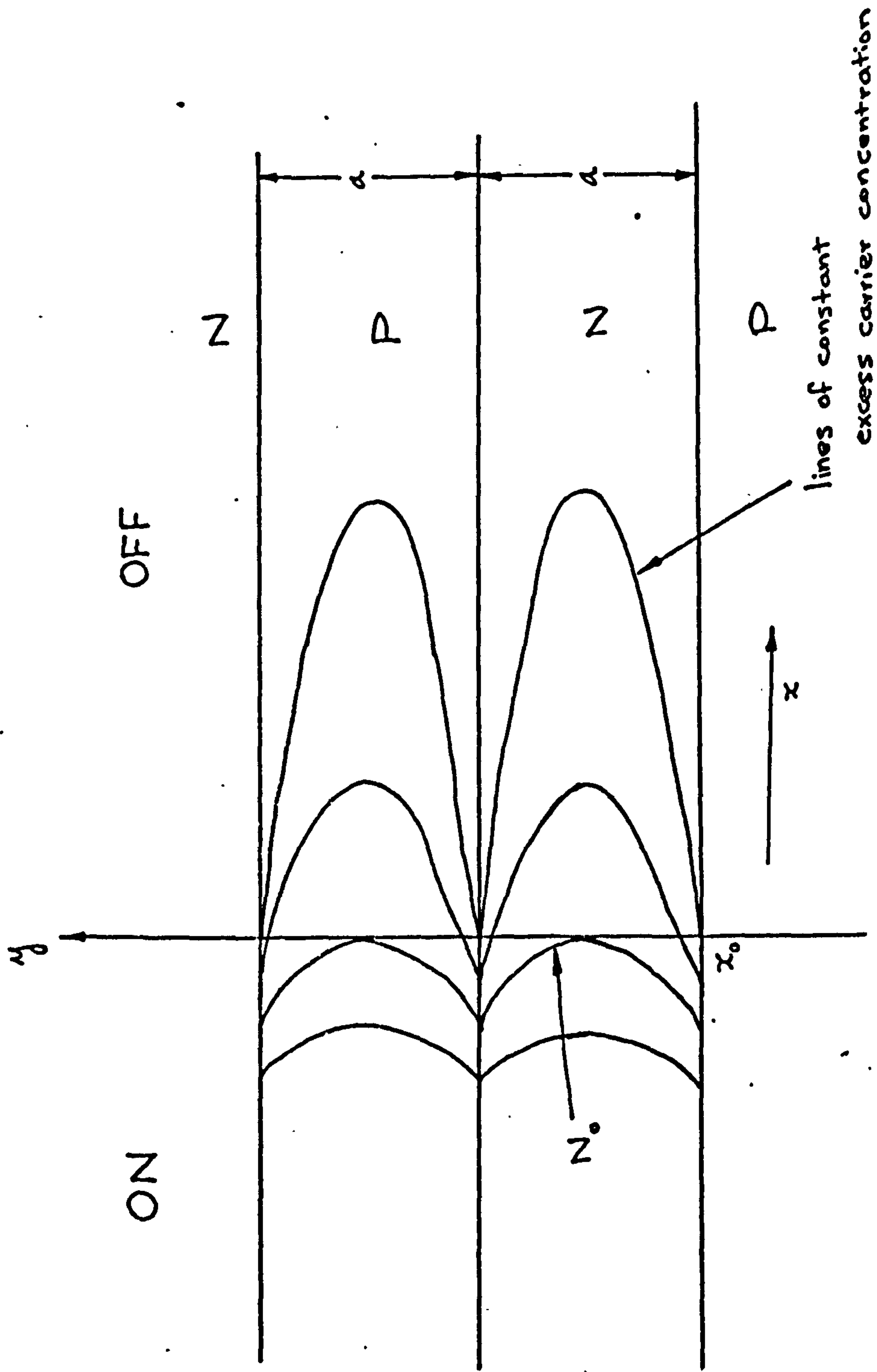
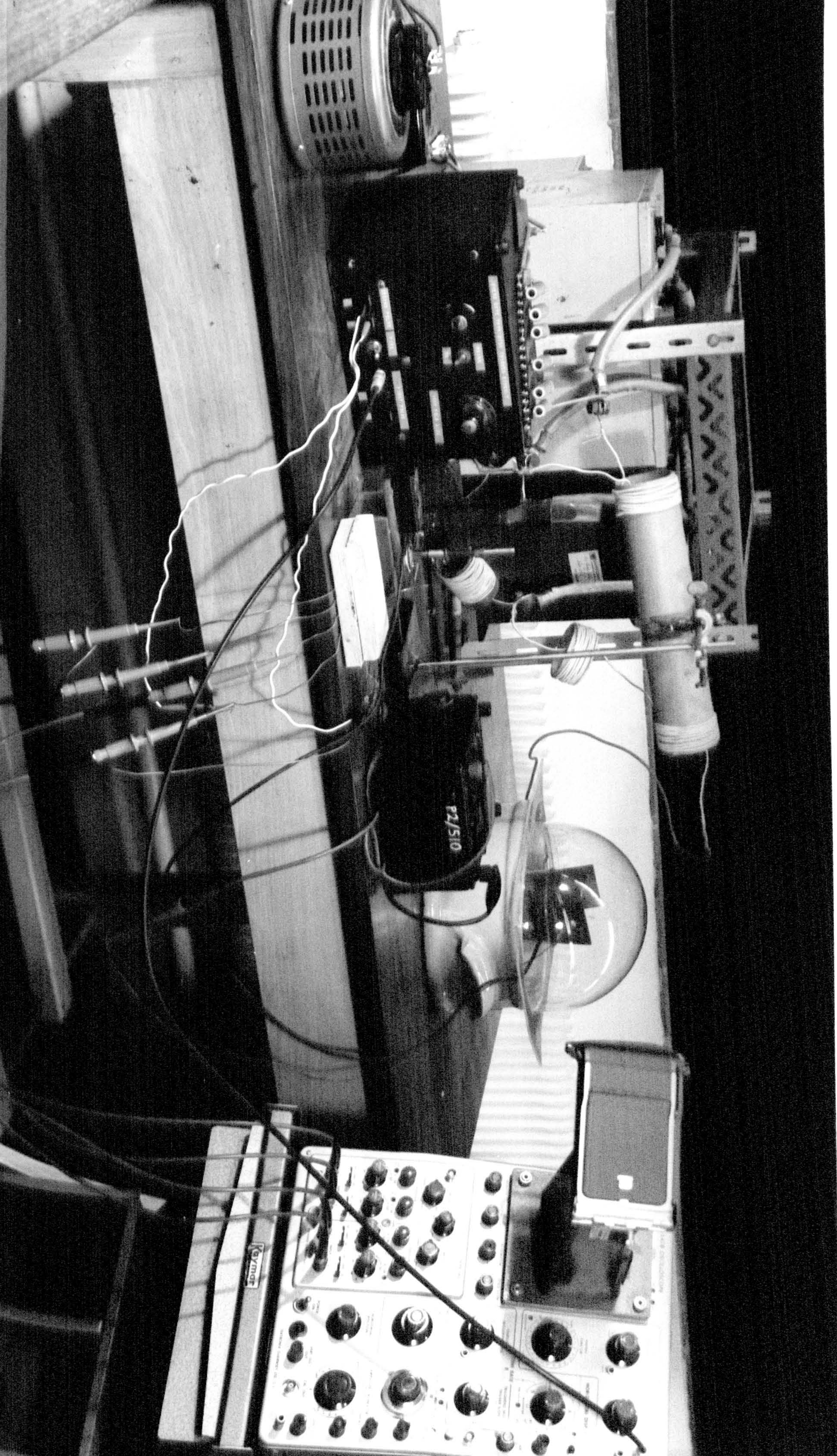


FIG. 21 Instantaneous minority carrier density plot  
 (From Longini and Melngailis (32))



2018/11

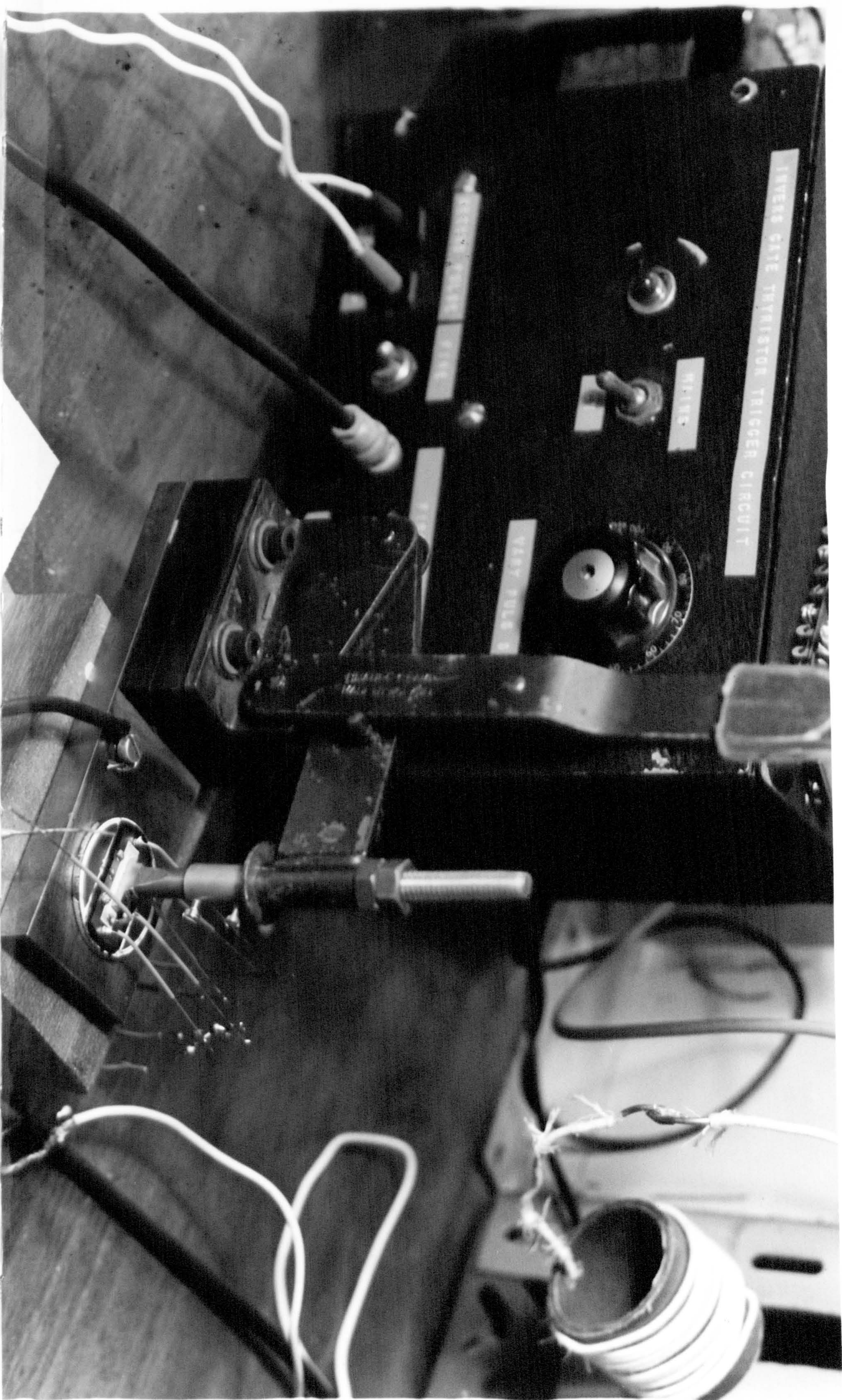


PLATE 2

PLATE 3

